REPORT DOCUMENTATION PAGE

Form Approved
OMB No. 0704-0188

1. AGENCY USE ONLY *(Leave Blank)*	2. REPORT DATE	3. REPORT TYPE AND DATES COVERED
	22-Jan-02	Final; 01-May-99 through 30-Jun-00

4. TITLE AND SUBTITLE
Density of Axisymmetric Models of Closed in-Vacuo Prolate Spheroidal Shells

5. FUNDING NUMBERS
G; N00014-99-1-0826

6. AUTHORS
Courtney B. Burroughs

7. PERFORMING ORGANIZATION NAME(S) AND ADDRESS(ES)
Applied Research Laboratory
The Pennsylvania State University
PO Box 30
State College PA 16804-0030

8. PERFORMING ORGANIZATION REPORT NUMBER

9. SPONSORING / MONITORING AGENCY NAME(S) AND ADDRESS(ES)
Office of Naval Research, ONR 321SS
Ballston Centre Tower One
800 North Quincy Street
Arlington VA 22217-5660

10. SPONSORING / MONITORING AGENCY REPORT NUMBER

11. SUPPLEMENTARY NOTES

12a. DISTRIBUTION / AVAILABILITY STATEMENT
Approved for Public Release

12b. DISTRIBUTION CODE

13. ABSTRACT *(Maximum 200 words)*

The objective is to develop simple expressions for the modal density of prolate spheroidal shells applicable at frequencies above where modal overlap renders the need to identify locations of individual modes unnecessary. The effort presented here is limited to axisymmetric modes which present the greatest challenge. Axisymmetric modes involve the zeroth-order circumferential modal response where the effects of curvature are strongest because of the ring in-plane stresses. Non-axisymmetric mods will be influenced less by curvature which should simplify the development of simple expressions for modal density. Thus, if we can obtain good estimates of the modal density for higher-order axisymmetric modes, it is likely that we can also obtain good estimates for modal densities for all higher-order modes for a closed prolate spheroidal shell.

14. SUBJECT TERMS
modal density
prolate spheroidal shells
axisymmetric modes

15. NUMBER OF PAGES
79

16. PRICE CODE

17. SECURITY CLASSIFICATION OF REPORT	18. SECURITY CLASSIFICATION OF THIS PAGE	19. SECURITY CLASSIFICATION OF ABSTRACT	20. LIMITATION OF ABSTRACT
unclassified	unclassified	unclassified	SAR

NSN 7540-01-280-5500

Standard Form 298 (Rev. 2-89)
Prescribed by ANSI Std. Z39-1
298-102

Density of Axisymmetric Modes of Closed in-Vacuo Prolate Spheroidal Shells

Dr. Courtney B. Burroughs
Applied Research Laboratory
The Pennsylvania State University
State College, PA 16804
cbb2@psu.edu

Final Report for
Grant No. N00014-99-1-0826
Office of Naval Research, Ballston Centre Tower One
800 North Quincy Street
Arlington, VA 22217-5660

24 January 2002

This material was based upon work supported by the Office of Naval Research under Award No. N00014-99-1-0826.

1.0 Introduction

When the modal bandwidth, determined by the damping, is on the order of three times the modal spacing, individual modes to not make significant contributions to the response of the shell as a function of frequency. Since damping changes slowly with frequency, whereas the modal spacing decreases with frequency, it is at the higher frequencies where modal overlap will be strong. The response of the shell to broadband, localized and/or transient excitation will then depend more on the modal density than on the locations of individual frequencies of resonance. However, estimation of modal density must rely on the estimation of the locations of the frequencies of resonance.

For prolate spheroidal shells, closed-form solutions for the resonant response are not available. Therefore, it is necessary to rely on either numerical methods or approximate analytical methods to obtain estimates of the frequencies of resonance for prolate spheroidal shells. Unfortunately, the computational effort for both numerical and approximate analytical methods increases with mode number, making it more difficult to obtain estimates of frequencies of resonance for the higher-order modes. However, because the importance of the exact locations of frequencies of resonance decreases with increasing mode number, the focus can be shifted from the location of the frequencies of resonance to obtaining estimates of modal density that are accurate where the modal overlap is high.

The objective of this report is to develop simple expressions for the modal density of prolate spheroidal shells applicable at frequencies above where modal overlap renders the need to identify locations of individual modes unnecessary. The effort presented here is limited to axisymmetric modes which present the greatest challenge. Axisymmetric

modes involve the zeroth-order circumferential modal response where the effects of curvature are strongest because of the ring in-plane stresses. Non-axisymmetric modes will be influenced less by curvature which should simplify the development of simple expressions for modal density. Thus, if we can obtain good estimates of the modal density for higher-order axisymmetric modes, it is likely that we can also obtain good estimates for the modal densities for all higher-order modes for a closed prolate spheroidal shell.

We base the effort to develop estimate for modal density on estimates of the frequencies of resonance of closed in-vacuo prolate spheroidal shells of constant thickness. Because the estimates of modal density will be based on the frequencies of resonance, we will retain the effects of material and geometric properties in the estimation of modal density.

2.0 Model for Frequencies of Resonance of Prolate Spheroidal Shell

The equations of motion for the axisymmetric nontorsional response of prolate spheroidal shells are given by [1]

$$JA_1\frac{\partial^2 u_\theta}{\partial\theta^2}+J^3A_2\cot\theta\frac{\partial u_\theta}{\partial\theta}-JA_3u_\theta+J^2A_4\sin^2\theta\frac{\partial^2\beta_\theta}{\partial\theta^2}+\sin\theta\cos\theta A_5\frac{\partial\beta_\theta}{\partial\theta}+$$
$$IJA_6\beta_\theta+IA_7\frac{\partial w}{\partial\theta}-\frac{IJ^2}{\Phi^2}A_8\sin\theta\cos\theta w+\Omega^2J(A_9u_\theta+A_{10}\beta_\theta)=0$$

$$k'\gamma JA_{11}\frac{\partial^2 w}{\partial\theta^2}+k'\gamma J^3A_{12}\cot\theta\frac{\partial w}{\partial\theta}-I^2JA_{13}w-IA_7\frac{\partial u_\theta}{\partial\theta}-IA_{14}\cot\theta u_\theta+$$
$$+A_{15}\frac{\partial\beta_\theta}{\partial\theta}+A_{16}\cot\theta\beta_\theta+\Omega^2JA_9w=0$$

$$J\frac{\partial^2\beta_\theta}{\partial\theta^2}+J^3\cot\theta\frac{\partial\beta_\theta}{\partial\theta}-JA_{17}\beta_\theta+\frac{IJ}{\Phi^2}\sin^2\theta\frac{\partial^2 u_\theta}{\partial\theta^2}+A_{18}\cos\theta\sin\theta\frac{\partial u_\theta}{\partial\theta}+$$
$$IJ^3A_{19}u_\theta+J^2A_{20}\frac{\partial w}{\partial\theta}+A_{21}\cos\theta\sin\theta w+\Omega^2J\Phi^2(A_{22}u_\theta+\beta_\theta)=0$$

where $A_1=1-c_1$, $A_2=1-c_1(3-4\sigma^2)$, $A_3=\nu I^2+\cot^2\left[1+\Phi^2c_2\right]$, $A_4=\dfrac{h_1T}{J^2\Phi^4}$,

$$A_5=h_1\left(\frac{IJ}{\Phi^4}\right)\left(3-\sigma^2\right),\ A_6=k'\gamma A_{11}+\frac{h_1}{J^2\Phi^4}\cos^2\theta,\ A_7=\nu+\left(1+k;\gamma\right)J^2-\left(1+\frac{3}{7}k'\gamma\right)J^2c_1$$

$$A_8=4+\sigma^2+h_1\left(\frac{I^2J^2}{\Phi^2}\right)\left(4-3\sigma^2+3\sigma^4+\sigma^6\right),\ A_9=\Phi^2+h_1I^2,\ A_{10}=h_1I\left(2+\sigma^2\right),$$

$$A_{11}=1-\frac{3}{7}c_1,\ A_{12}=1-\frac{3}{7}c_1\left(3-4\sigma^2\right),$$

$$A_{13}=2\nu+J^2\left(2+2\sigma^2+\sigma^4\right)+\frac{\sin^2\theta}{\Phi^2}c_1\left(3+3\sigma^2+\sigma^4\right),$$

$$A_{14}=\nu J^2+1+c_2k'\gamma J^4\left(1-2\sigma^2\right)\left(1-7c_1\right),\ A_{15}=k'\gamma\left(1-\frac{3}{7}c_1\right)-c_1,$$

$$A_{16}=c_2+k'\gamma\left[1-\frac{9}{7}J^2c_1\left(1-\sigma^2\right)\right],\ A_{17}=\cot^2\theta+\gamma I^2+\frac{k'\gamma}{h_1}\Phi^2\left(1-\frac{3}{7}c_1\right),$$

$$A_{18} = \frac{IJ^3}{\Phi^2}\left(3-\sigma^2\right),\ A_{19} = \frac{\cos^2\theta}{J^2\Phi^2} + \frac{k'\gamma\Phi^2}{h_1}\left(1-c_1\right),\ A_{20} = \frac{\Phi^2}{h_1}\left[c_1 - k'\gamma\left(1-\frac{3}{7}c_1\right)\right],$$

$$A_{21} = \frac{I^2J^4}{\Phi^2}\left(4-\sigma^2+\sigma^4\right) \text{ and } A_{22} = IJ^2\left(2+\sigma^2\right).$$

In the above, $c_1 = h_1\frac{I^2}{\Phi^4}\sin^2\theta$, $c_2 = h_1\frac{T^2}{\Phi^4}\sin^2\theta$, $I = \frac{\cosh b}{\Phi}$, $J = \frac{\sinh b}{\Phi}$, $T = \coth b$,

$h_1 = \frac{h^2}{12a^2}$, $\sigma = \frac{\sin\theta}{\sinh b}$, $\gamma = \frac{1-\nu}{2}$, $k' = \frac{5}{6}$ and $\Phi = \left(\sinh^2 b + \sin^2\theta\right)^{1/2}$,

and $\cosh b = \frac{a}{\left(a^2-b^b\right)^{1/2}}$, where $2a$ is the major axis and $2b$ is the minor axis, h is the shell thickness, and the eccentricity is $e = \frac{1}{\cosh b}$. The nondimensional frequency is $\Omega = \frac{\omega a_f}{c_l}$, where $c_l = \sqrt{\frac{E}{\rho\left(1-\nu^2\right)}}$ is the longitudinal wave phase speed in a plate, where E is Young's modulus, ρ is the material density and ν is Poisson' ratio. The nondimensional frequencies are $u_\theta = \frac{u_\theta'}{a_f \sinh b}$, where u_θ' is the in-plane displacement in the meridian (θ) direction and a_f is half the interfocal distance, β_θ is the rotational of an element relative to the normal to the middle surface in the θ-direction and $w = \frac{w'}{a_f \sinh b}$ where w' is the displacement normal to the middle surface of the shell.

These displacements are illustrated in Figure 1.

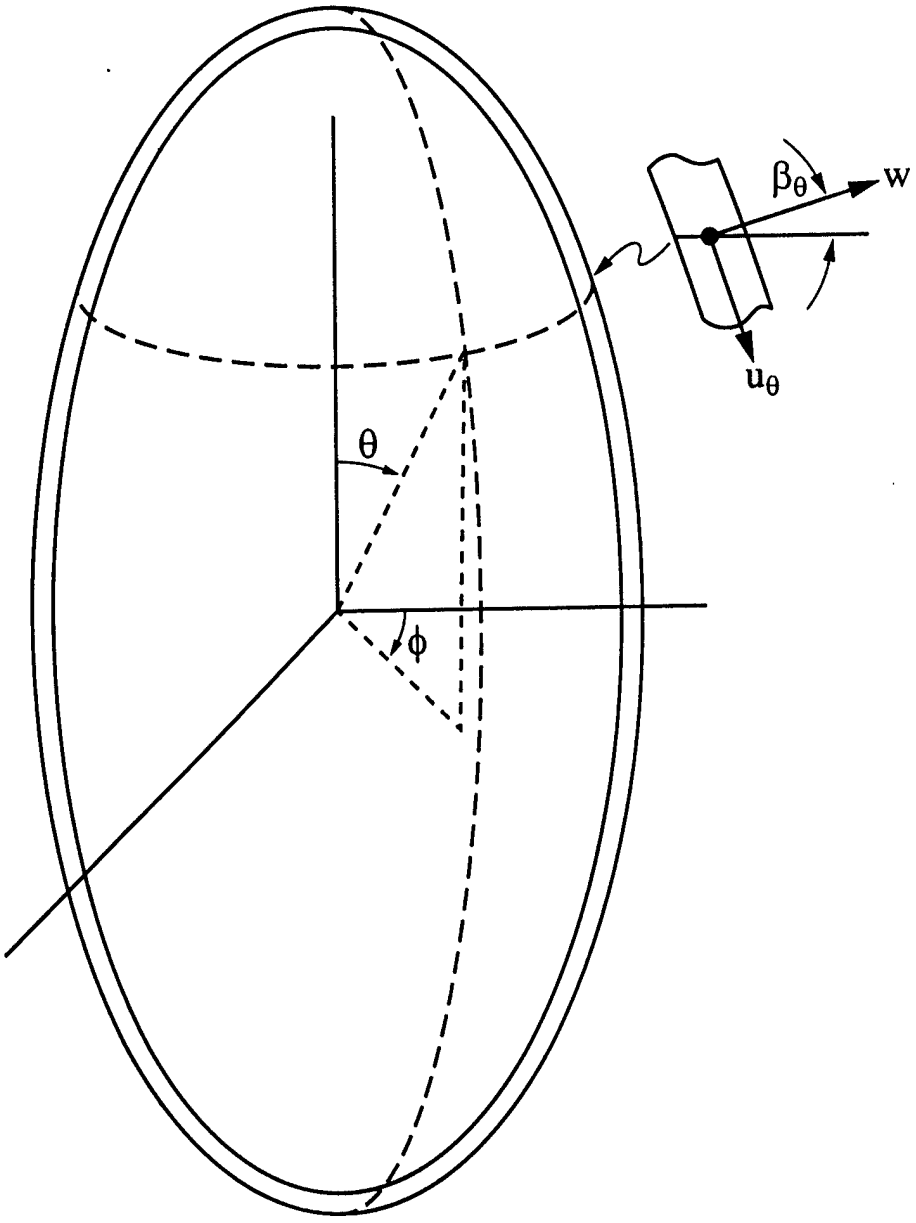

Figure 1. Nontorsional displacements for axisymmetric motion of a closed prolate spheroidal shell

Galerkin's variational method is applied to obtain approximate solutions to the above shell equations. Basically, Galerkin's method involves the approximation of the solution with a series of functions that form a complete set and satisfy the boundary conditions exactly. The expansion coefficients are then selected to approximate the differential equations, knowing that the boundary conditions will be satisfied exactly. For axisymmetric motion of a closed shell, the boundary conditions are

$$u_\theta = \frac{\partial w}{\partial \theta} = \beta_\theta = 0 \;\; at \;\; \theta = 0, \pi$$

The solutions can then be expressed as

$$u_\theta = \sum_{n=0}^{N} C_{1n} \sin(n\theta)$$
$$w = \sum_{n=0}^{N} C_{2n} \cos(n\theta)$$
$$\beta_\theta = \sum_{n=0}^{N} C_{3n} \sin(n\theta)$$

Substituting these approximate solutions into the governing differential equations for the shell, operating on the first and third equation with $\int_0^\pi \sin(n'\theta) d\theta$ and the second equation with $\int_0^\pi \cos(n'\theta)$, and using the orthogonality conditions yields

$$\sinh b \sum_{n=0}^{N} C_{1n} \Lambda_{1nk} + \cosh b \sum_{n=0}^{N} C_{2n} \Lambda_{2nk} + T \sum_{n=0}^{N} C_{3n} \Lambda_{3nk} = 0$$
$$\cosh b \sum_{n=0}^{N} C_{1n} \Lambda_{4nk} + \sinh b \sum_{n=0}^{N} C_{2n} \Lambda_{5nk} + \sum_{n=0}^{N} C_{3n} \Lambda_{6nk} = 0$$
$$T \sum_{n=0}^{N} C_{1n} \Lambda_{7nk} + \sum_{n=0}^{N} C_{2n} \Lambda_{8nk} + \frac{\cosh b}{\sinh b} \sum C_{3n} \Lambda_{9nk} = 0$$

where Λ_{ink} are defined in Appendix of ref. 1.

In order to obtain a nontrivial solution for the expansion coefficients, C_{in}, the determinant of the matrix formed by Λ_{ink} must vanish, i.e. $|\Lambda| = 0$. The values of Ω^2 for

which $|\Lambda| = 0$ then define the frequencies of resonance. To obtain estimates for the frequencies of resonance for higher-order modes, larger numbers of terms must be included in the summation. As the number of terms in the solutions increases, the approximate solution approaches the exact solution from above.

3.0 Estimates of Frequencies of Resonances

Estimates of the frequencies of resonance were obtained for the nontorsional, axisymmetric modes for the in-vacuo, closed prolate spheroidal shells with the geometric properties given in Table 1.

The convergence of the estimates for the square of the nondimensional frequencies of resonance are shown in Table 2 for Case 1a as a function of the number of terms used in the approximate solution. The solution for the n=1 mode converged to the third decimal place for the number of terms in the solution between 5 and 10. For the n=20 mode, 90 terms were needed to obtain accuracy to the third decimal place. With 90 terms in the solution, the n=25 mode converged only to the first decimal place.

With 90 terms in the solution, the size of the matrix is 270 by 270, showing the need for a more computationally efficient method of estimating modal density for axisymmetric modes with mode numbers greater than n=20.

Using 90 terms in the solution, the square of the nondimensional frequencies of resonance are given in Tables 3, 4 and 5 for Cases 1, 2 and 3 shown in Table 1. Frequencies of resonance obtained from the values in Tables 3, 4 and 5 will be used below to obtain approximations to modal densities applicable to higher-order modes, i.e. for modes with mode number greater than approximately 10.

Table 1. Geometric Parameters used in Estimating Frequencies of Resonance.

Case	Interfocal Distance (inches)	Minor axis (inches)	Major axis (inches)	Thickness (inches)
1a	328	297.5	442.8	0.25
b	"	"	"	0.50
c	"	"	"	0.75
d	"	"	"	1.00
e	"	"	"	1.25
f	"	"	"	1.50
2a	187	261.7	321.6	0.25
b	"	"	"	0.50
c	"	"	"	0.75
d	"	"	"	1.00
e	"	"	"	1.25
f	"	"	"	1.50
3a	628	287.8	690.8	0.25
b	"	"	"	0.50
c	"	"	"	0.75
d	"	"	"	1.00
e	"	"	"	1.25
f	"	"	"	1.50

Table 2a. Convergence of Frequencies of Resonance for Case 1a Shell for 1 to 14 Mode Number

N*	Mode Number													
	1	2	3	4	5	6	7	8	9	10	11	12	13	14
5	0.517	0.847	1.176	1.440										
10	0.516	0.827	0.919	1.037										
15	-	0.826	0.902	0.941										
20		0.826	0.896	0.924	0.958									
25		-	0.895	0.915	0.940	0.967								
30			0.895	0.912	0.927	0.950	0.980							
35			-	0.911	0.923	0.938	0.964	0.989						
40				0.911	0.921	0.934	0.951	0.975	1.003					
45				-	0.921	0.932	0.947	0.963	0.990	1.016				
50					-	0.932	0.945	0.960	0.980	1.004	1.032	1.072		
55						0.931	0.945	0.959	0.978	0.997	1.023	1.050	1.089	1.128
60						-	-	-	-	1.018	1.044	1.072	1.111	1.206
65										1.017	1.041	1.068	1.099	1.135
70										-	1.041	1.067	1.097	1.128
75											-	-	1.096	1.128
80													-	-
90														

Table 2b. Convergence of Frequencies of Resonance for Case 1a Shell for 15 to 25 Mode Number

N*	Mode Number										
	15	16	17	18	19	20	21	22	23	24	25
5											
10											
15											
20											
25											
30											
35											
40											
45											
50											
55											
60	1.206	1.256	1.338								
65	1.135	1.175	1.227	1.335	1.424						
70	1.128	1.167	1.206	1.259	1.309	1.383					
75	1.126	1.164	1.201	1.245	1.294	1.348					
80	-	1.164	1.201	1.244	1.288	1.339	1.392	1.458	1.523	1.611	1.687
90		-	-	-	1.287	1.337	1.384	1.438	1.495	1.550	1.603

* Number of terms in approximate solutions

Table 3. Frequencies of Resonance for Case 1 Prolate Spheroidal Shell – Interfocal Distance = 328 inches and Thickness – a) 0.25, b) 0.50, c) 0.75, d) 1.00, e) 1.25 and f) 1.50 inches

Mode No.	Case a)	Case b)	Case c)	Case d)	Case e)	Case f)
1	0.516	0.516	0.516	0.516	0.516	0.516
2	0.826	0.826	0.826	0.826	0.826	0.826
3	0.895	0.896	0.897	0.898	0.899	0.901
4	0.911	0.916	0.920	0.924	0.929	0.933
5	0.921	0.932	0.942	0.952	0.962	0.971
6	0.931	0.949	0.966	0.981	0.996	1.010
7	0.945	0.972	0.995	1.017	1.037	1.057
8	0.959	0.995	1.027	1.057	1.085	1.112
9	0.977	1.203	1.064	1.102	1.138	1.248
10	0.994	1.055	1.107	1.156	1.203	1.425
11	1.017	1.089	1.153	1.214	1.272	1.528
12	1.041	1.130	1.209	1.284	1.355	1.648
13	1.076	1.172	1.267	1.357	1.444	1.743
14	1.096	1.223	1.337	1.444	1.547	1.920
15	1.127	1.275	1.409	1.536	1.656	2.079
16	1.164	1.337	1.493	1.641	1.755	2.248
17	1.201	1.400	1.581	1.736	1.920	2.437
18	1.244	1.473	1.680	1.875	2.064	2.640
19	1.287	1.548	1.746	2.010	2.225	2.866
20	1.336	1.632	1.899	2.152	2.397	3.107
21	1.384	1.715	2.023	2.309	2.589	3.375
22	1.438	1.759	2.154	2.475	2.791	3.659
23	1.495	1.817	2.297	2.659	3.107	3.969
24	1.550	1.921	2.448	2.853	3.150	4.301
25	1/603	2.029	2.613	3.067	3.256	4.655

Table 4. Frequencies of Resonance for Case 2 Prolate Spheroidal Shell – Interfocal Distance = 187 inches and Thickness – a) 0.25, b) 0.50, c) 0.75, d) 1.00, e) 1.25 and f) 1.50 inches.

Mode No.	Case a)	Case b)	Case c)	Case d)	Case e)	Case f)
1	0.533	0.533	0.533	0.533	0.533	0.533
2	0.787	0.783	0.783	0.783	0.783	0.784
3	0.871	0.871	0.872	0.874	0.875	0.876
4	0.900	0.904	0.908	0.913	0.918	0.923
5	0.916	0.927	0.937	0.947	0.958	0.968
6	0.929	0.948	0.967	0.984	1.001	1.018
7	0.943	0.972	0.998	1.024	1.050	1.074
8	0.961	1.001	1.037	1.071	1.105	1.137
9	0.979	1.034	1.083	1.129	1.173	1.217
10	1.002	1.069	1.131	1.189	1.245	1.300
11	1.027	1.112	1.188	1.259	1.325	1.390
12	1.053	1.157	1.249	1.335	1.416	1.497
13	1.085	1.208	1.314	1.413	1.512	1.614
14	1.117	1.263	1.389	1.508	1.627	1.751
15	1.155	1.320	1.465	1.611	1.761	1.918
16	1.194	1.386	1.556	1.728	1.905	2.091
17	1.236	1.452	1.656	1.866	2.080	2.302
18	1.282	1.530	1.765	2.007	2.257	2.519
19	1.329	1.614	1.894	2.178	2.463	2.755
20	1.383	1.705	2.022	2.348	2.680	3.028
21	1.435	1.810	2.176	2.538	2.897	3.270
22	1.497	1.915	2.327	2.744	3.168	3.620
23	1.560	2.041	2.496	2.939	3.400	3.916
24	1.630	2.161	2.676	3.192	3.732	4.335
25	1.707	2.302	2.847	3.403	4.025	4.728

Table 5 Frequencies of Resonance for Case 3Prolate Spheroidal Shell – Interfocal Distance = 628 inches and Thickness – a) 0.25, b) 0.50, c) 0.75, d) 1.00, e) 1.25 and f) 1.50 inches.

Mode No.	Case a)	Case b)	Case c)	Case d)	Case e)	Case f)
1	0.384	0.384	0.384	0.384	0.384	0.384
2	0.809	0.809	0.809	0.809	0.809	0.809
3	0.854	0.854	0.854	0.854	0.854	0.854
4	0.910	0.912	0.913	0.915	0.917	0.920
5	0.916	0.920	0.926	0.931	0.937	0.943
6	0.921	0.930	0.937	0.944	0.951	0.958
7	0.928	0.944	0.959	0.974	0.990	1.006
8	0.935	0.953	0.968	0.982	0.996	1.009
9	0.946	0.982	1.005	1.032	1.055	1.076
10	0.952	0.982	1.008	1.035	1.066	1.160
11	0.968	1.019	1.058	1.094	1.128	1.236
12	0.972	1.020	1.068	1.121	1.178	1.263
13	0.998	1.065	1.119	1.170	1.218	1.390
14	1.002	1.075	1.193	1.239	1.320	1.448
15	1.030	1.120	1.200	1.262	1.436	1.541
16	1.040	1.145	1.280	1.371	1.458	1.595
17	1.070	1.176	1.382	1.443	1.495	1.720
18	1.100	1.230	1.440	1.500	1.612	1.815
19	1.150	1.240	1.490	1.541	1.677	1.920
20	1.200	1.320	1.520	1.650	1.791	2.072
21	1.250	1.430	1.600	1.718	1.895	2.164
22	1.350	1.460	1.660	1.822	1.996	2.354
23	1.400	1.580	1.730	1.987	2.147	2.460
24	1.500	1.620	1.800	2.100	2.365	2.716
25	1.550	1.720	1.950	2.250	2.510	2.760

4.0 Estimation of Modal Density

The approach to the estimation of modal density is to 'unwrap' each half of the prolate spheroidal shell into two flat circular plates with a radii equal to the chord length (L) from the apex ($\theta = 0 or \pi$) to the middle of the shell ($\theta = \pi/2$), as shown in Figure 2. The spreading in the circumferential (ϕ) direction should not affect the bending wavenumber in the meridian (θ) direction so that the resonant wavenumber for the shell before and after unwrapping should be the same when the curvature in the θ-direction is not a factor. Once the wavenumber of resonance in the θ-direction is modeled, then effects of the axisymmetric, zero wavenumber in the ϕ-direction must be included. This effect can not be ignored in the plate model where the in-plane stresses decouple from the radial displacements in the plate.

There are two types of axisymmetric modes in the shell; those which are symmetric about the middle of the shell, i.e. even in the θ-direction about $\theta = \pi/2$, and those which are nonsymmetric about $\theta = \pi/2$, i.e. odd in the θ-direction. For the symmetric modes, the slope and the shear in the middle of the shell are zero. Thus for the unwrapped plate the boundary conditions for the even modes are

$$\frac{\partial w}{\partial \theta} = \frac{\partial^3 w}{\partial \theta^3} = 0 \quad at\, r = L$$

For the symmetric modes, the displacement and moment are zero in the middle of the shell. Thus for the unwrapped plate the boundary conditions for the odd modes are

$$w = \frac{\partial^2 w}{\partial \theta^2} = 0 \quad at\, r = L$$

where $r = L$ is the radius of the plate.

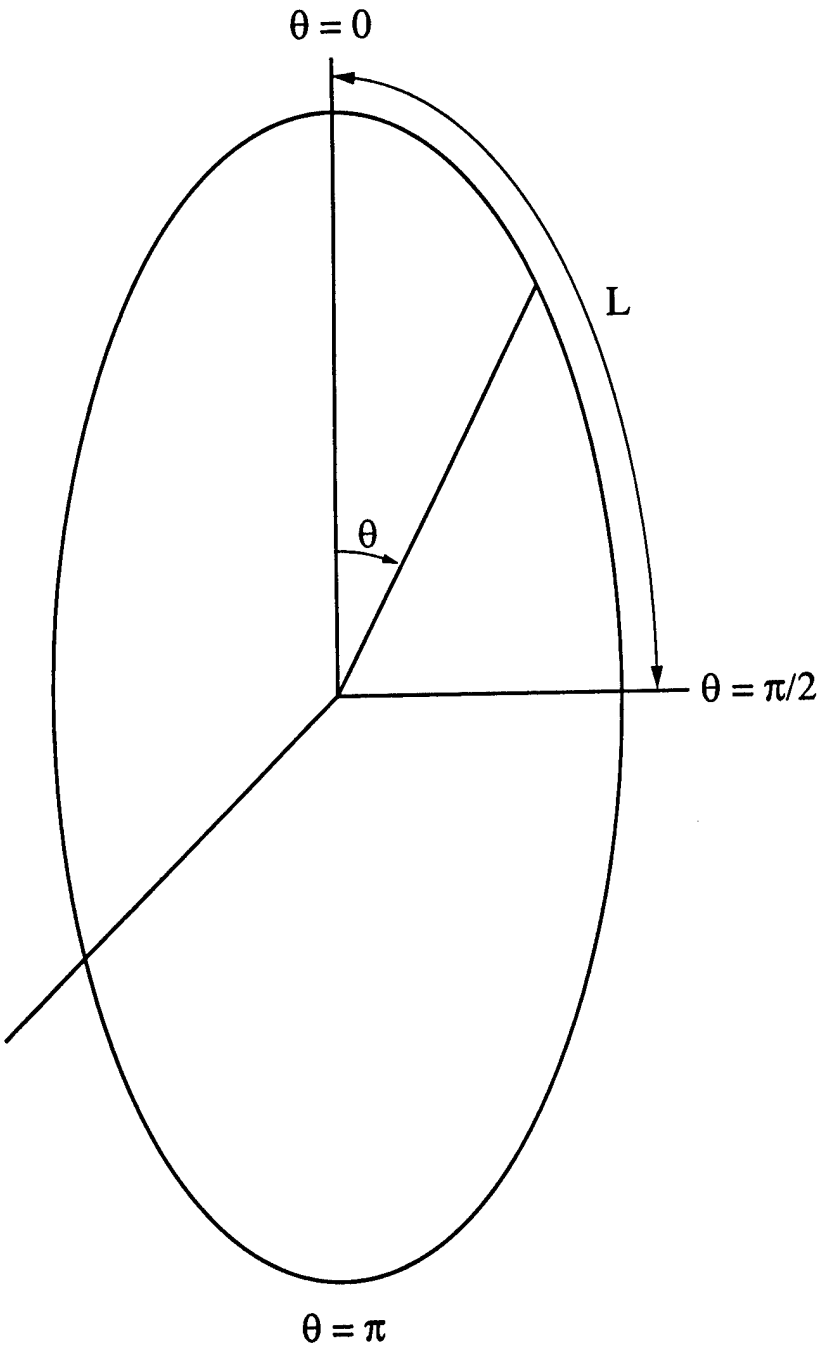

Figure 2. Meridian Arc Length for the Prolate Spheroidal Shell.

The radius of the unwrapped plate is the arc length of the shell from the apex located at $x = a, y = 0$ to the middle of the shell, given by $x = 0, y = b$, as shown in Figure 3. The arc length is then given by

$$L = \int_0^a \left\{1 + \left(\frac{\partial y}{\partial x}\right)^2\right\}^{1/2} dx$$

where $y = -\frac{b}{a}\frac{x}{\left(a^2 - x^2\right)^{1/2}}$ for the meridian arc length on the shell for ϕ=constant. For the prolate spheroidal shell with a major axis = $2a$ and minor axis = $2b$, the arc length is

$$L = \int_0^a \left[\frac{1 - k^2 y^2}{1 - y^2}\right]^{1/2} dy = aE\left(\frac{\pi}{2}, k\right)$$

where $E\left(\frac{\pi}{2}, k\right)$ is the elliptic integral and $k^2 = \frac{a^2 - b^2}{a^2}$.

The solution for the axisymmetric displacement of a circular plate is

$$w(r) = AJ_0(kr) + BI_0(kr)$$

where J_0 is the Bessel function of the first kind of zero order, I_0 is the modified Bessel function of the first kind of zero order, and k is the bending wavenumber. Applying the boundary condtions for the symmetric modes leads to $J_1(kL) = 0$ as the solution for the nondimensional frequency,

$$(kL)^2 = 2\pi f L^2 \left[\frac{12\rho(1 - \nu^2)}{Eh^2}\right]$$

where f is the frequency in Hz. Applying the boundary conditions for the nonsymmetric modes leads to [2]

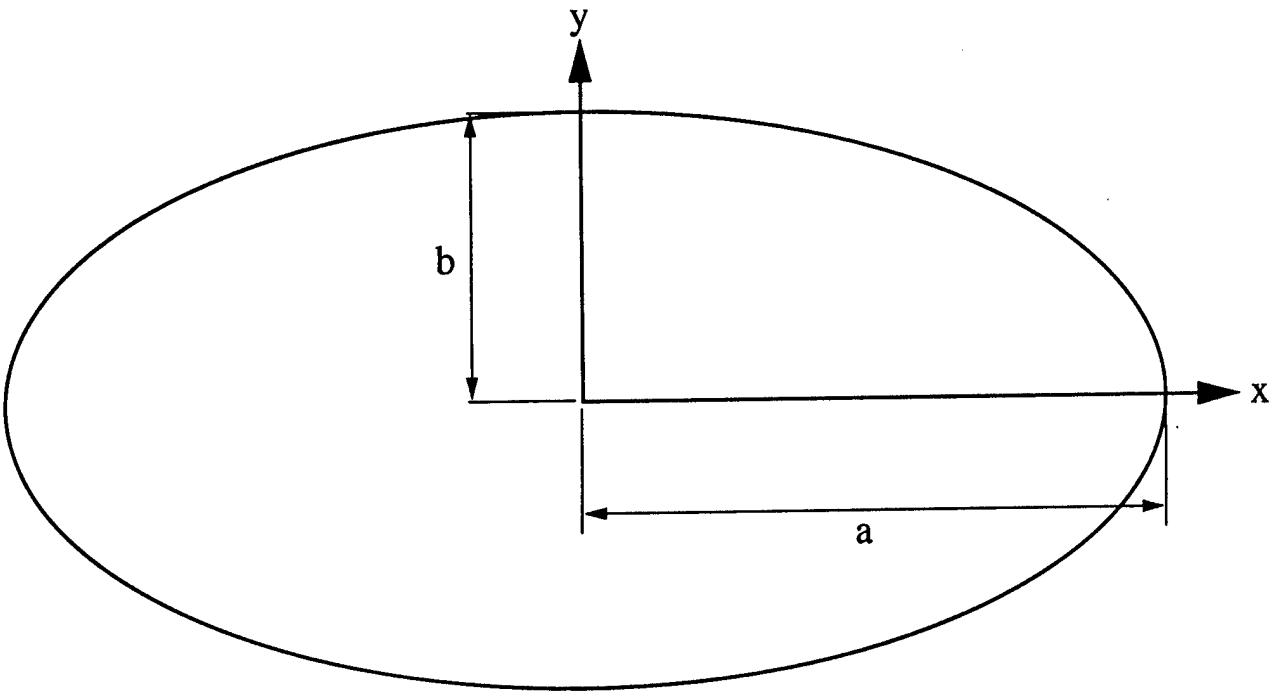

Figure 3. Half of Major and Minor Axis for Prolate Spheroidal Shell

$$\frac{J_1(kL)}{J_0(kL)} + \frac{I_1(kL)}{I_0(kL)} = \frac{2kL}{1-\nu}$$

For large kL (i.e. above $\cong 5$), this becomes $J_0(kL) \approx 0$.

The frequencies of resonance for the unwrapped shell were then obtained by alternating between symmetric and nonsymmetric modes. The frequencies of resonance for the plate are compared to the frequencies of resonance for the shell for Case 1a in Figure 4. The ring stresses in the shell keep the frequencies of resonance for the shell far above the frequencies of resonance for the plate. The differences between the plate and shell frequencies of resonance are much greater for the lower-order modes where coupling between the in-plane and transverse displacements along the meridian of the shell are greatest. For the higher-order modes, this coupling decreases so that only the in-plane stresses around the circumference of the shell (i.e. the ring stresses) are holding the frequencies of resonance for the shell above the frequencies of resonance for the plate. Thus, we need to include the effects of the ring in-plane stresses, which will be the same for all modes in the meridian (θ) direction.

The frequency of resonance for a ring of radius R is [3]

$$\Omega^2 = 1 = \frac{\rho(1-\nu^2)R^2\omega^2}{E}$$

Since the influence of the ring stresses in a prolate spheroidal shell are maximum in the middle and decrease to nearly zero at the apex, and the radius decreases from $R = b$ at the middle of the shell to zero at the apex, we can approximate the effect of the ring stresses in the shell by using an effective radius for the shell by integrating over the arc length of the shell and including the orientation of the ring stresses. This leads to

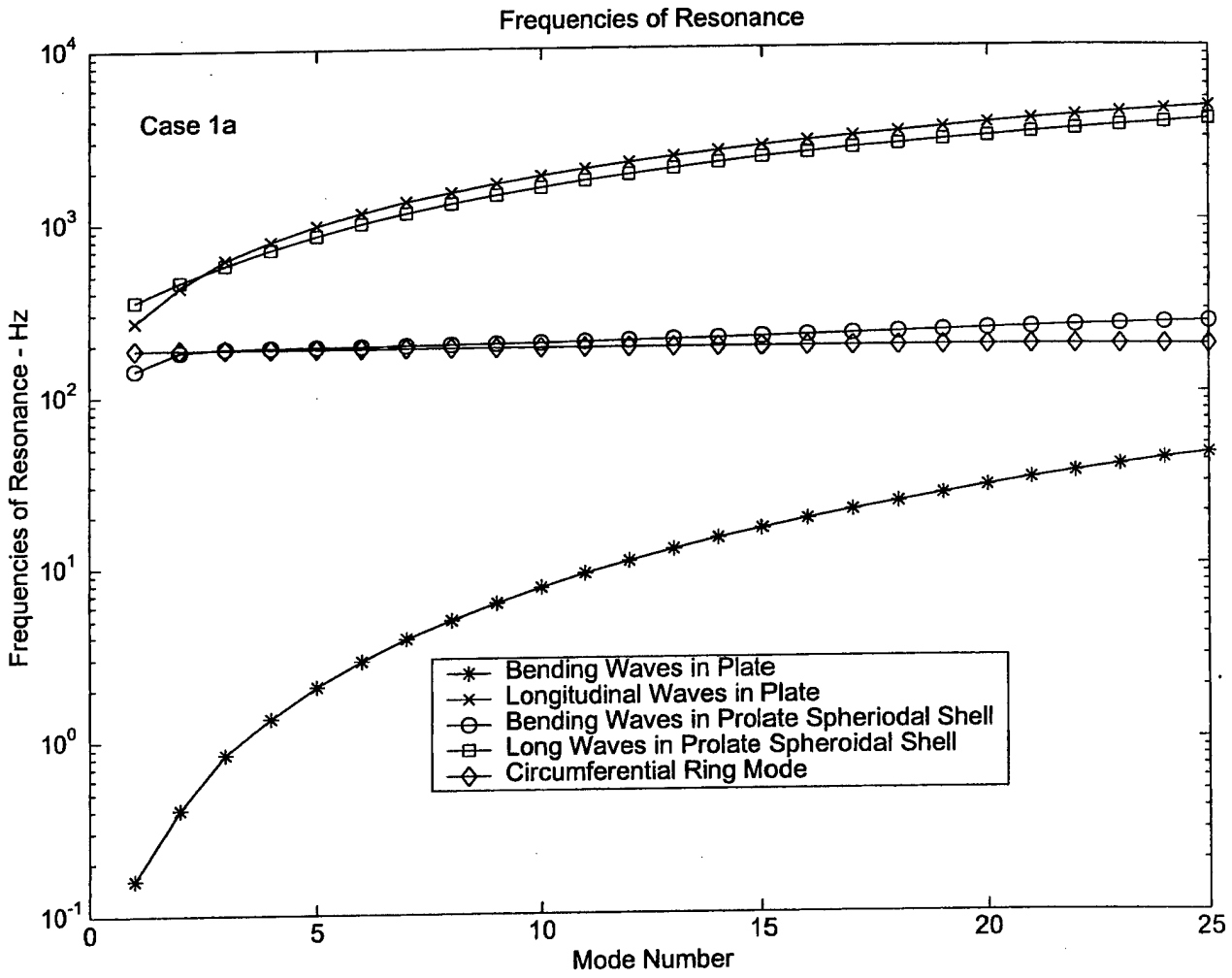

Figure 4. Frequency of Resonance for Case 1a Prolate Spheroidal Shell and And Corresponding Unwrapped Plate.

$$R_e = \frac{1}{a}\int_0^a \frac{y}{\cos\theta} d$$

where $\cos\theta = \frac{y}{(x^2+y^2)^{1/2}}$. Performing the integration yields

$$R_e = \frac{a}{2} + \frac{b^2}{2(a^2-b^2)} \ln\left[\frac{(a^2-b^2)^{1/2}+a}{b}\right]$$

This equation is used in the equation for the frequency of resonance for the circumferential ring mode. This ring frequency of resonance is compared to the frequencies of resonance for the bending waves in the prolate spheroidal shell in Figure 4. The fact that the frequency of resonance for the circumferential ring mode is close to the frequencies of resonance for the bending waves in the shell implies that the frequencies of resonance for the shell are controlled by the axisymmetric ring mode in the circumferential direction.

In addition to the above comparisons, Figure 4 also shows comparisons between the frequencies of resonance for in-plane modes in the shell to the in-plane modes in the plate. For the plate, the frequencies of resonance for the symmetric modes (where $u_\theta = 0 \ \ at\, r = L$) and nonsymmetric modes (where $\frac{\partial u_\theta}{\partial \theta} \ \ at\, r = L$) are given by $J_0(k_l L) = 0$ and $J_1(k_l L) = 0$, respectively, where $k_l = \frac{\omega}{c_l}$ and $c_l^2 = \frac{E}{\rho(1-\nu^2)}$. The in-plane frequencies of resonance for the plate and shell are in close agreement indicating that the shell in-plane axisymmetric modes can be approximated with the much simpler model of the plate. Thus, we will concentrate in the following on the bending modes to

obtain an approximation for the modal density for the axisymmetric bending waves in the shell.

A quadratic fit to the bending wave frequencies of resonance for the Case 1a prolate spheroidal shell is shown in Figure 5. This fit is then used to extrapolate the frequencies of resonance out to the n=50 bending wave mode number. These extrapolated frequencies of resonance are compared to the frequencies of resonance for the unwrapped plate and the circumferential ring mode frequency of resonance in Figure 6. At the higher mode numbers, the influence of bending along the meridian (θ) direction becomes apparent. For Case 1a, which is the thinnest of the Case 1 shells (h=0.25 inches), the influence of the ring mode in the circumferential direction and the bending modes in the unwrapped plate (i.e in the shell without the effects of curvature) on the frequencies of resonance for the bending waves in the shell appear to be nearly equal near the n=50 mode.

The same approach was applied to Cases 1b through 1f with the results shown in Figures 7 through 21. As the thickness of the shell increases, the influence of the bending waves in the meridian direction increase to the point where the unwrapped plate provides an increasingly accurate approximation for the frequencies of resonance for the shell.

Results for the other two shells (Cases 2 and 3) are shown in Figures 23 through 57. For both of these shells, the trends in the frequencies of resonance are similar to the frequencies of resonance for the Case 1 shell. The influence of the bending waves in the meridian direction increases with increasing shell thickness. The frequencies of resonance for the plate provide a better fit to the frequencies of resonance for the shell at the higher-order modes for the Case 2 and 3 shells than for the Case 1 shell. For the Case

3 shell, the frequencies of resonance exceed the frequencies of resonance for the plate. This may be because the Case 3 shell has the largest interfocal distance of the three shells, and has the longest and thinnest profile.

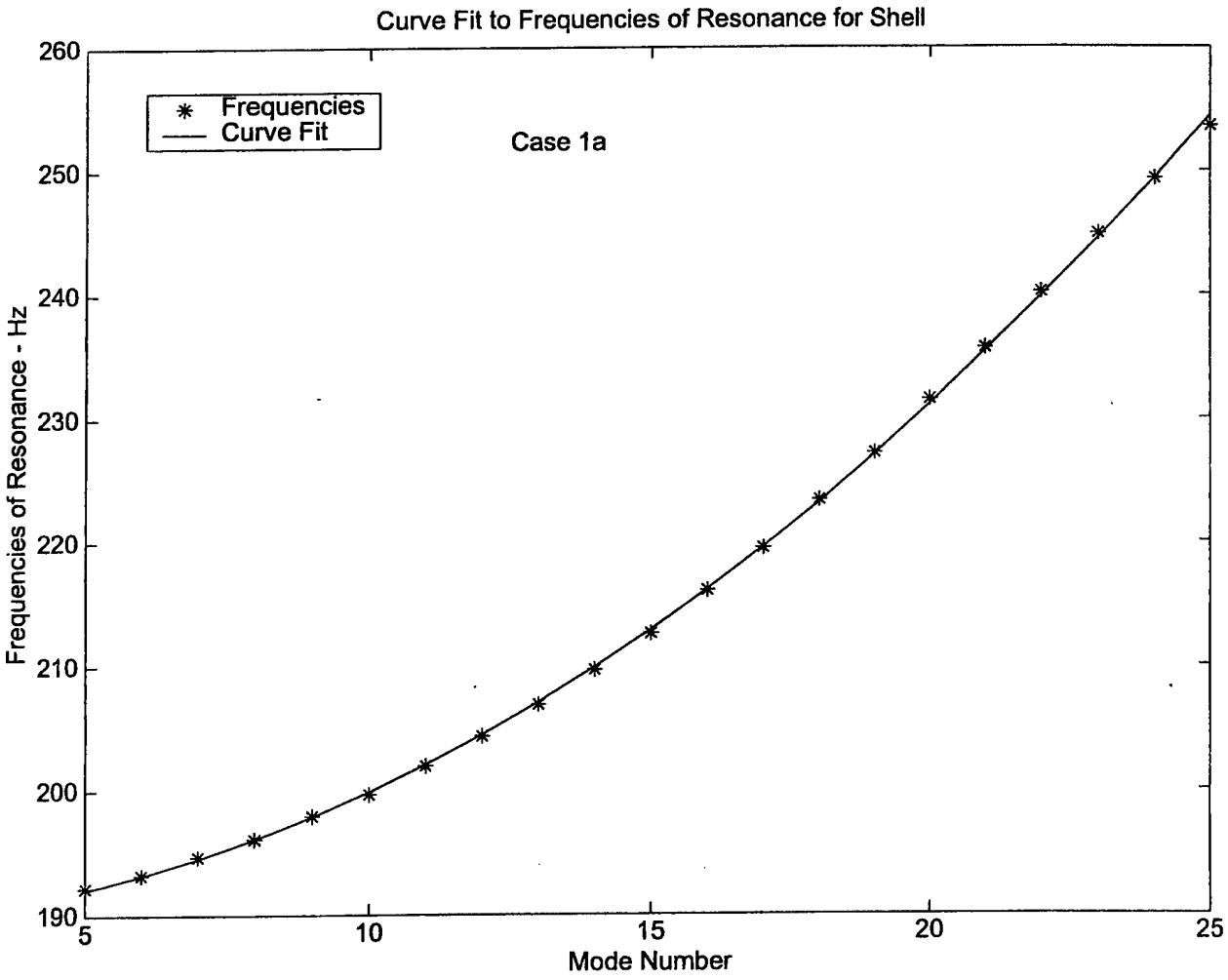

Figure 5. Quadratic Curve Fit to Bending Wave Frequencies of Resonance for Case 1a Prolate Spheroidal Shell

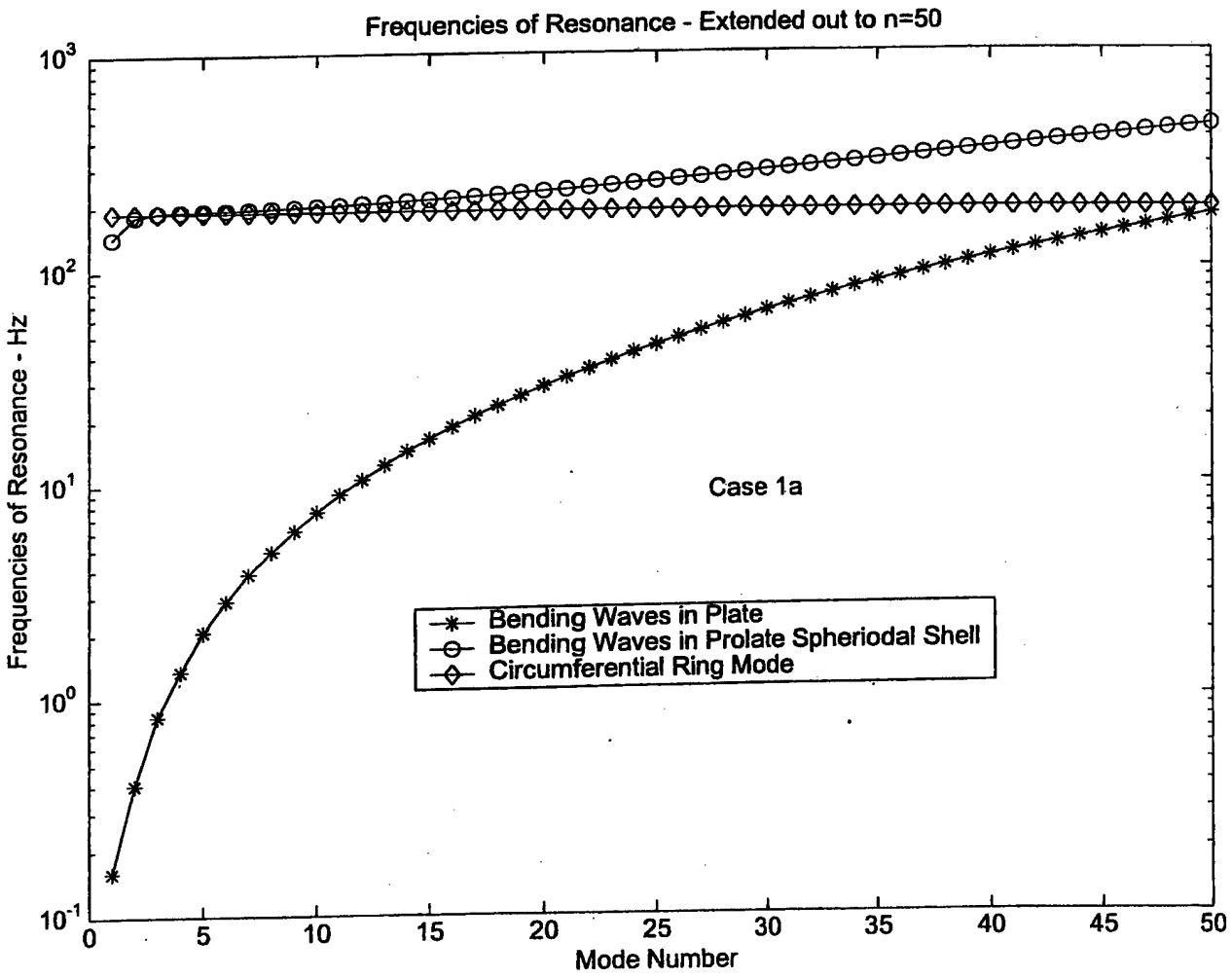

Figure 6. Extrapolation of Frequencies of Resonance for Case 1a Shell and Plate to Mode Number, n=50.

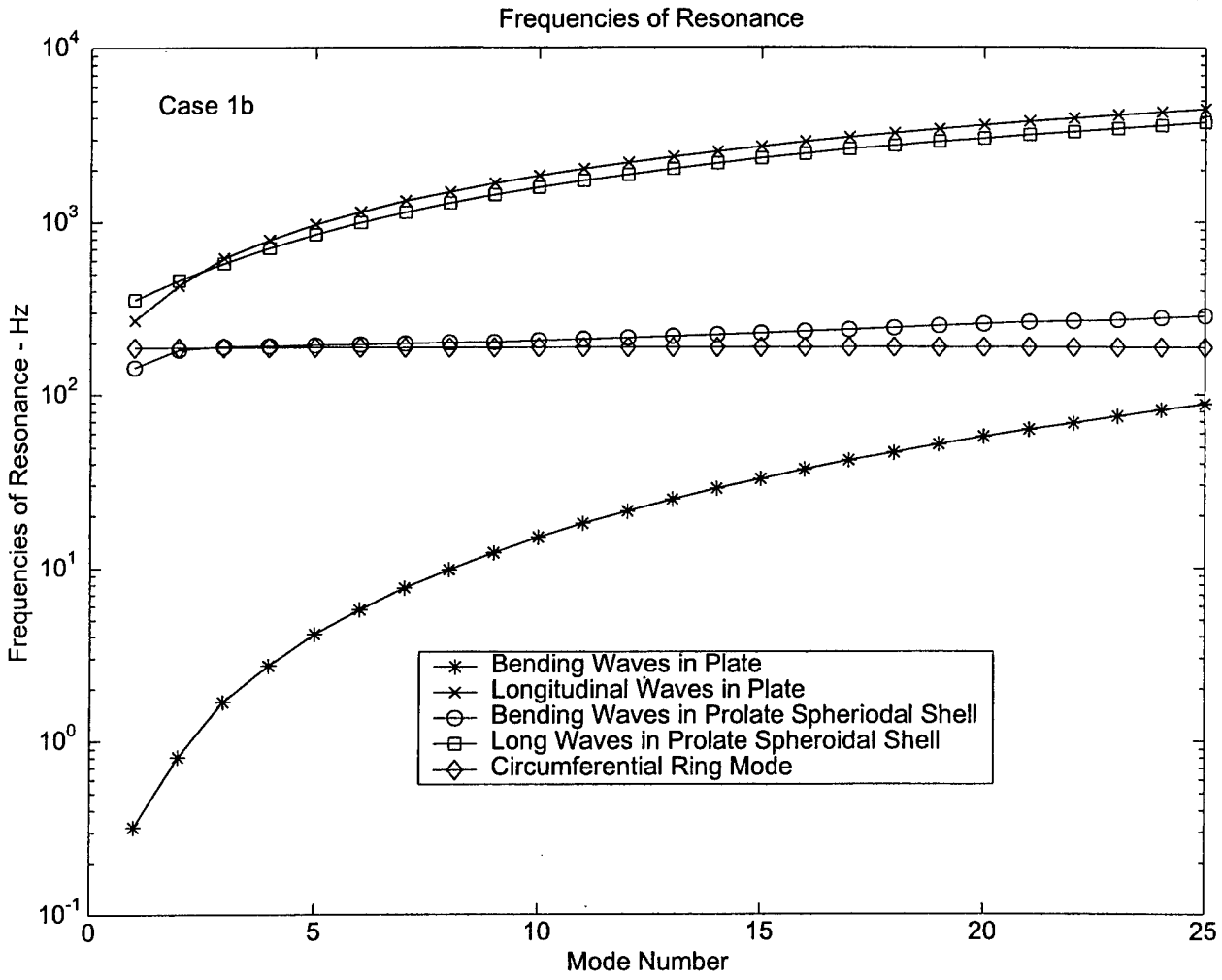

Figure 7. Frequency of Resonance for Case 1b Prolate Spheroidal Shell and And Corresponding Unwrapped Plate.

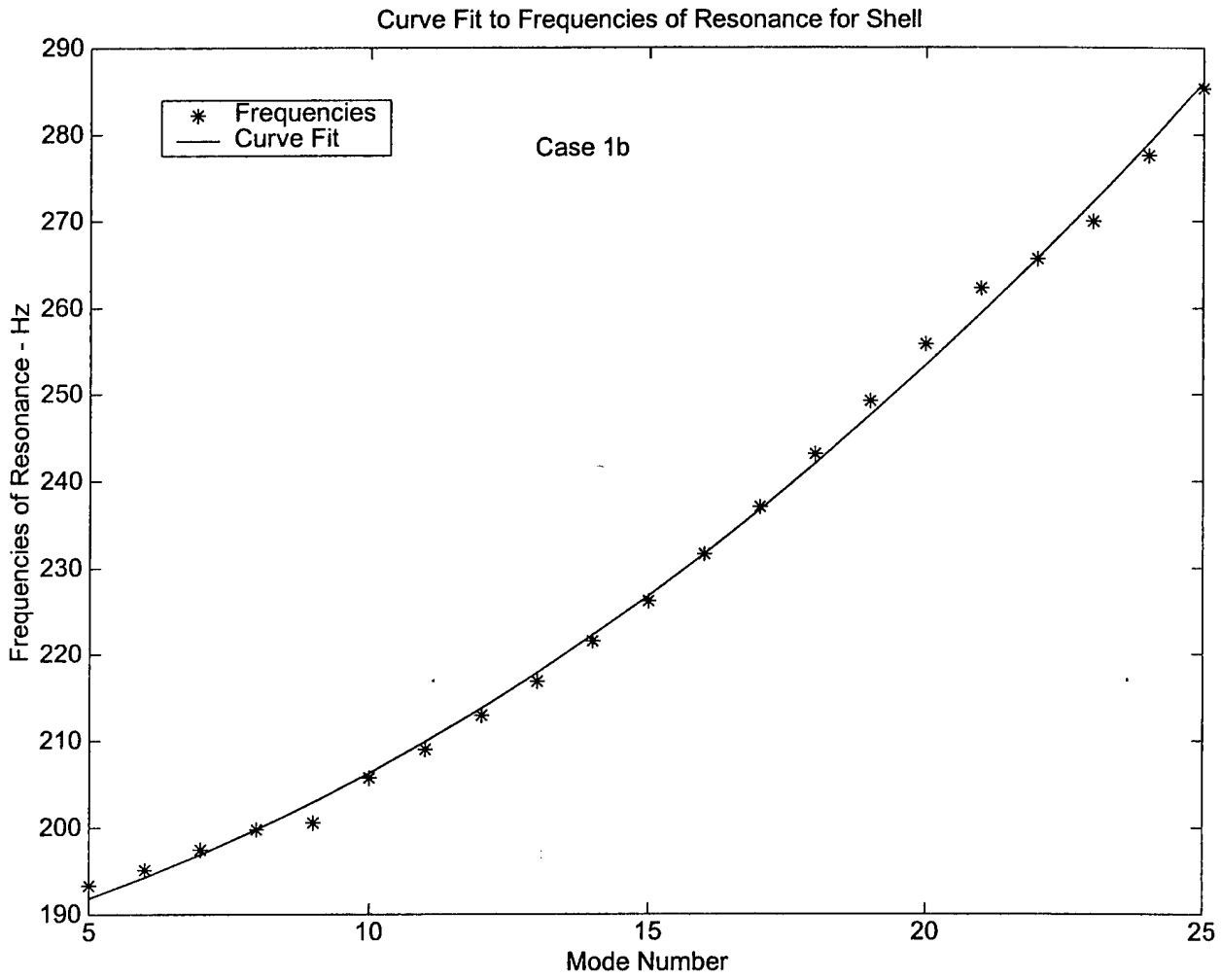

Figure 8. Quadratic Curve Fit to Bending Wave Frequencies of Resonance for Case 1b Prolate Spheroidal Shell

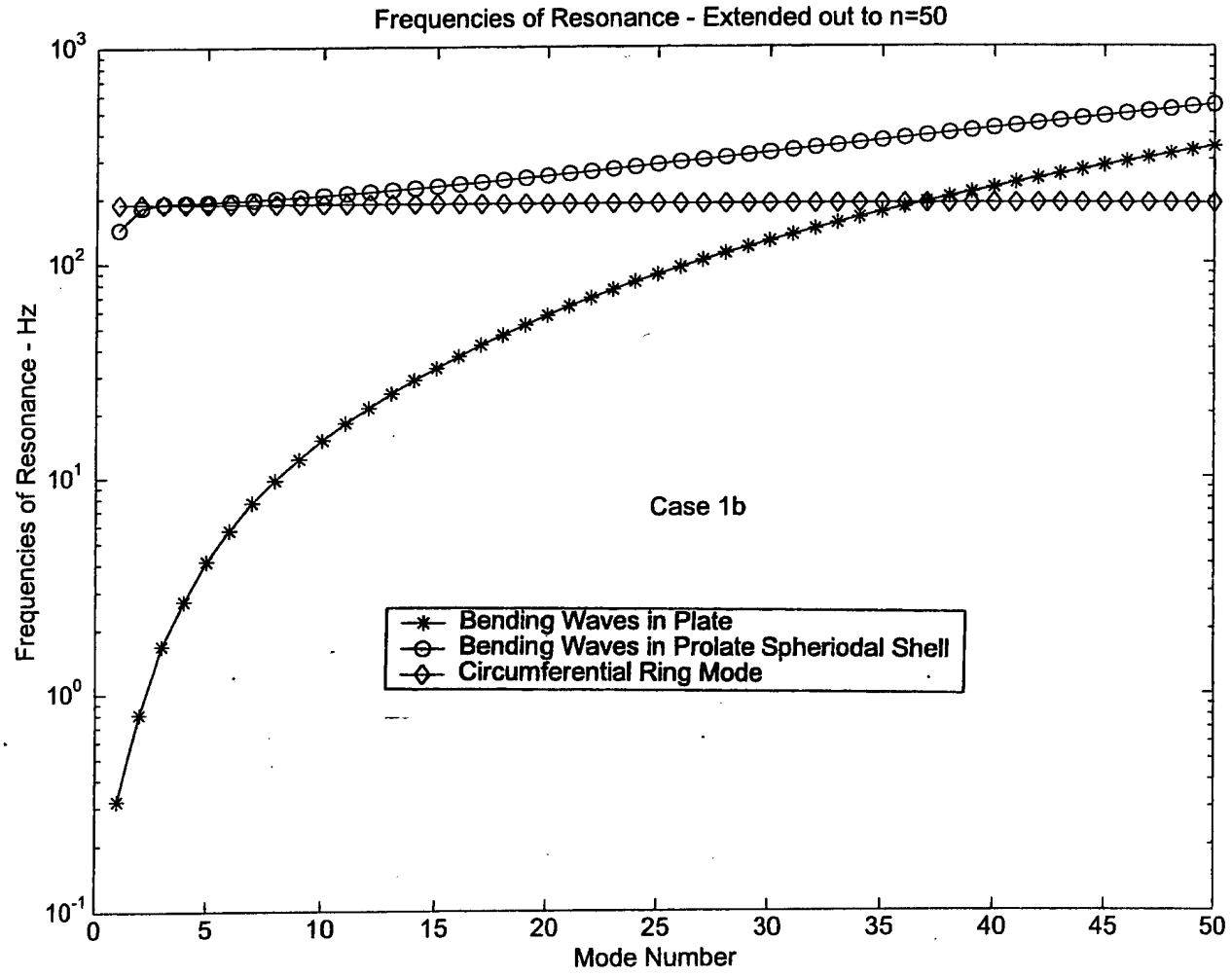

Figure 9. Extrapolation of Frequencies of Resonance for Case 1b Shell and Plate to Mode Number, n=50.

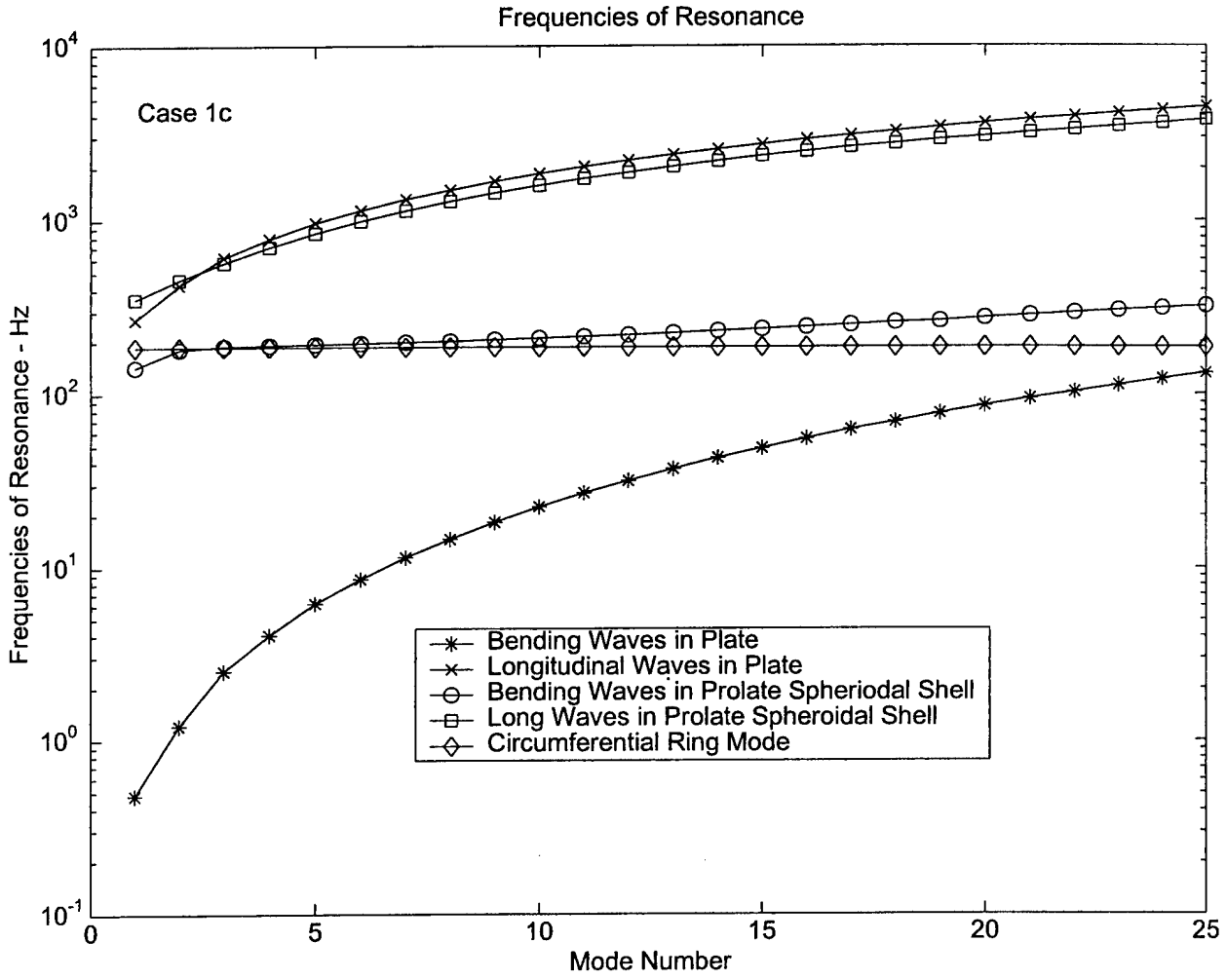

Figure 10. Frequency of Resonance for Case 1c Prolate Spheroidal Shell and And Corresponding Unwrapped Plate.

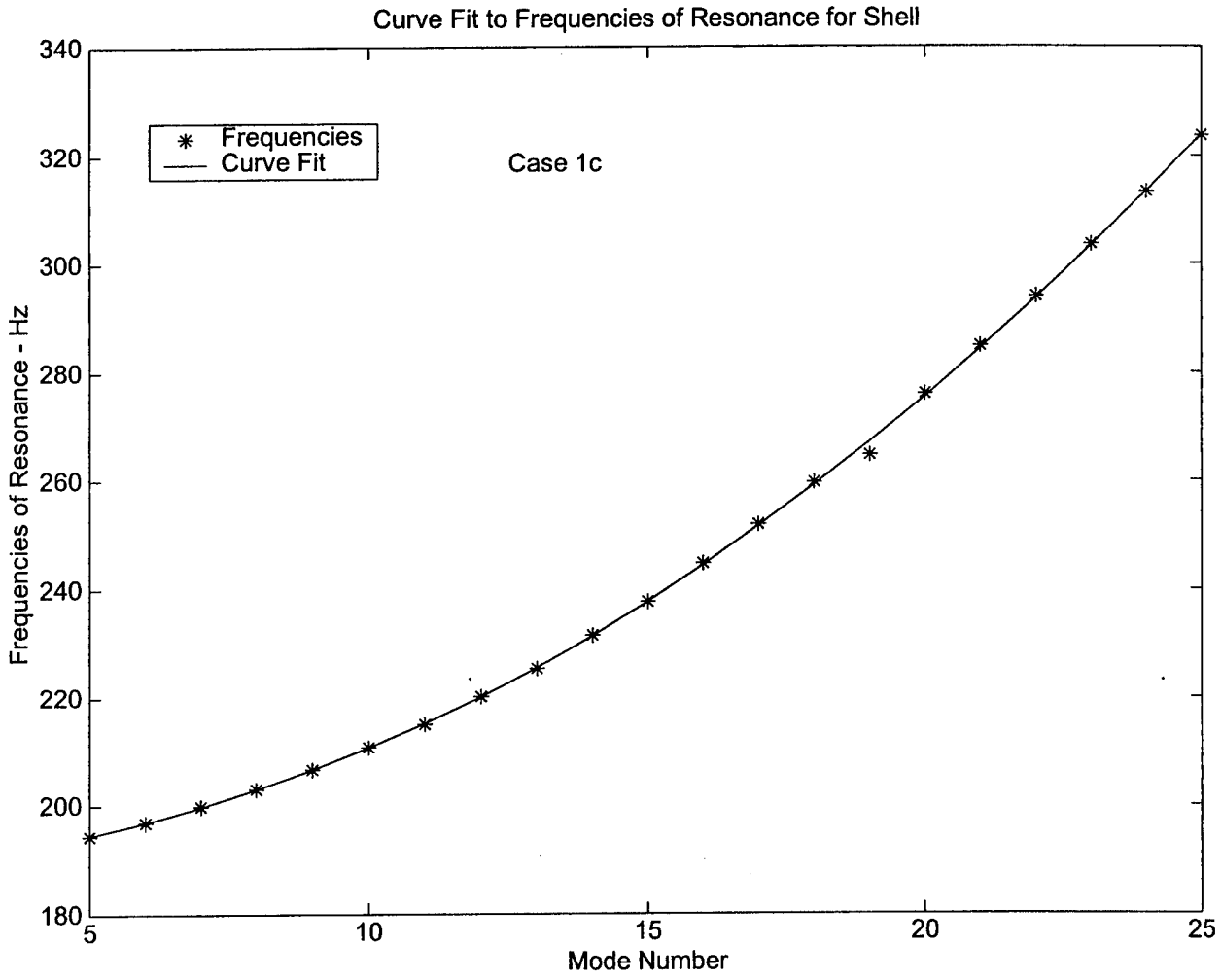

Figure 11. Quadratic Curve Fit to Bending Wave Frequencies of Resonance for Case 1c Prolate Spheroidal Shell

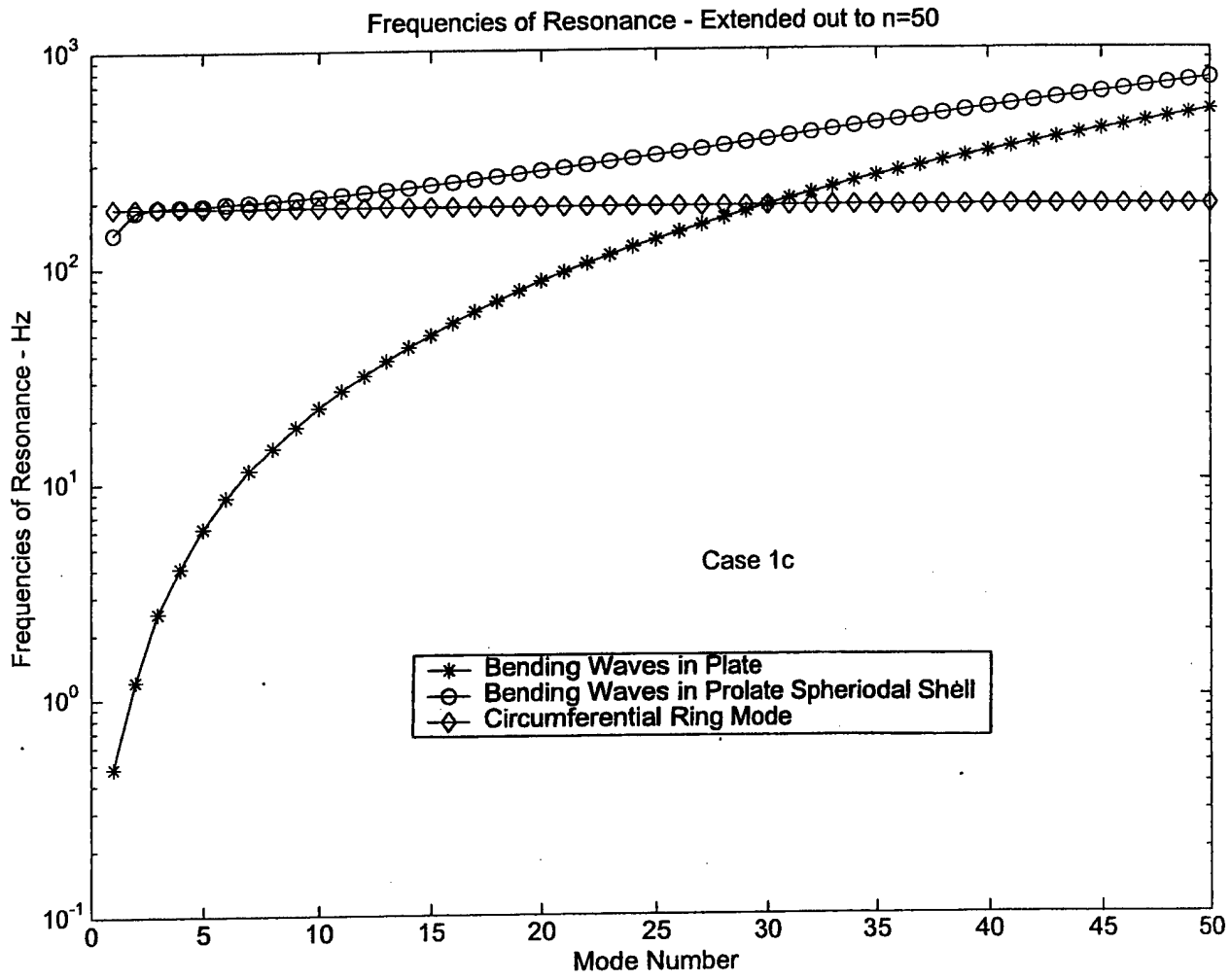

Figure 12. Extrapolation of Frequencies of Resonance for Case 1c Shell and Plate to Mode Number, n=50.

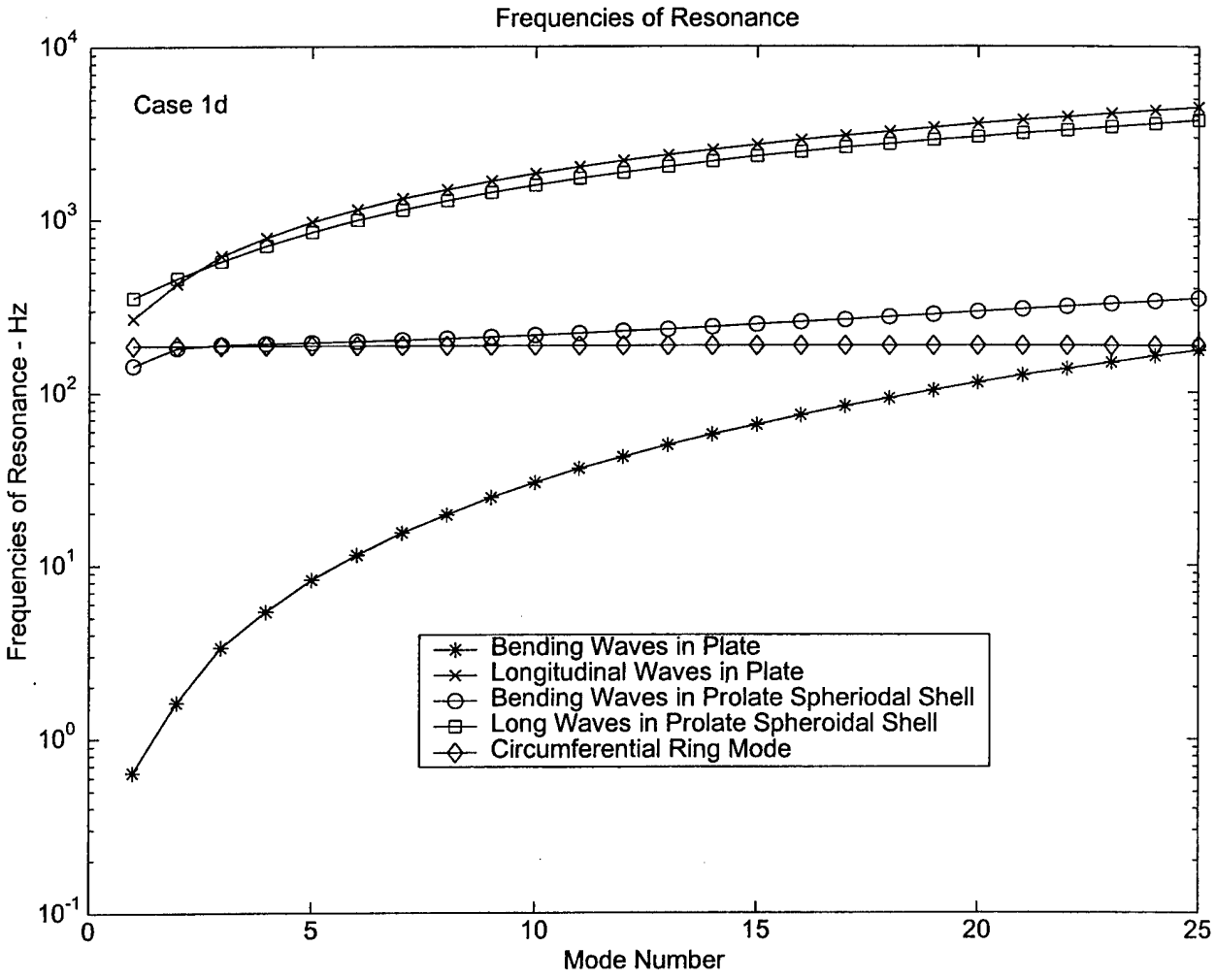

Figure 13. Frequency of Resonance for Case 1d Prolate Spheroidal Shell and And Corresponding Unwrapped Plate.

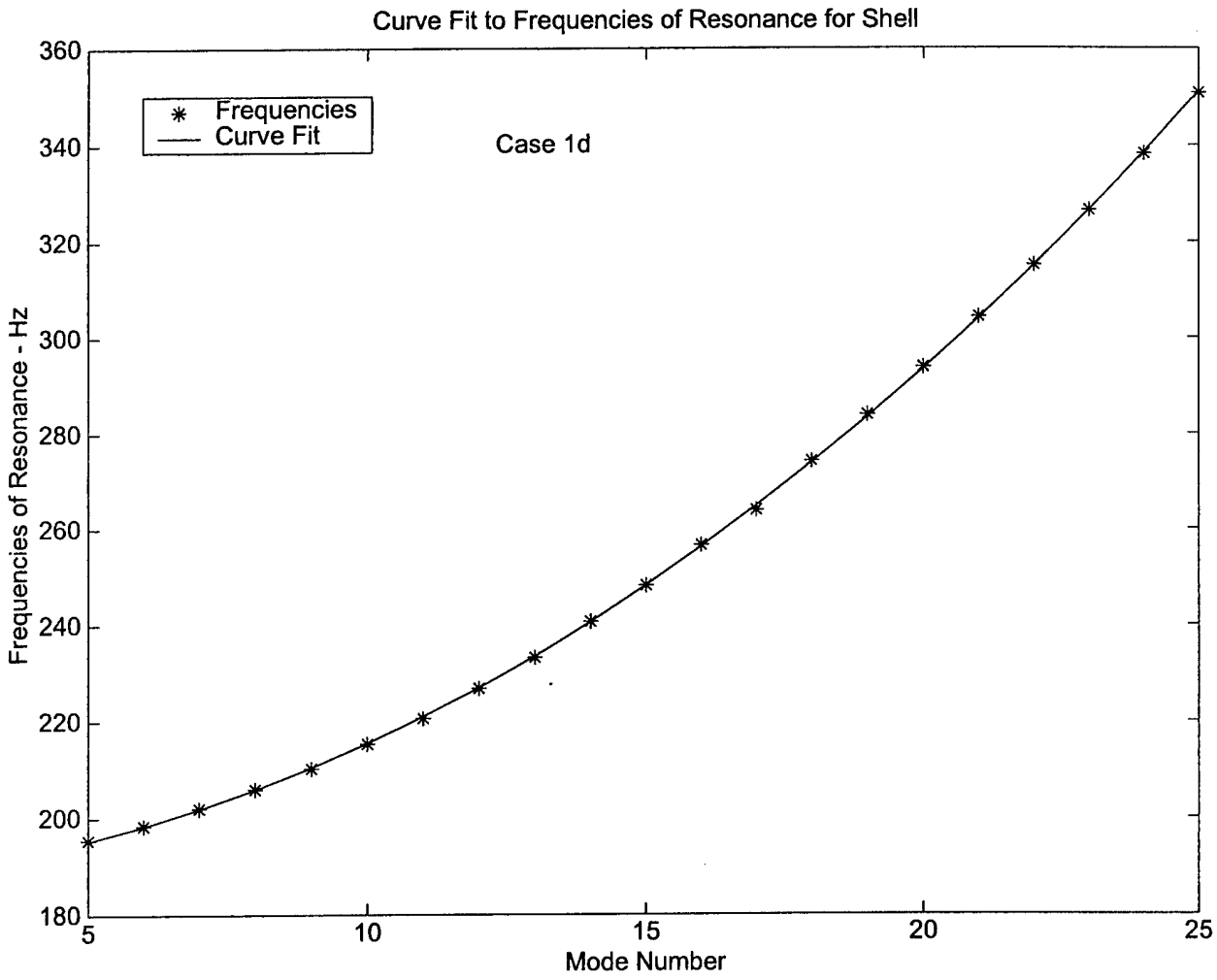

Figure 14. Quadratic Curve Fit to Bending Wave Frequencies of Resonance for Case 1d Prolate Spheroidal Shell

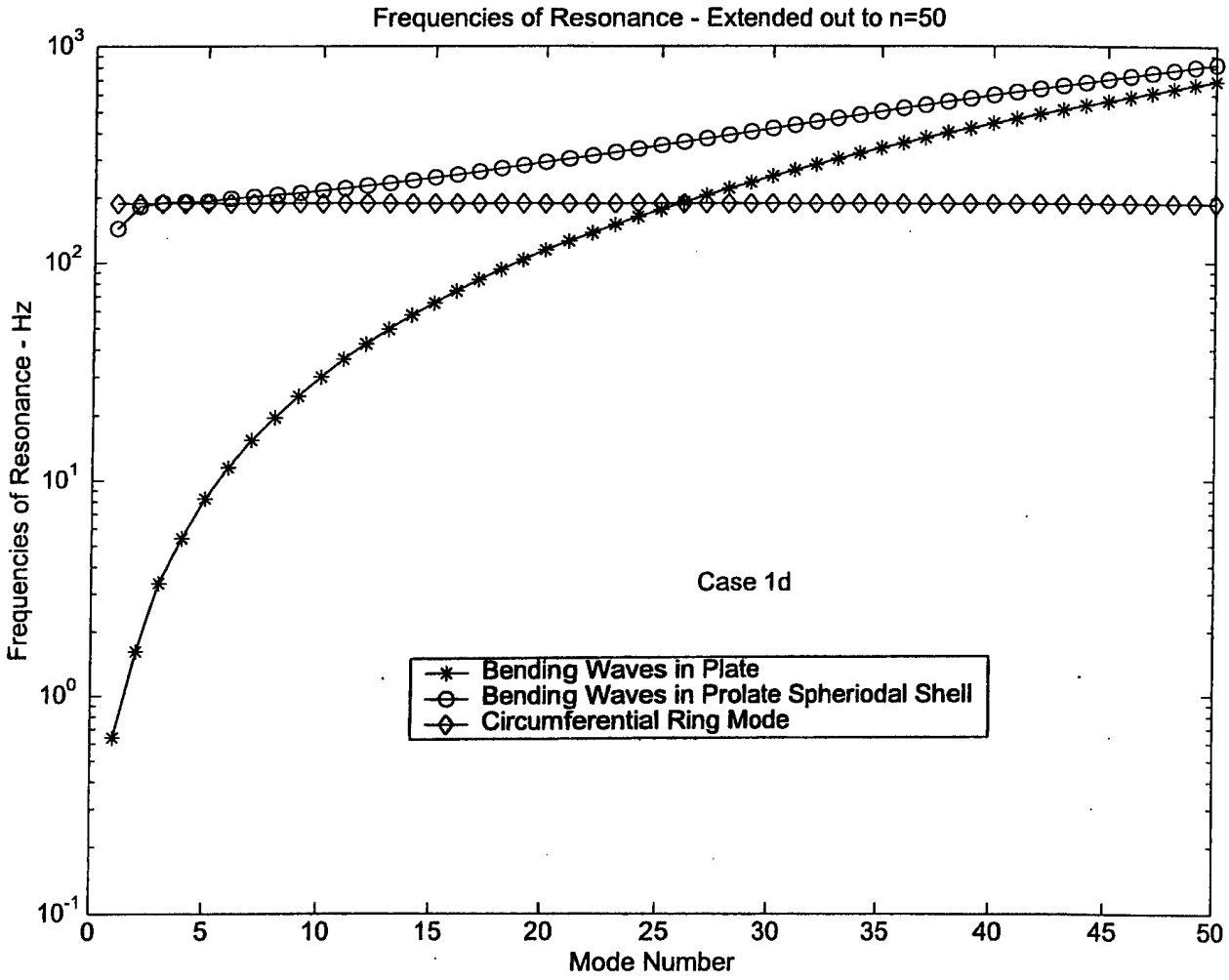

Figure 15. Extrapolation of Frequencies of Resonance for Case 1d Shell and Plate to Mode Number, n=50.

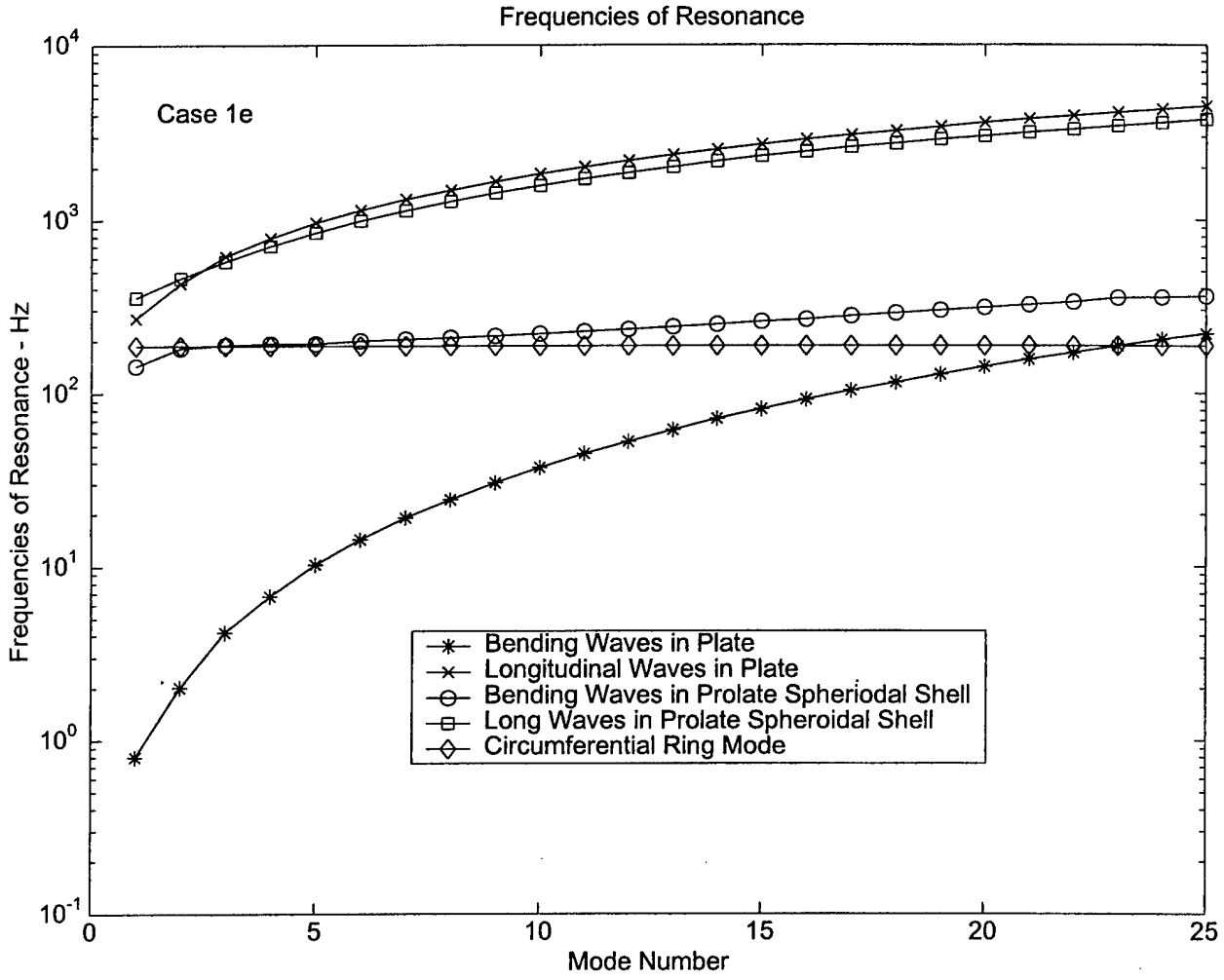

Figure 16. Frequency of Resonance for Case 1e Prolate Spheroidal Shell and And Corresponding Unwrapped Plate.

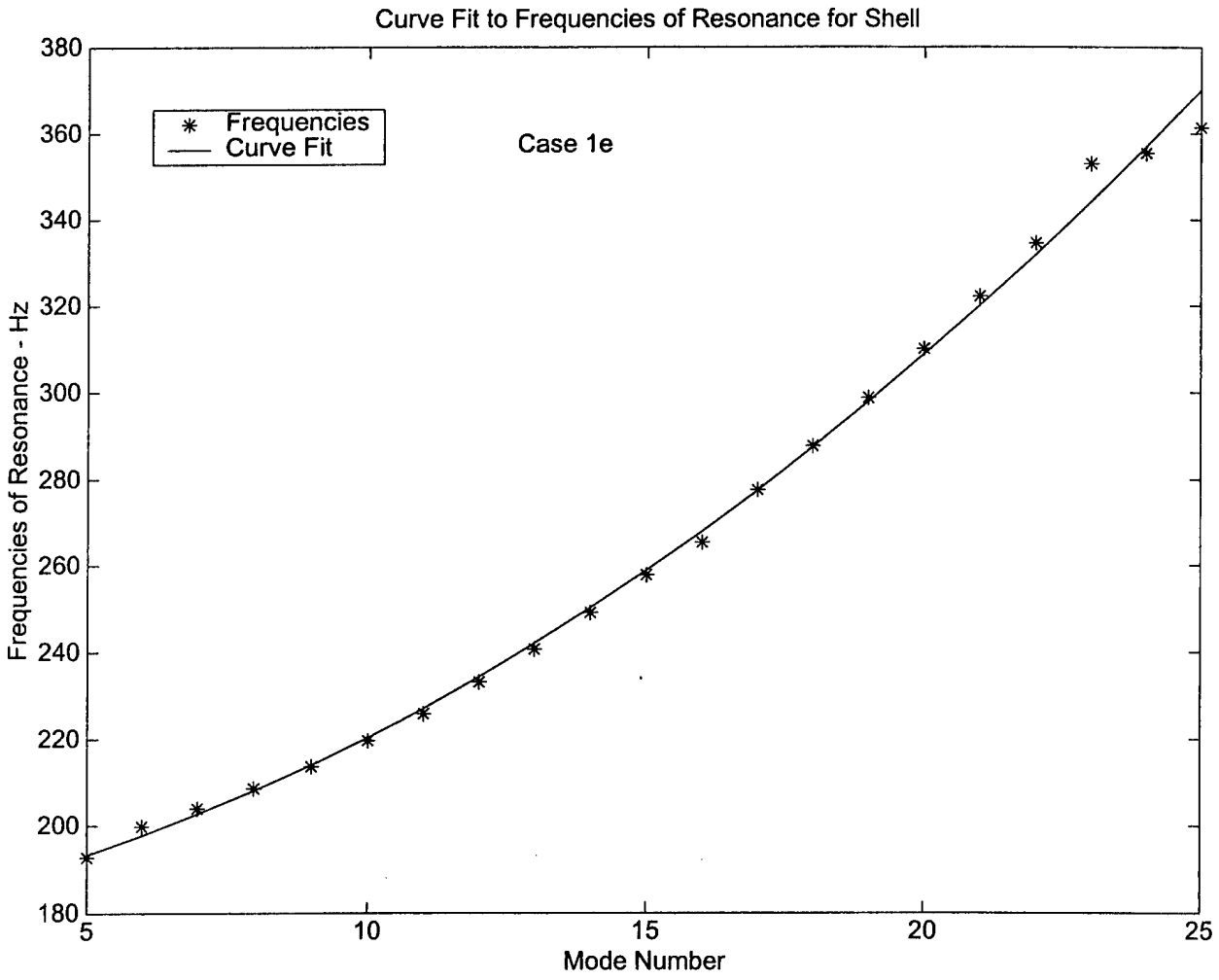

Figure 17. Quadratic Curve Fit to Bending Wave Frequencies of Resonance for Case 1e Prolate Spheroidal Shell

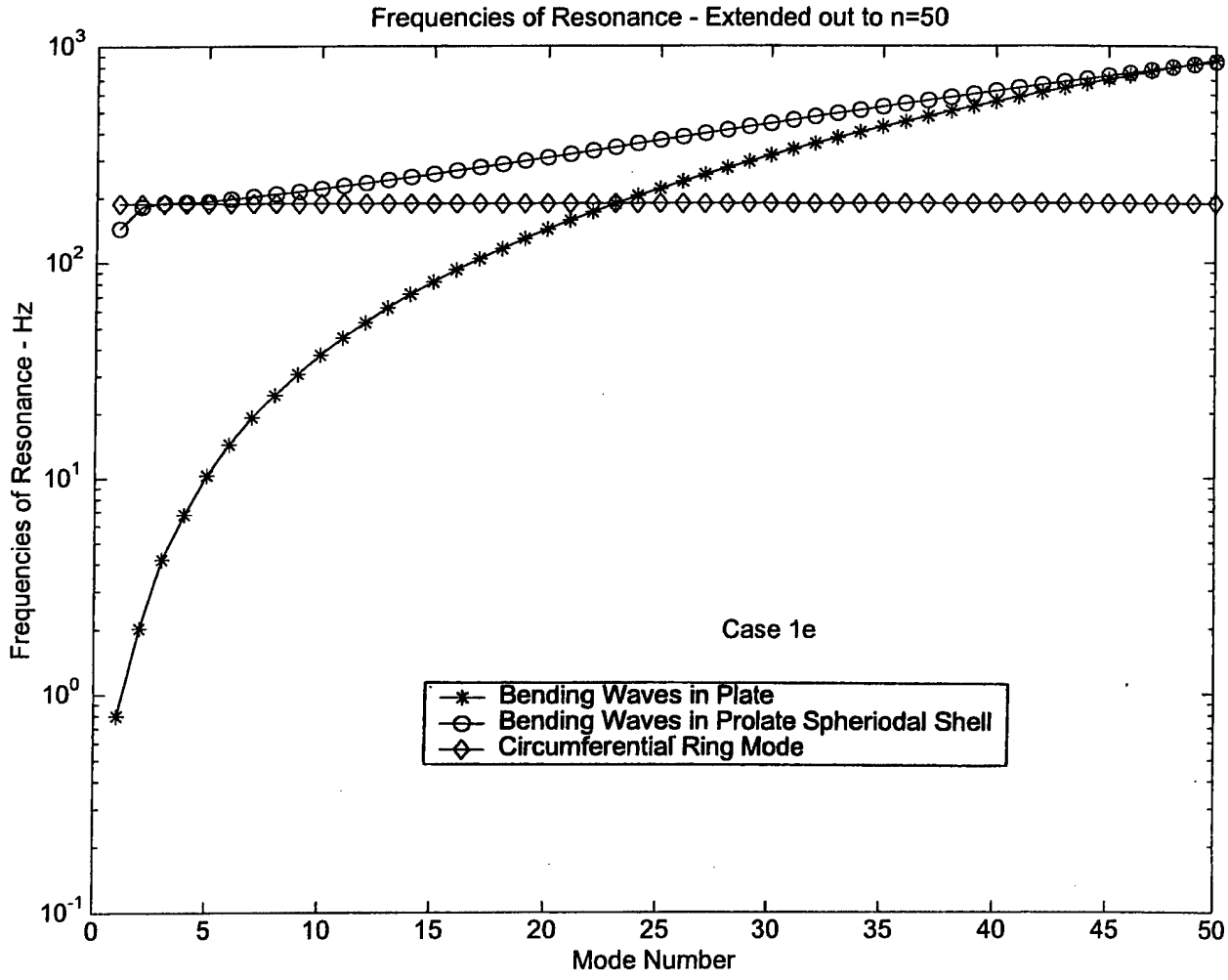

Figure 18. Extrapolation of Frequencies of Resonance for Case 1e Shell and Plate to Mode Number, n=50.

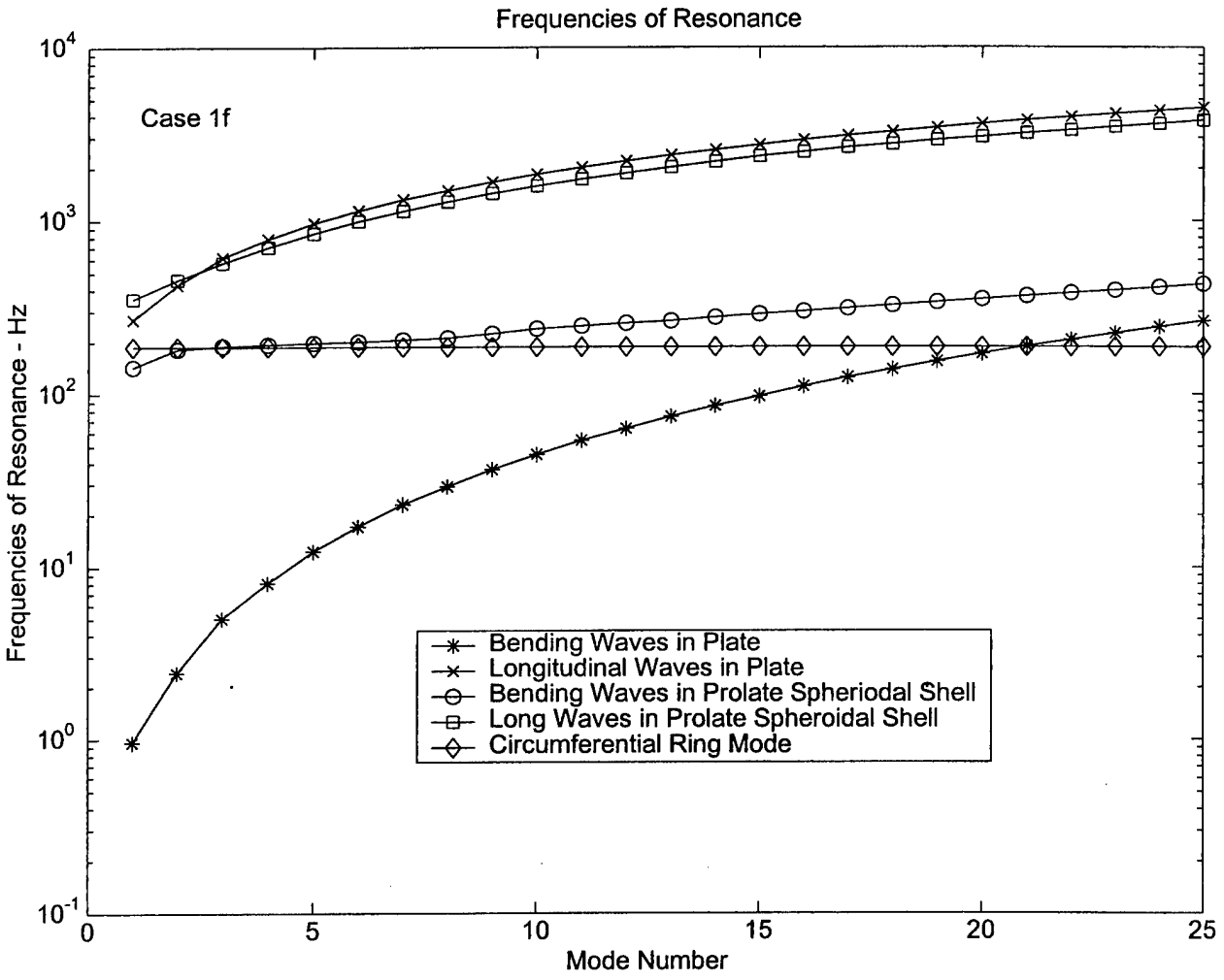

Figure 19. Frequency of Resonance for Case 1f Prolate Spheroidal Shell and And Corresponding Unwrapped Plate.

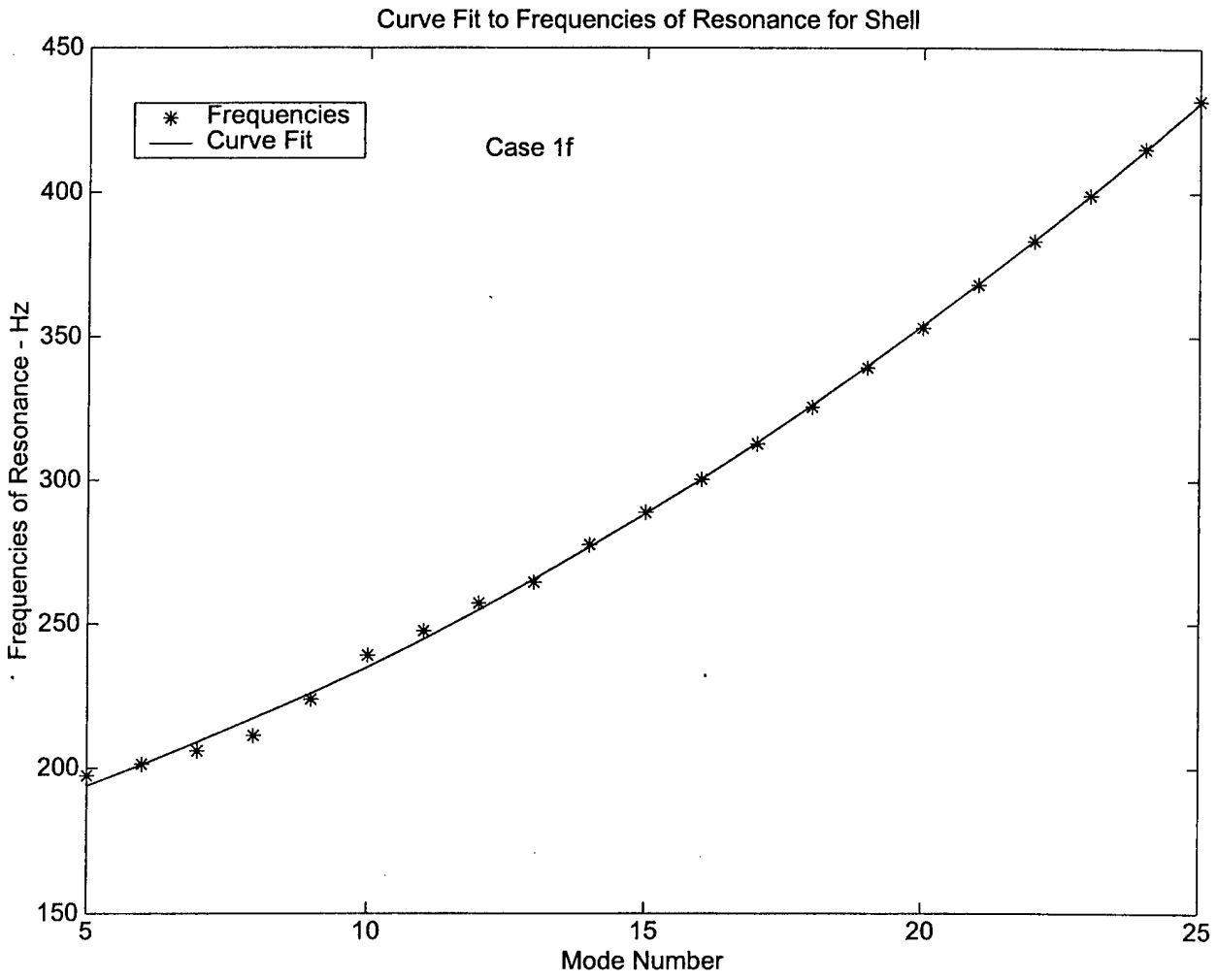

Figure 20. Quadratic Curve Fit to Bending Wave Frequencies of Resonance for Case 1f Prolate Spheroidal Shell

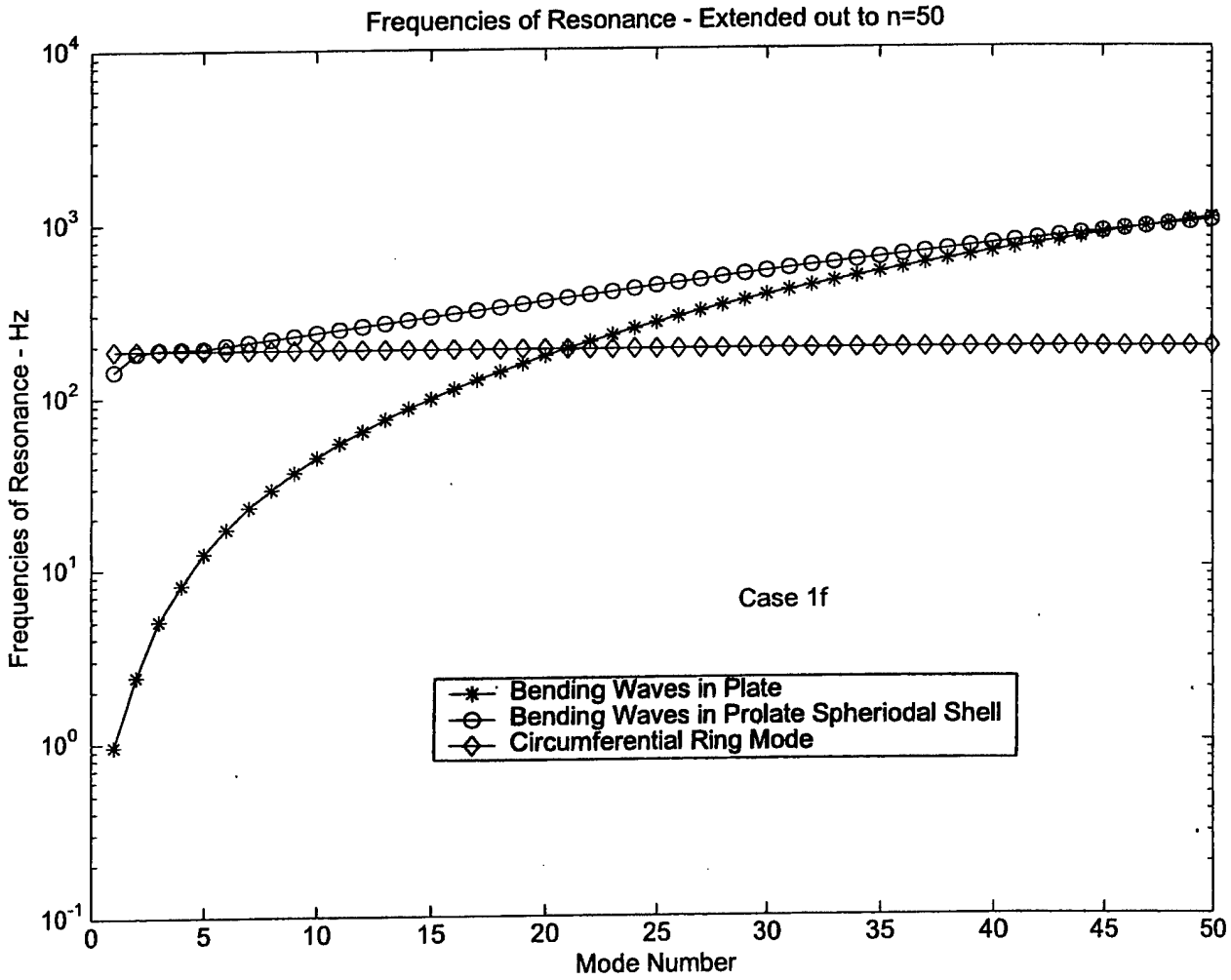

Figure 21. Extrapolation of Frequencies of Resonance for Case 1f Shell and Plate to Mode Number, n=50

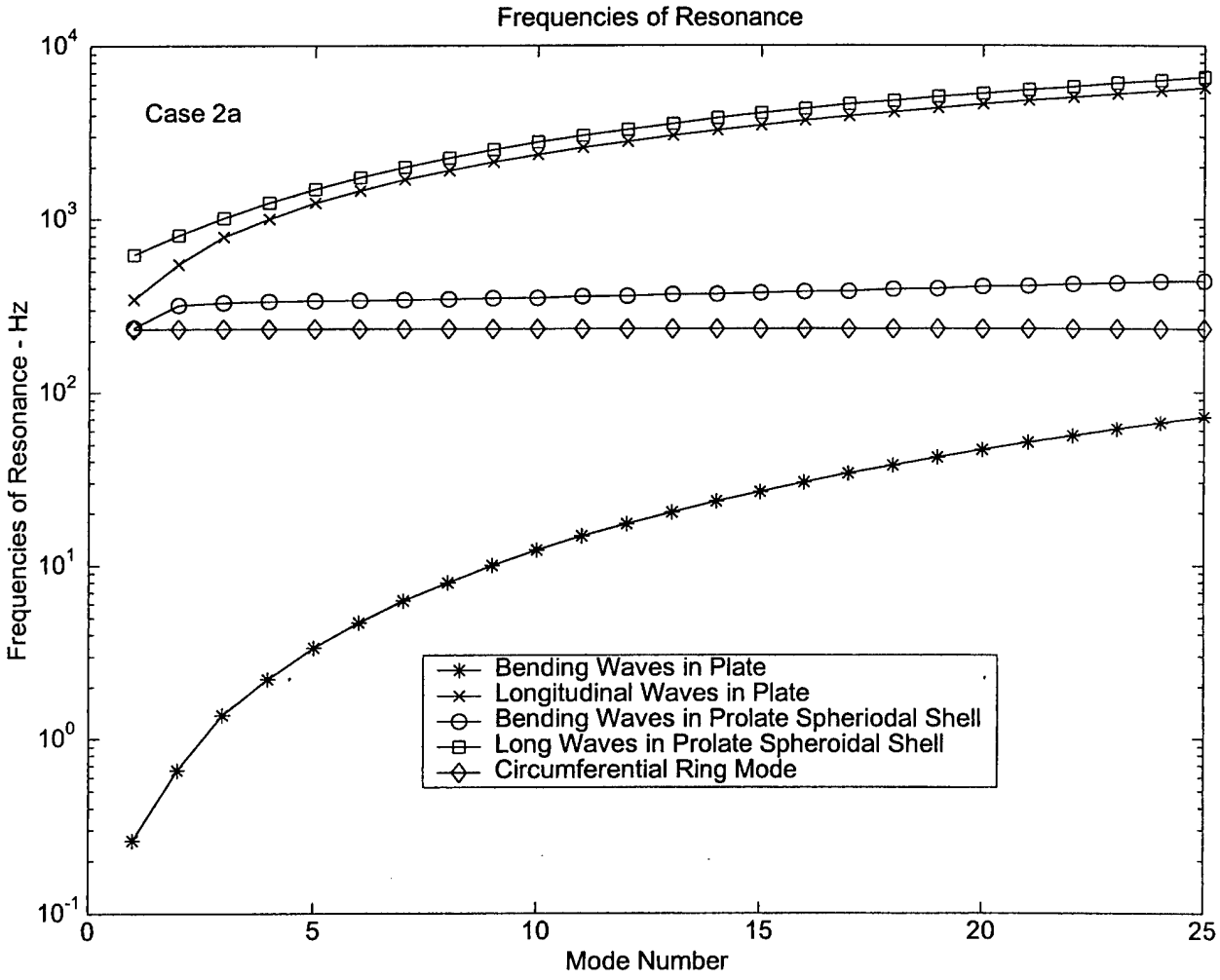

Figure 22. Frequency of Resonance for Case 2a Prolate Spheroidal Shell and And Corresponding Unwrapped Plate.

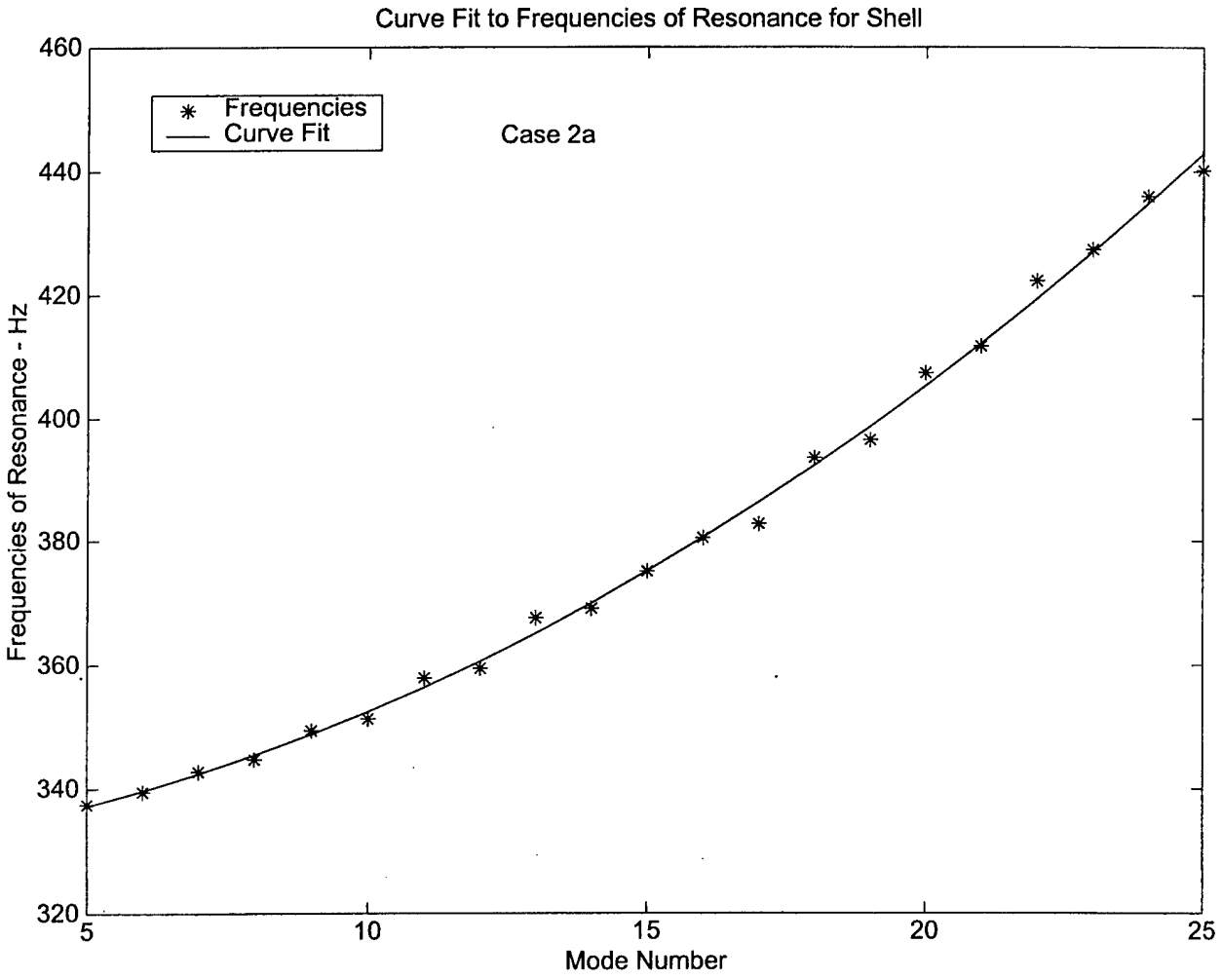

Figure 23. Quadratic Curve Fit to Bending Wave Frequencies of Resonance for Case 2a Prolate Spheroidal Shell

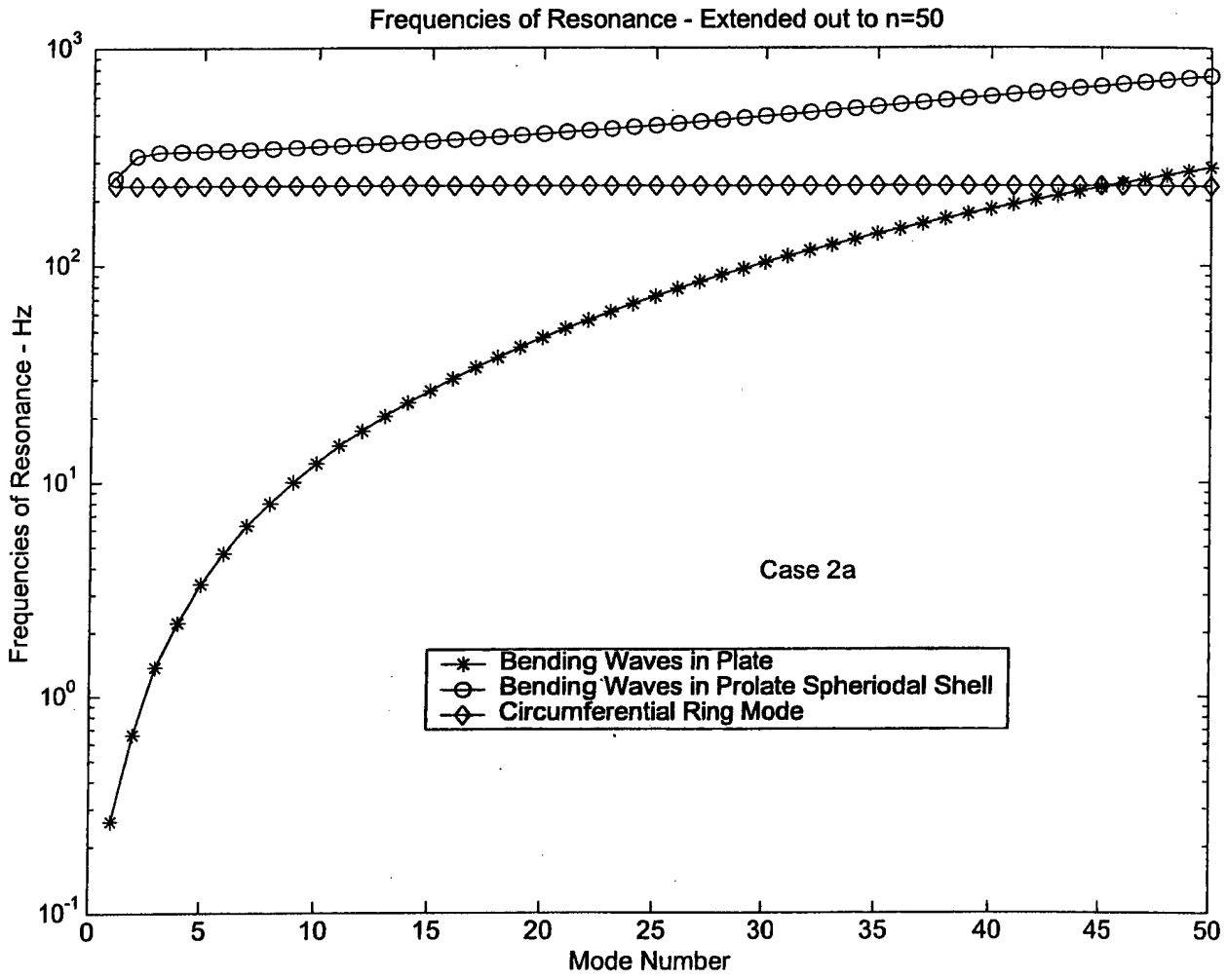

Figure 24. Extrapolation of Frequencies of Resonance for Case 2a Shell and Plate to Mode Number, n=50

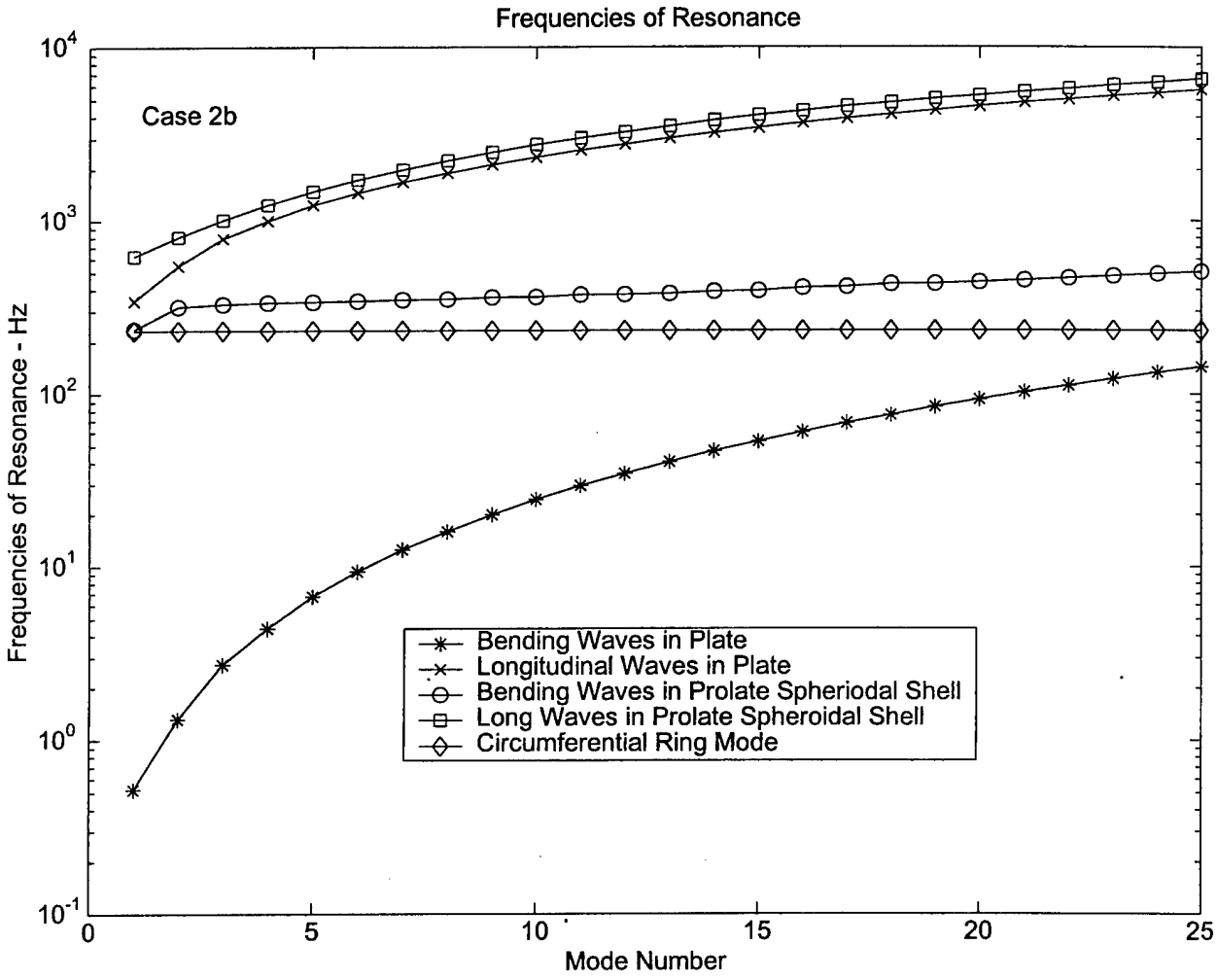

Figure 25. Frequency of Resonance for Case 2b Prolate Spheroidal Shell and And Corresponding Unwrapped Plate.

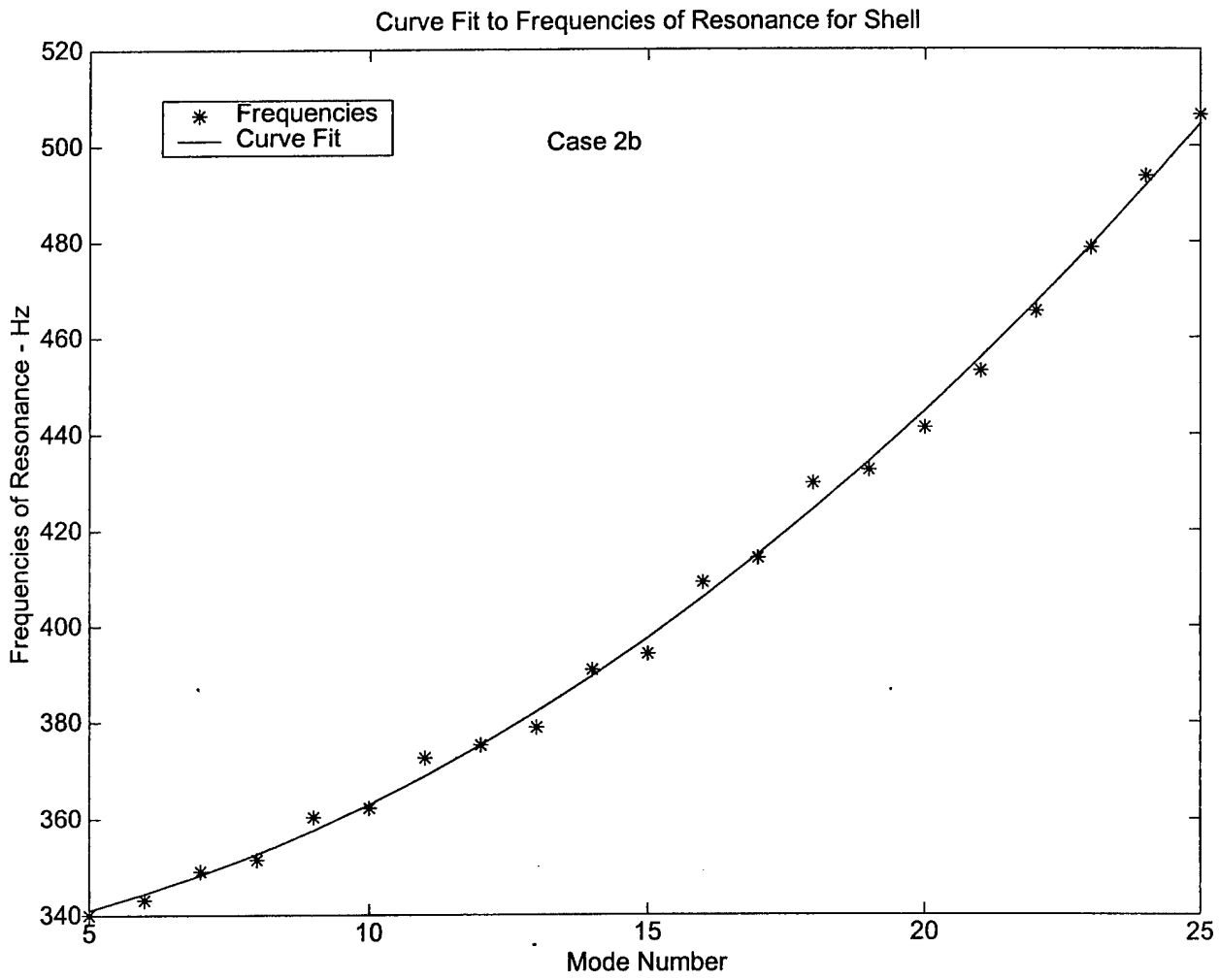

Figure 26. Quadratic Curve Fit to Bending Wave Frequencies of Resonance for Case 2b Prolate Spheroidal Shell

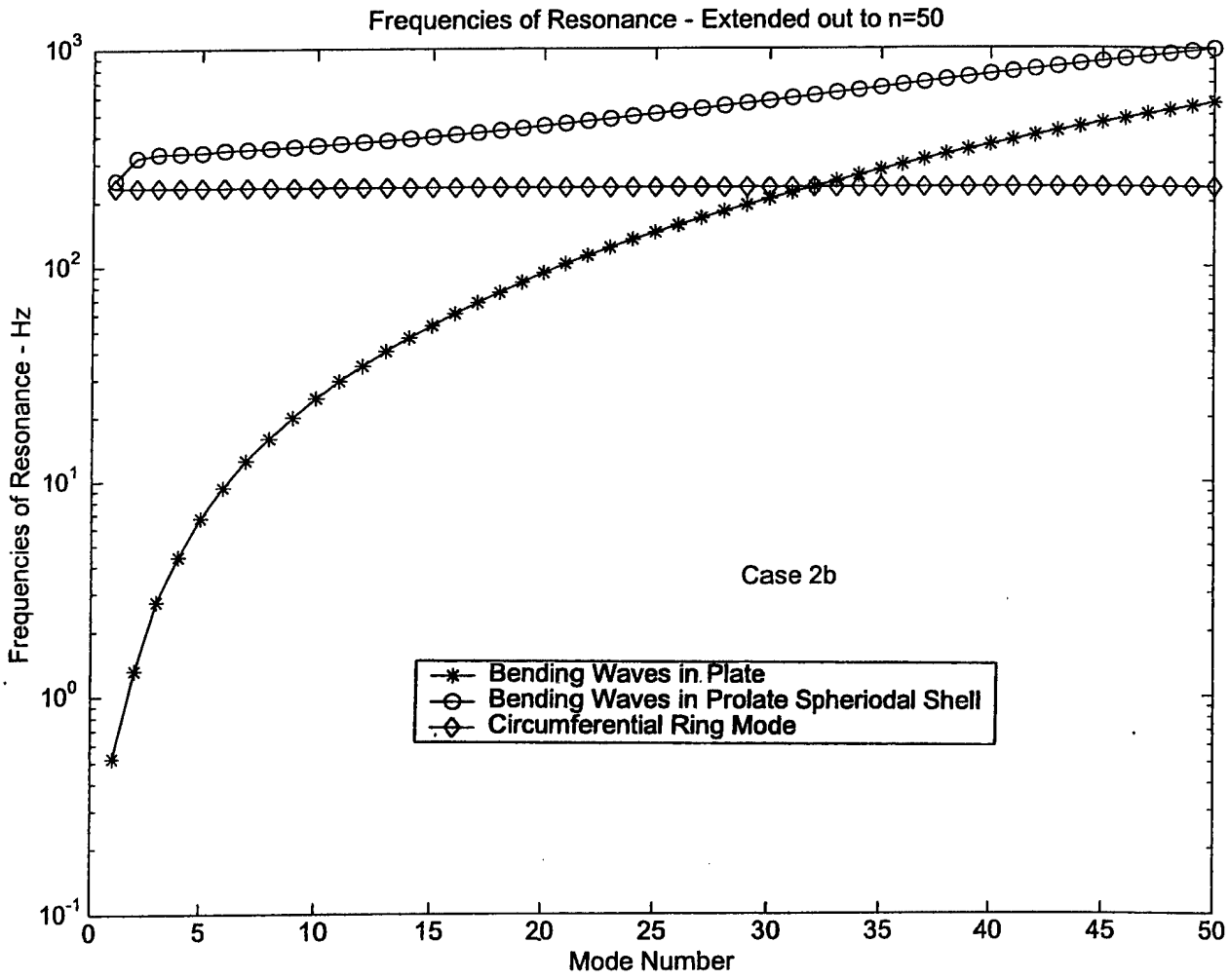

Figure 27. Extrapolation of Frequencies of Resonance for Case 2b Shell and Plate to Mode Number, n=50

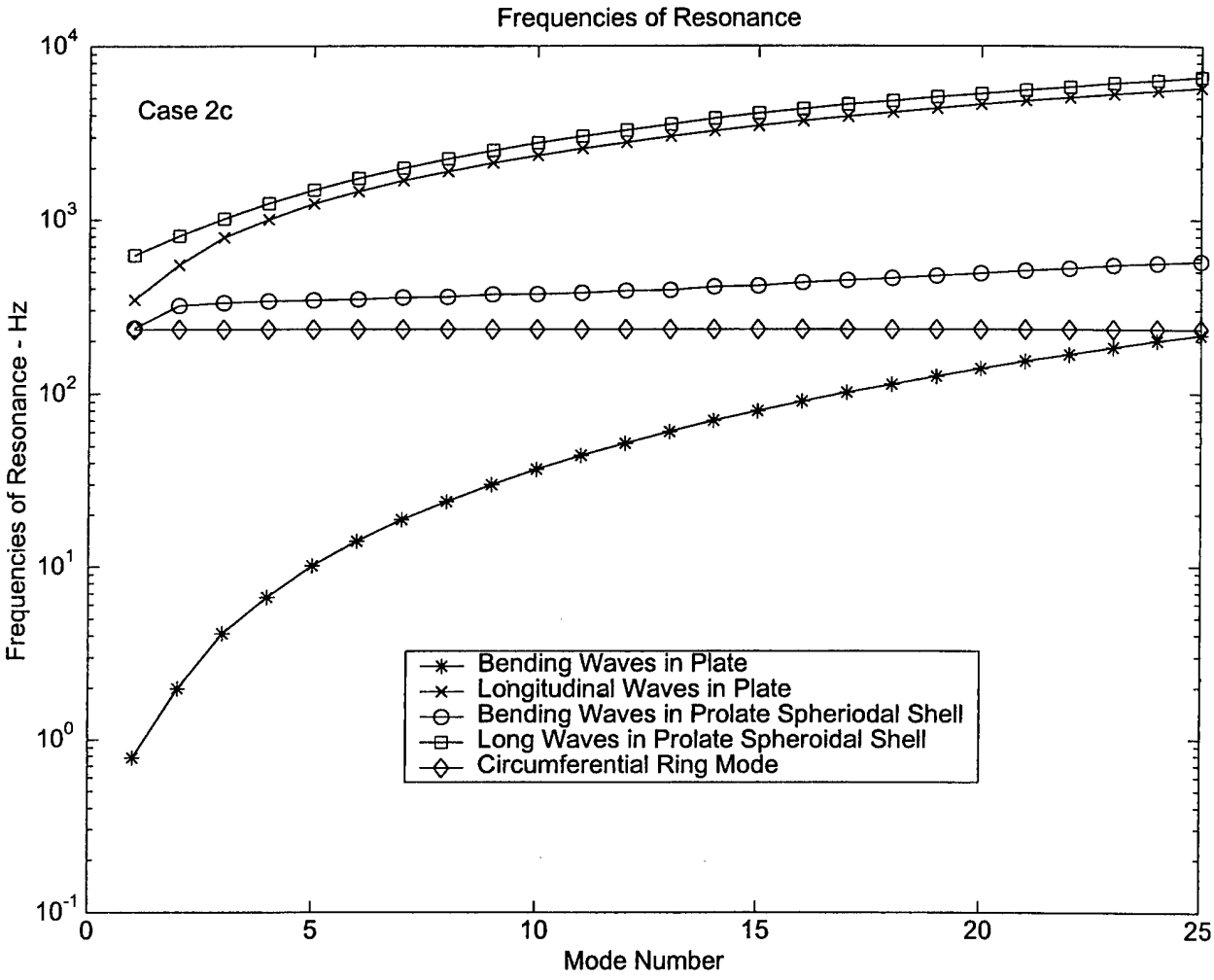

Figure 28. Frequency of Resonance for Case 2c Prolate Spheroidal Shell and And Corresponding Unwrapped Plate.

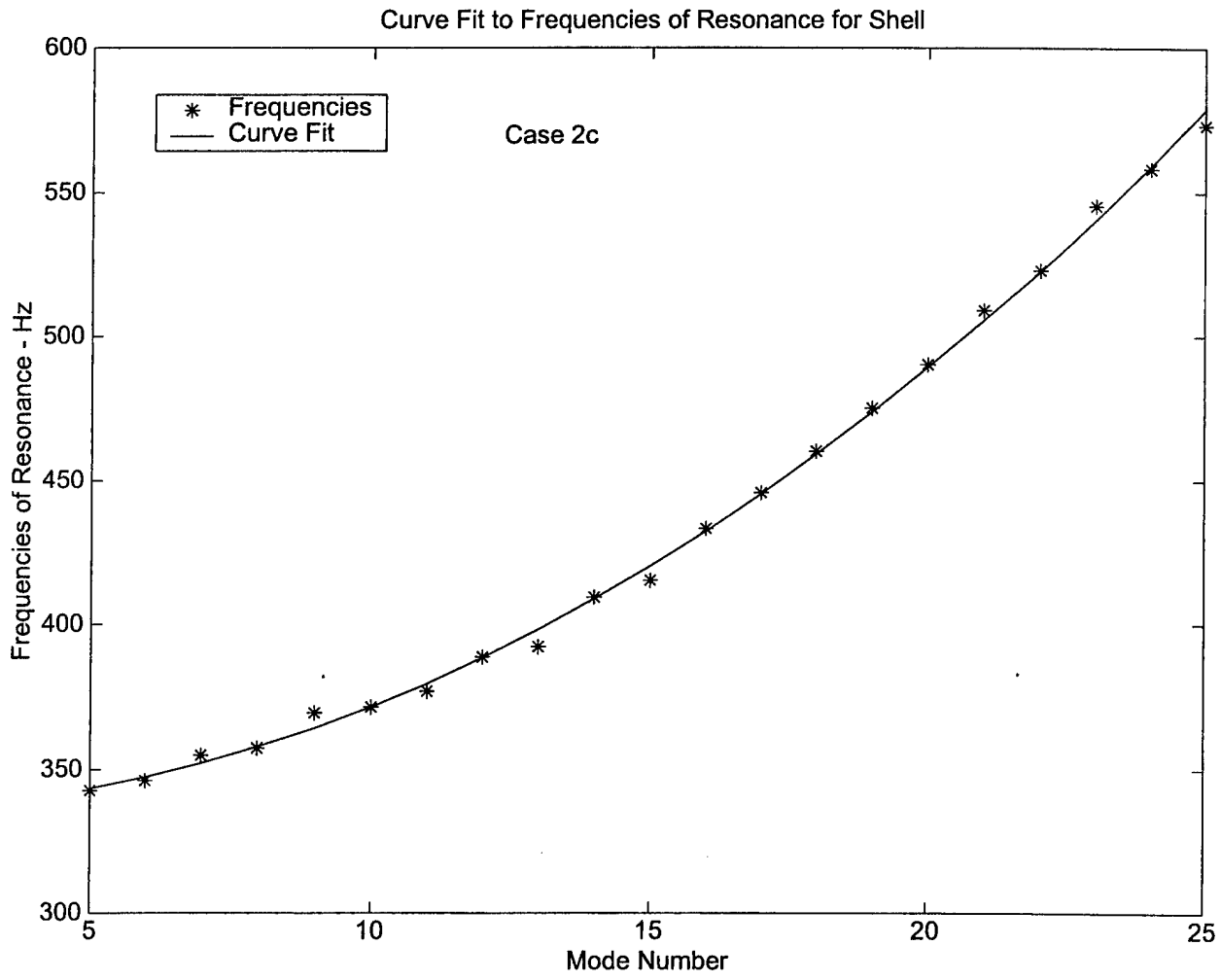

Figure 29. Quadratic Curve Fit to Bending Wave Frequencies of Resonance for Case 2c Prolate Spheroidal Shell

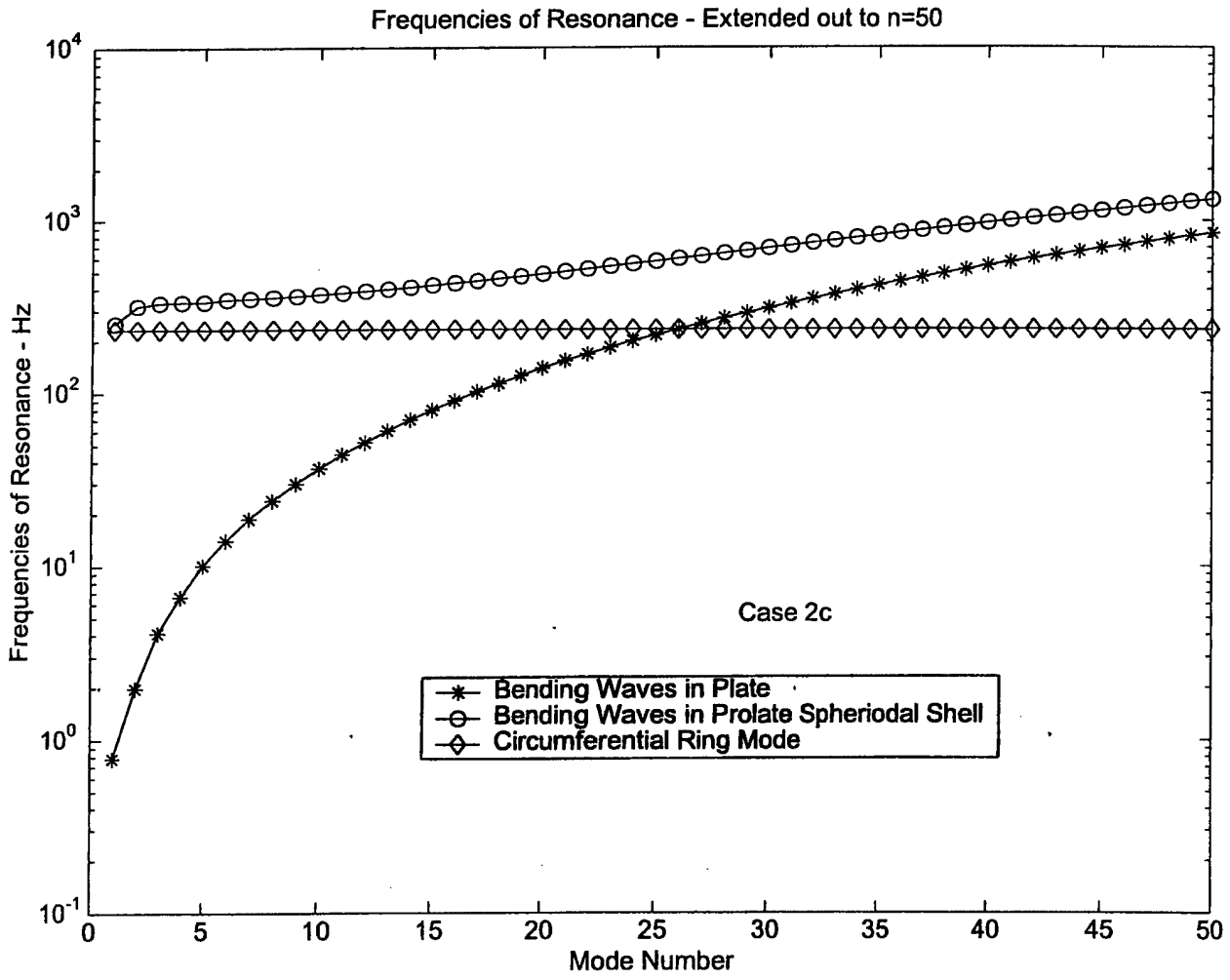

Figure 30. Extrapolation of Frequencies of Resonance for Case 2c Shell and Plate to Mode Number, n=50

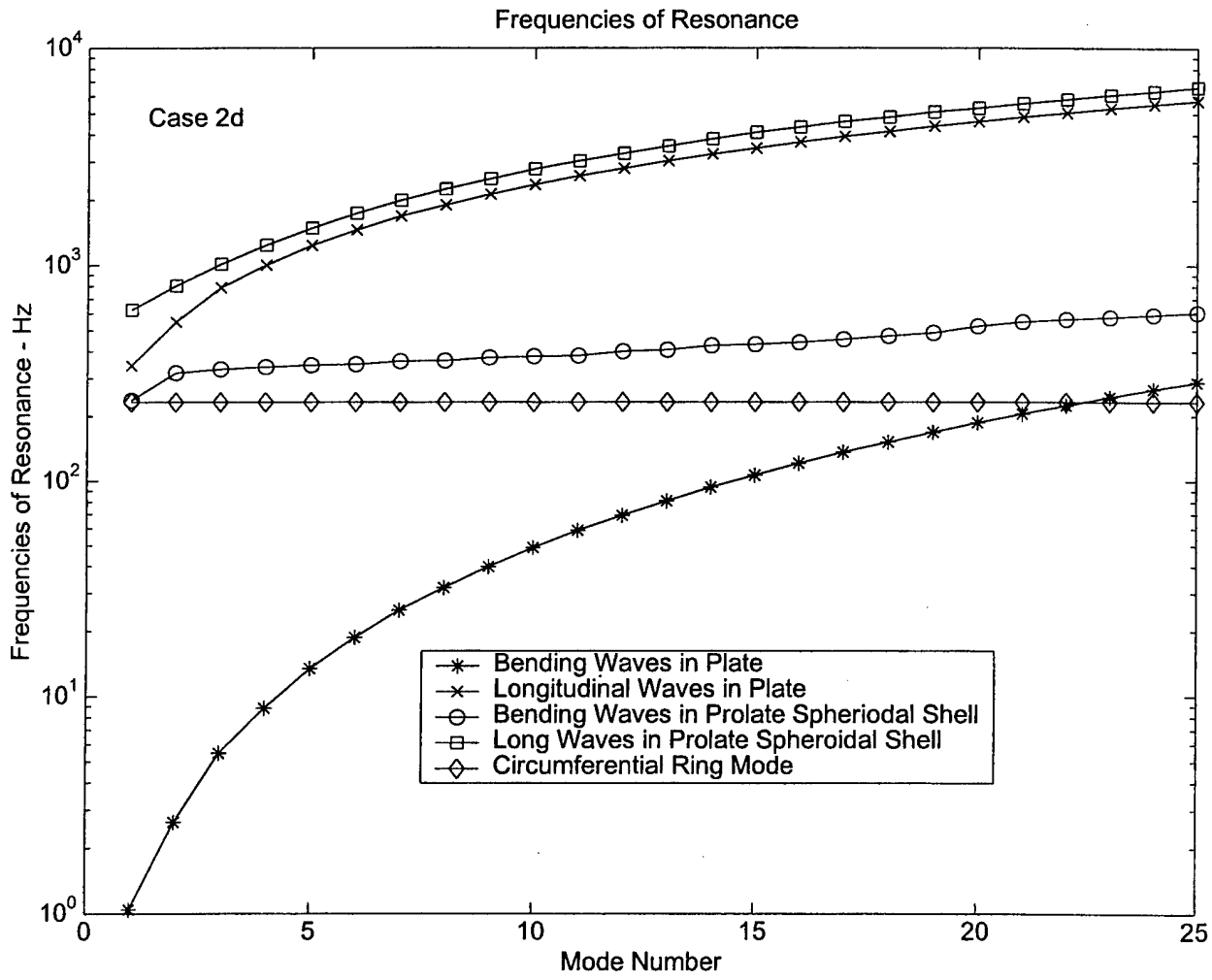

Figure 31. Frequency of Resonance for Case 2d Prolate Spheroidal Shell and And Corresponding Unwrapped Plate.

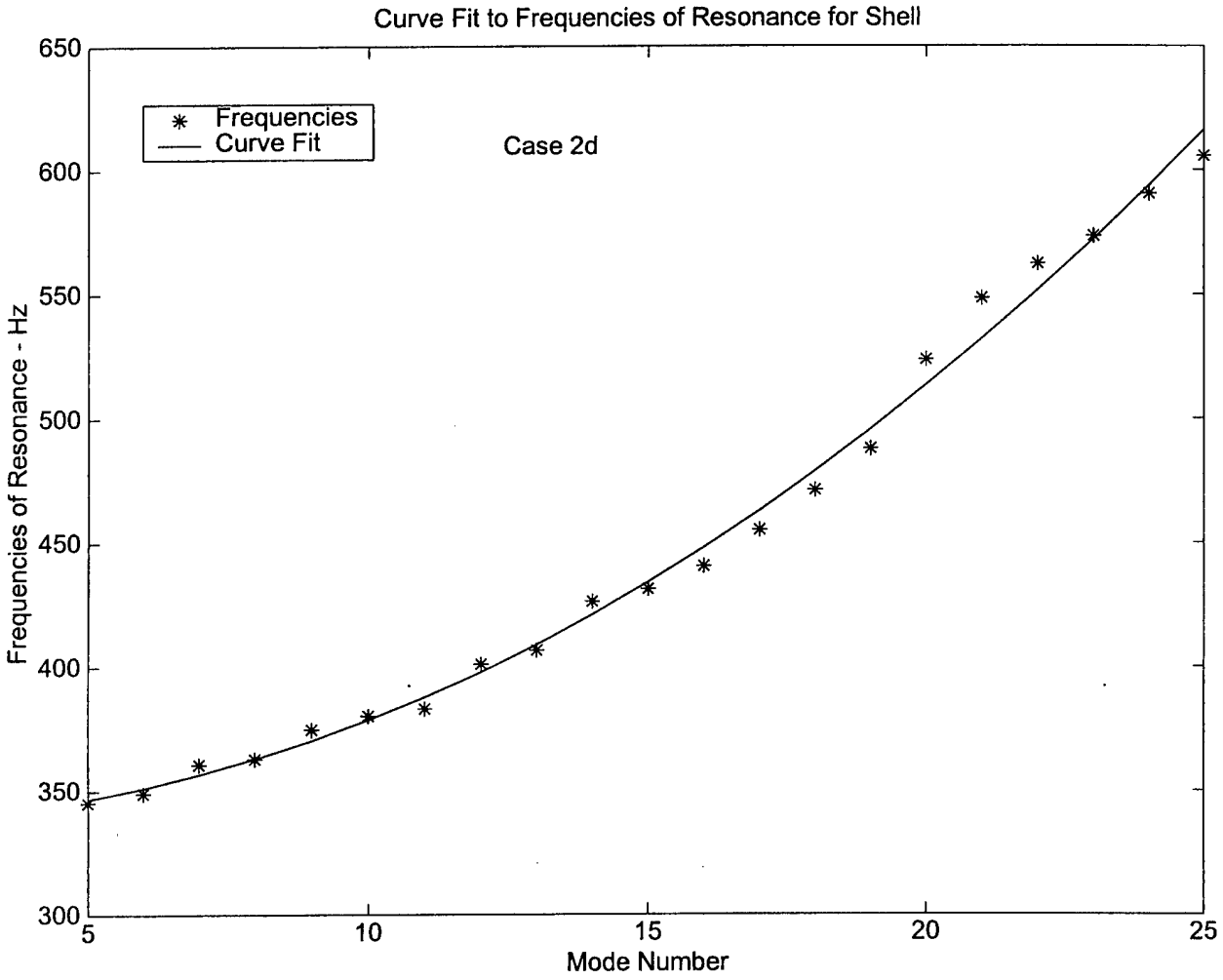

Figure 32. Quadratic Curve Fit to Bending Wave Frequencies of Resonance for Case 2d Prolate Spheroidal Shell

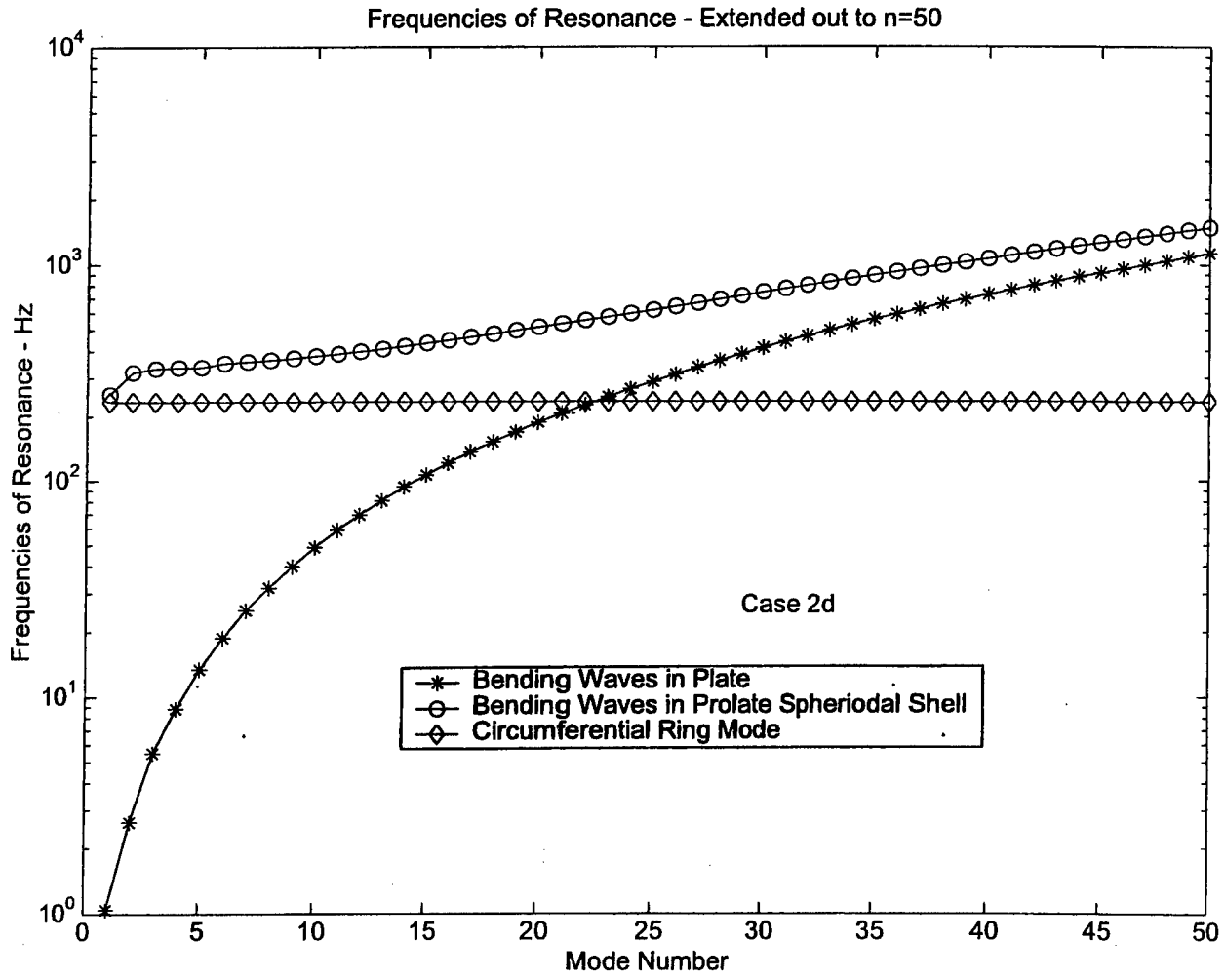

Figure 33. Extrapolation of Frequencies of Resonance for Case 2d Shell and Plate to Mode Number, n=50

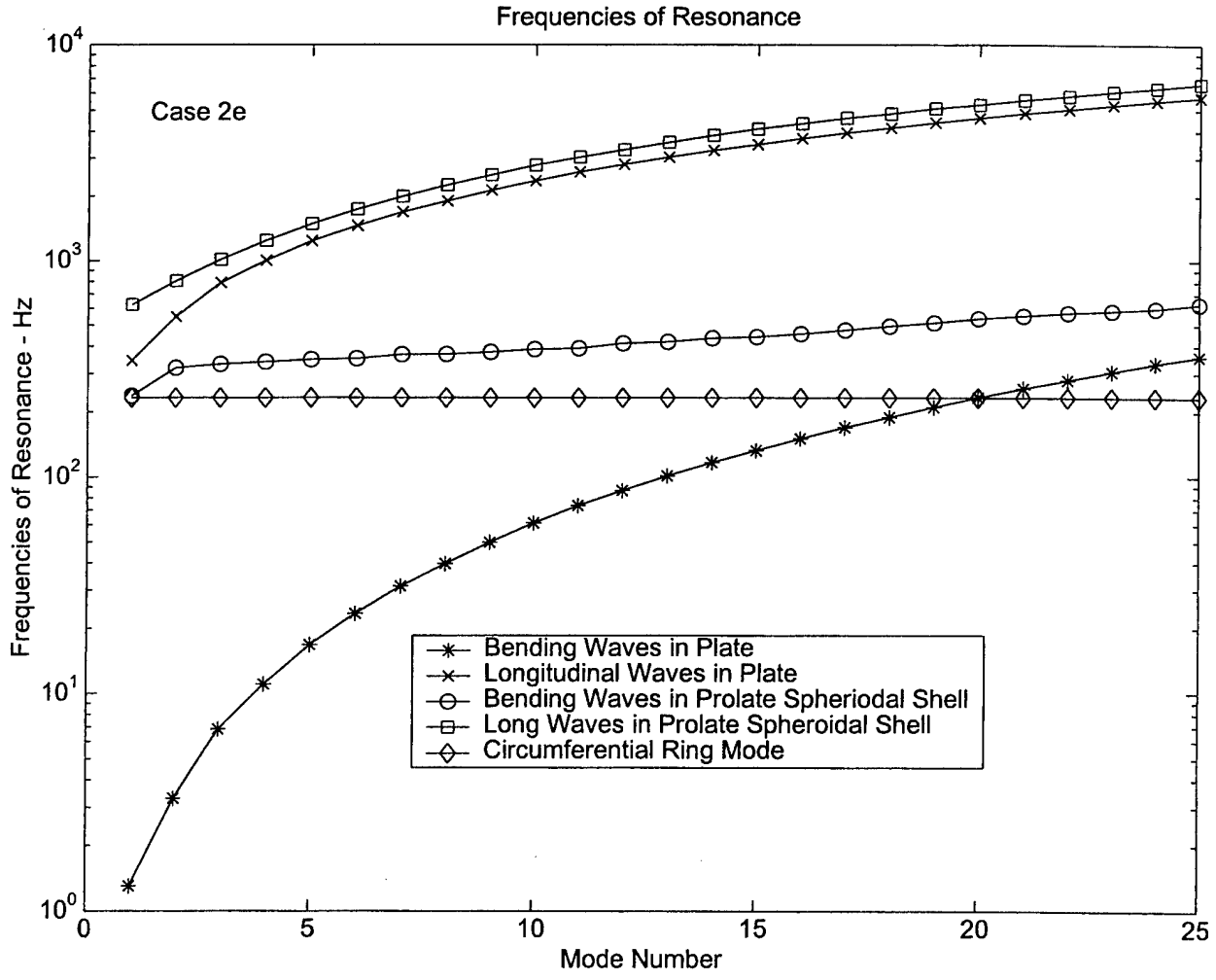

Figure 34. Frequency of Resonance for Case 2e Prolate Spheroidal Shell and And Corresponding Unwrapped Plate.

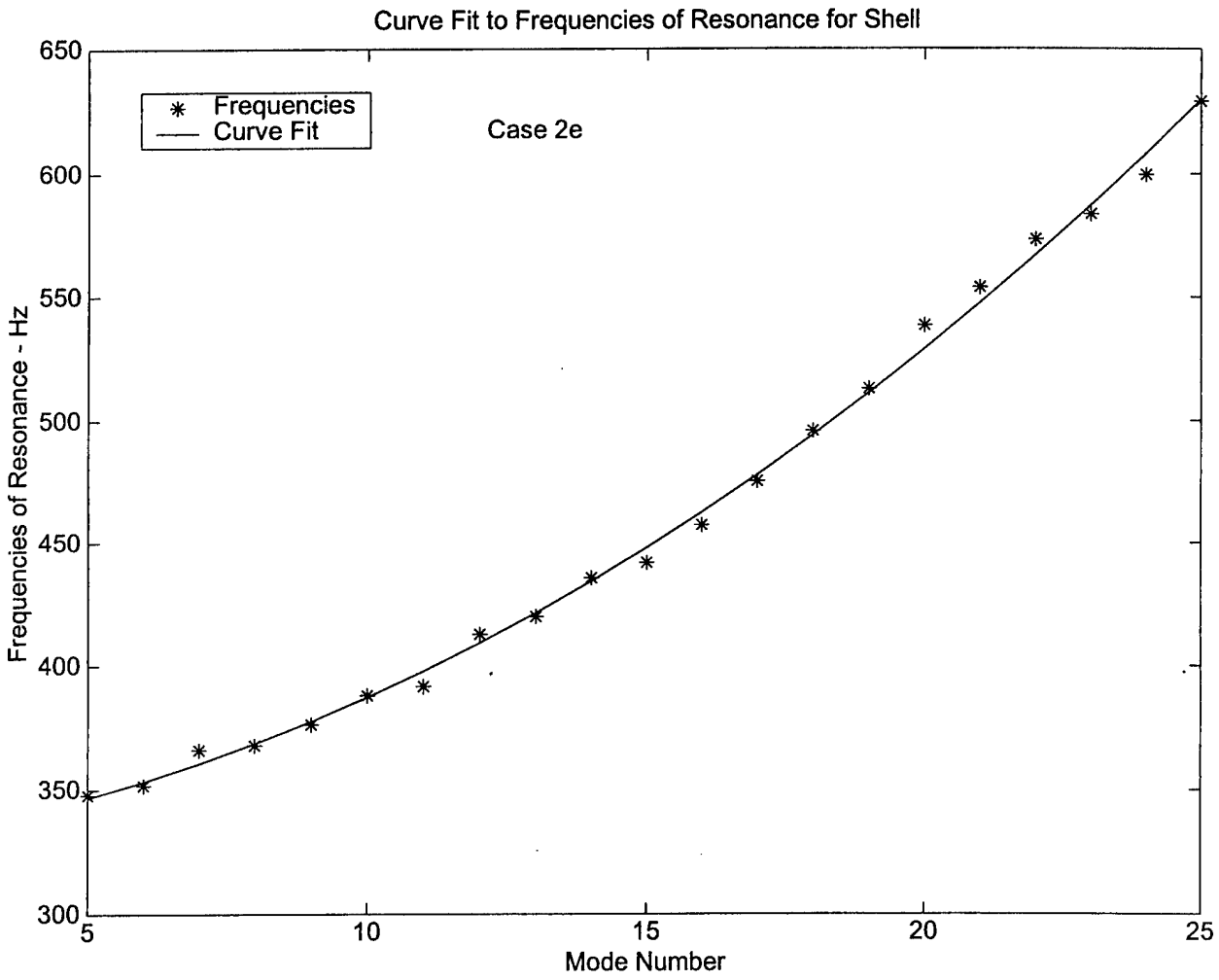

Figure 35. Quadratic Curve Fit to Bending Wave Frequencies of Resonance for Case 2e Prolate Spheroidal Shell

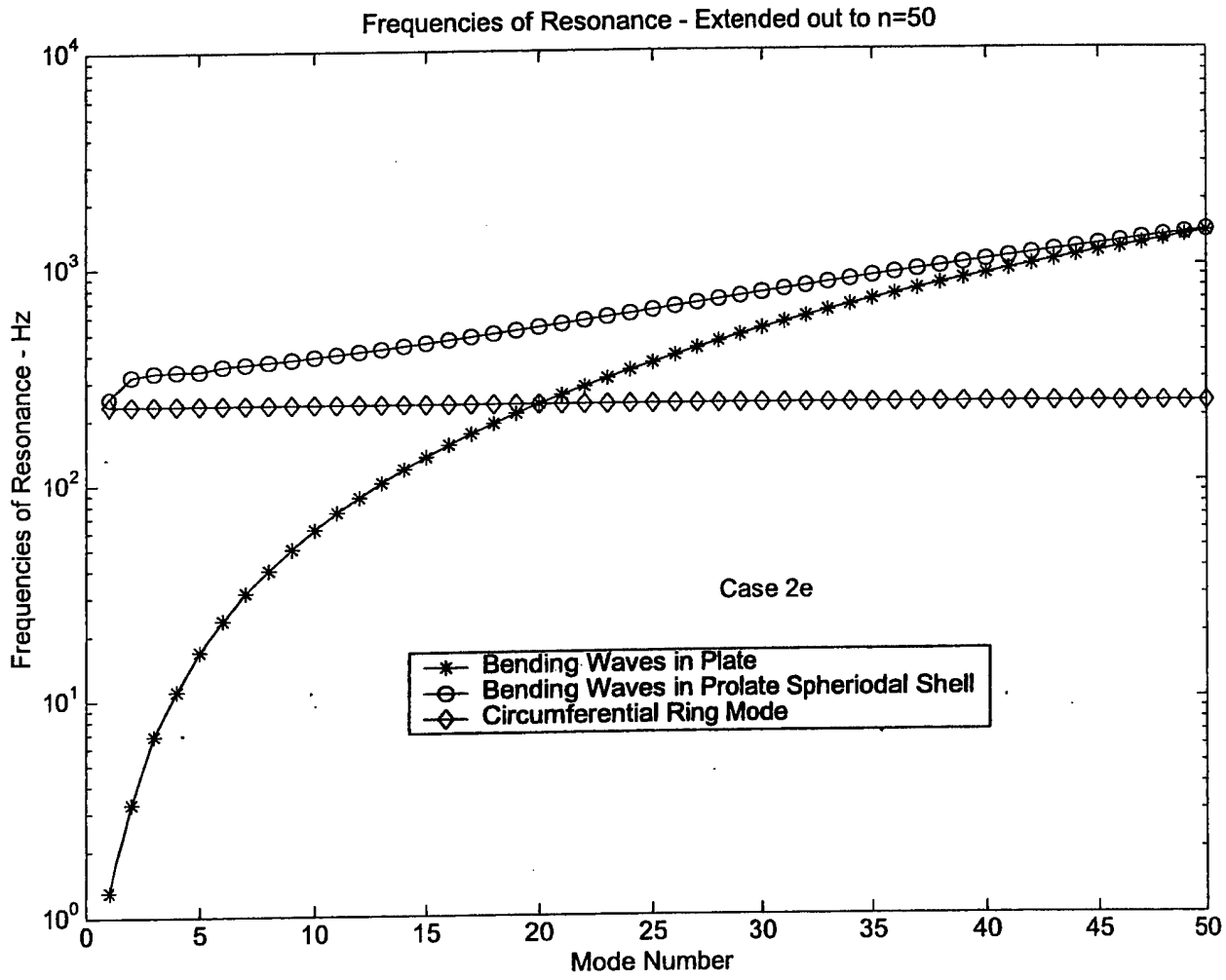

Figure 36. Extrapolation of Frequencies of Resonance for Case 2e Shell and Plate to Mode Number, n=50

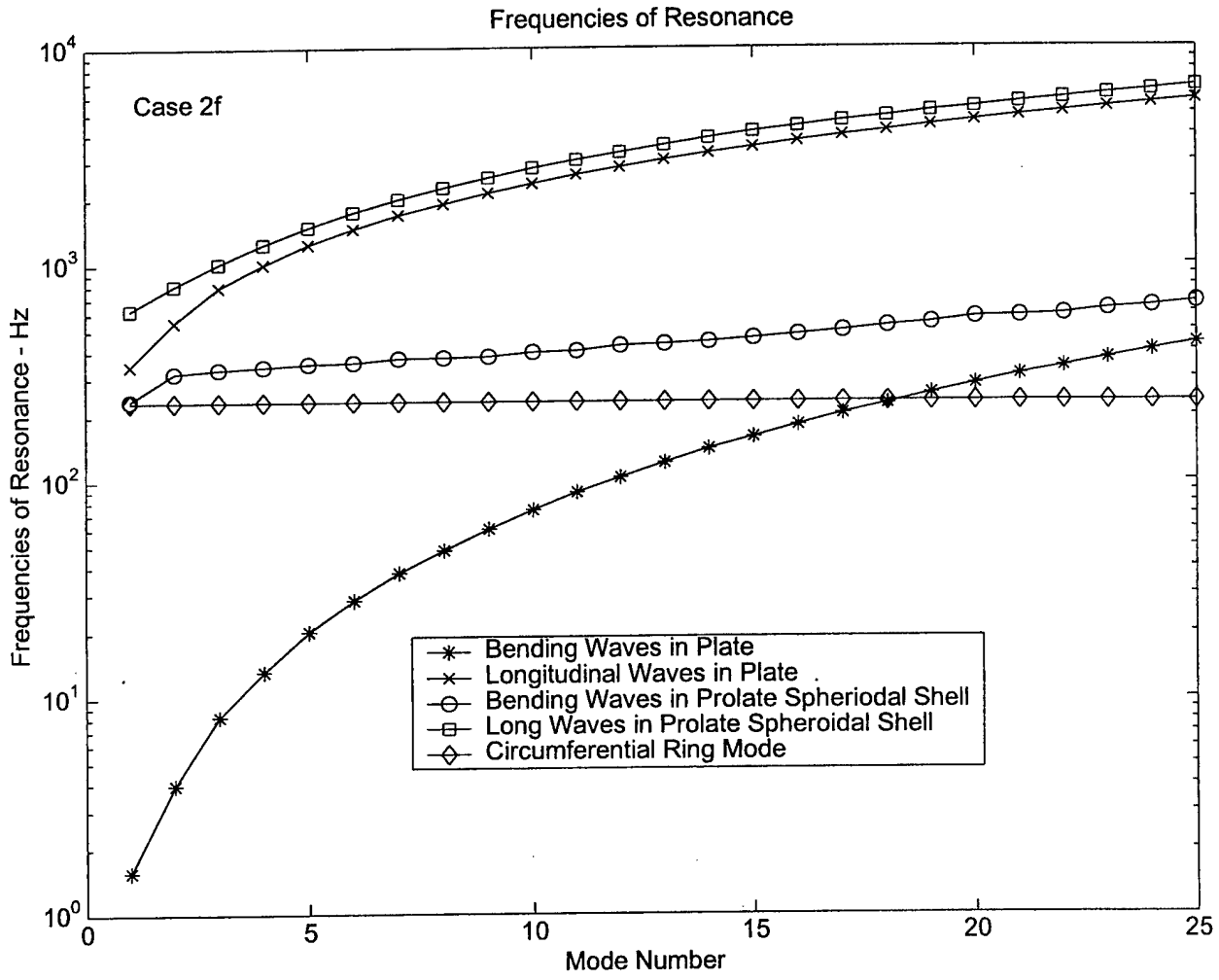

Figure 37. Frequency of Resonance for Case 2f Prolate Spheroidal Shell and And Corresponding Unwrapped Plate.

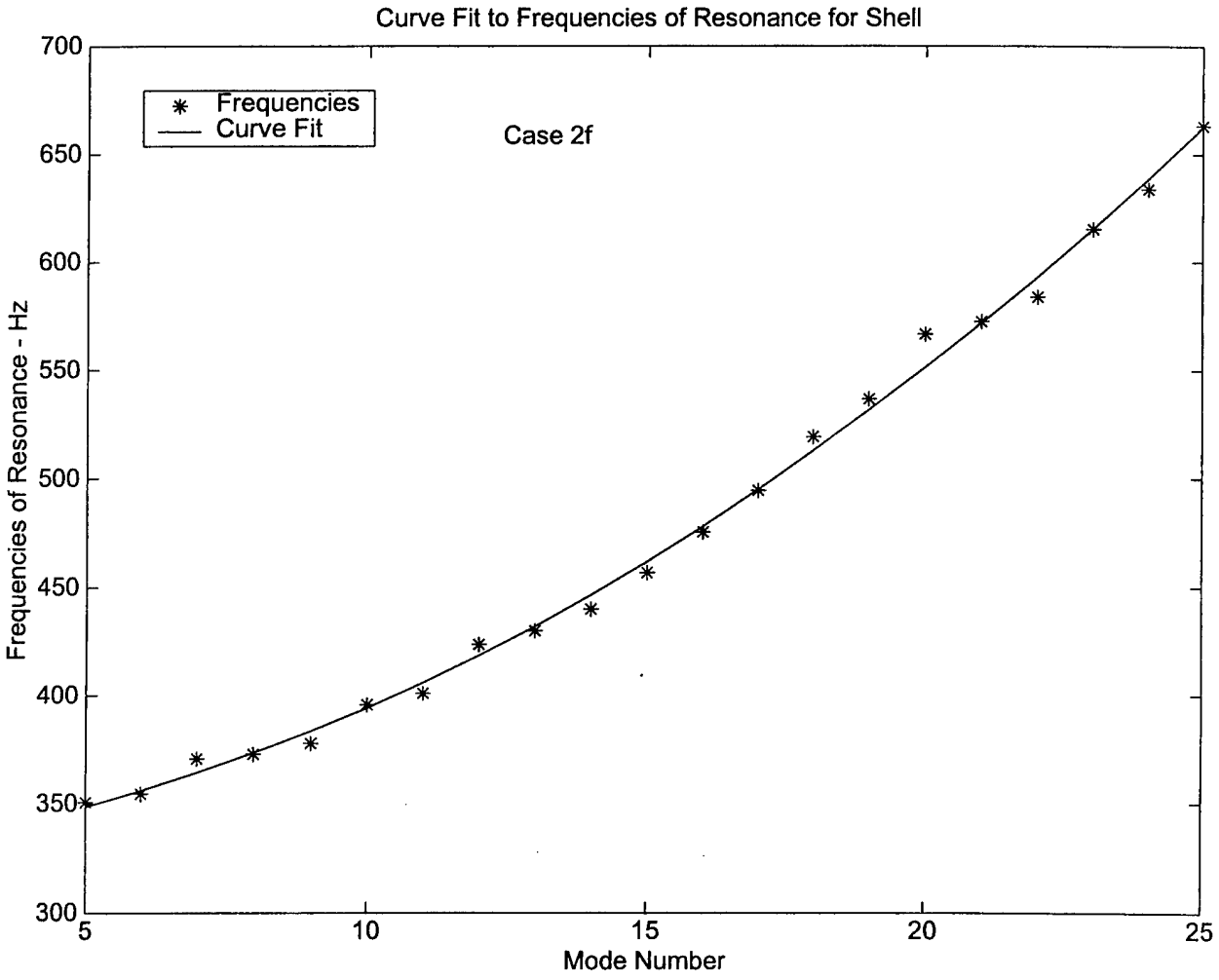

Figure 38. Quadratic Curve Fit to Bending Wave Frequencies of Resonance for Case 2f Prolate Spheroidal Shell

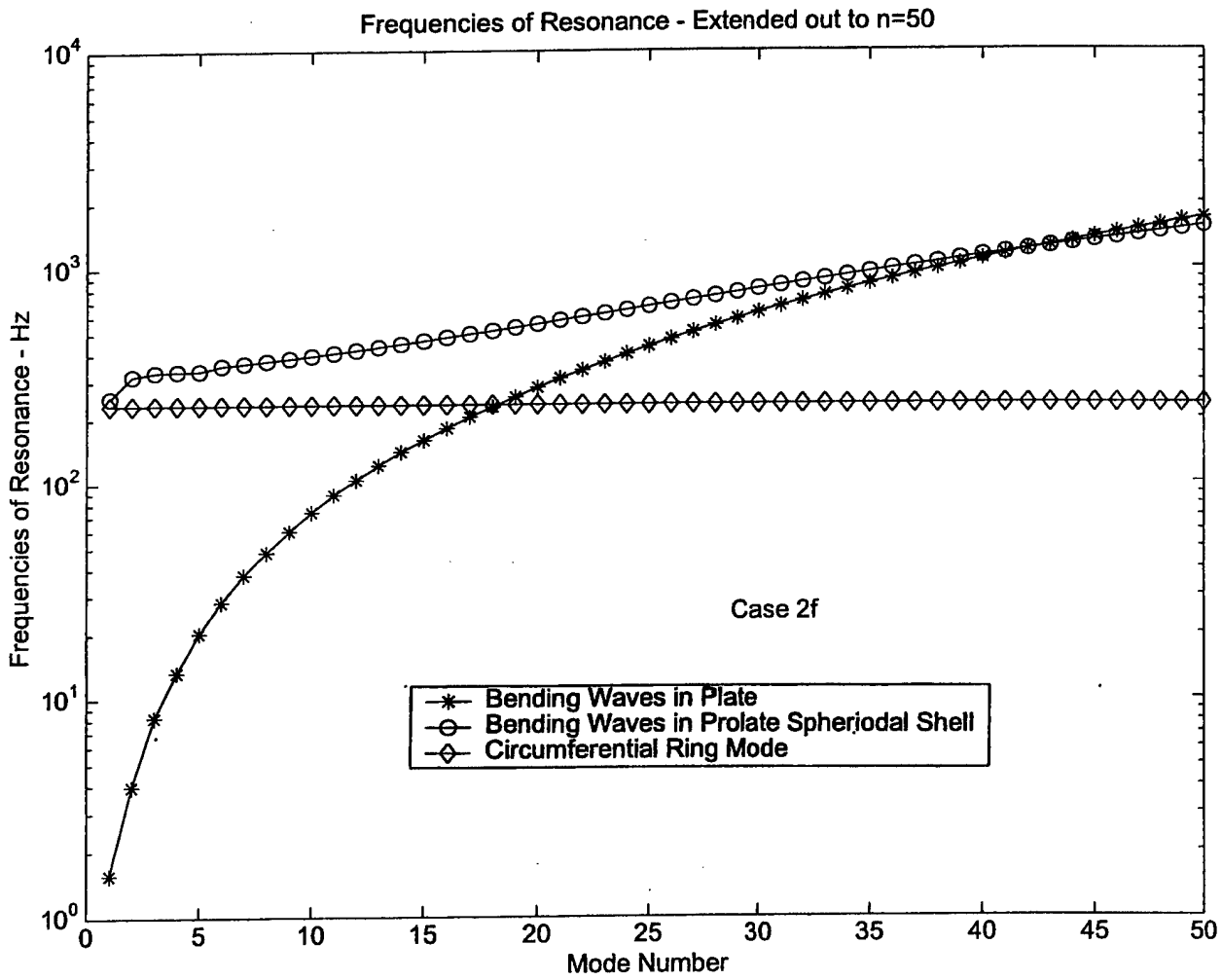

Figure 39. Extrapolation of Frequencies of Resonance for Case 2f Shell and Plate to Mode Number, n=50

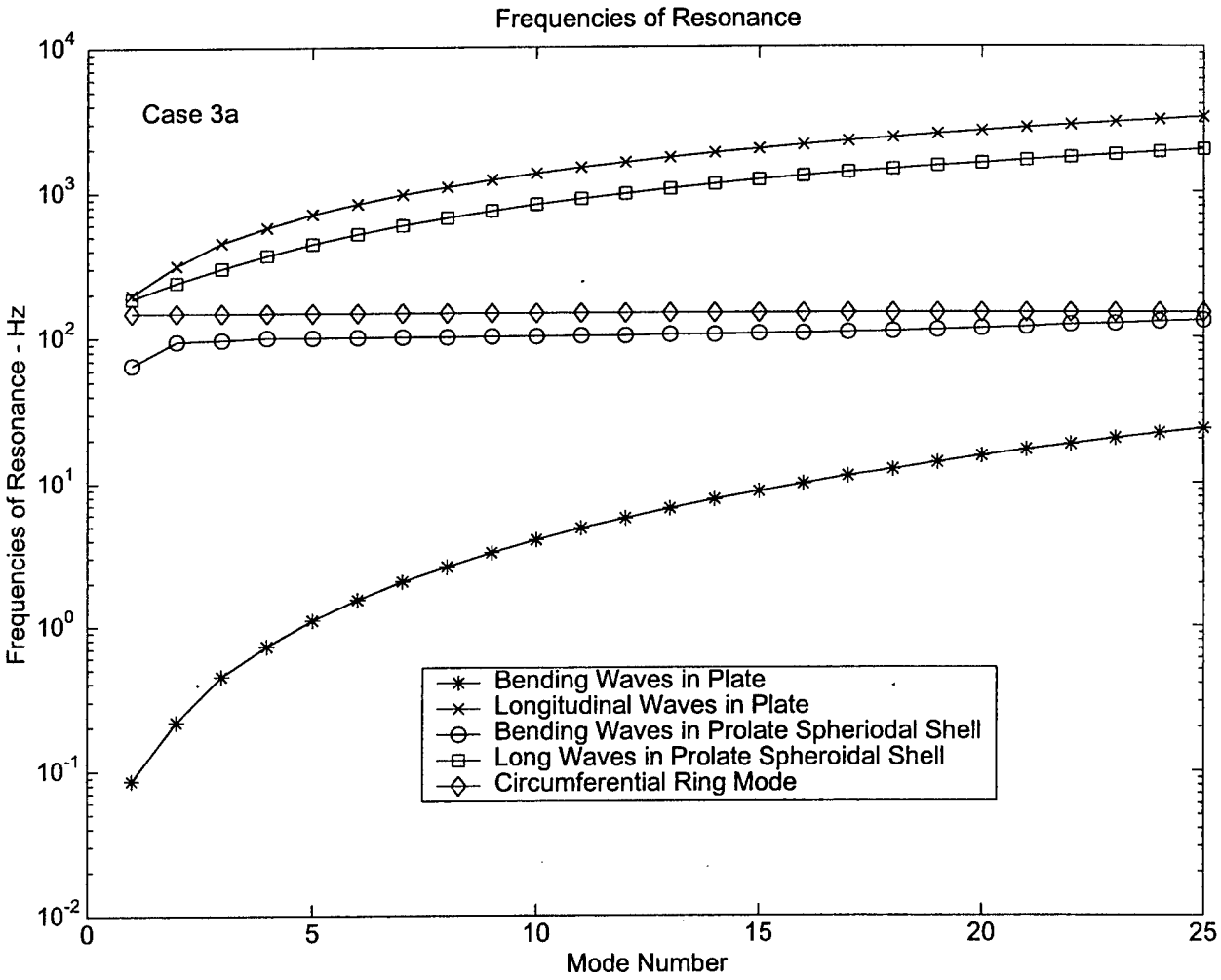

Figure 40. Frequency of Resonance for Case 3a Prolate Spheroidal Shell and And Corresponding Unwrapped Plate.

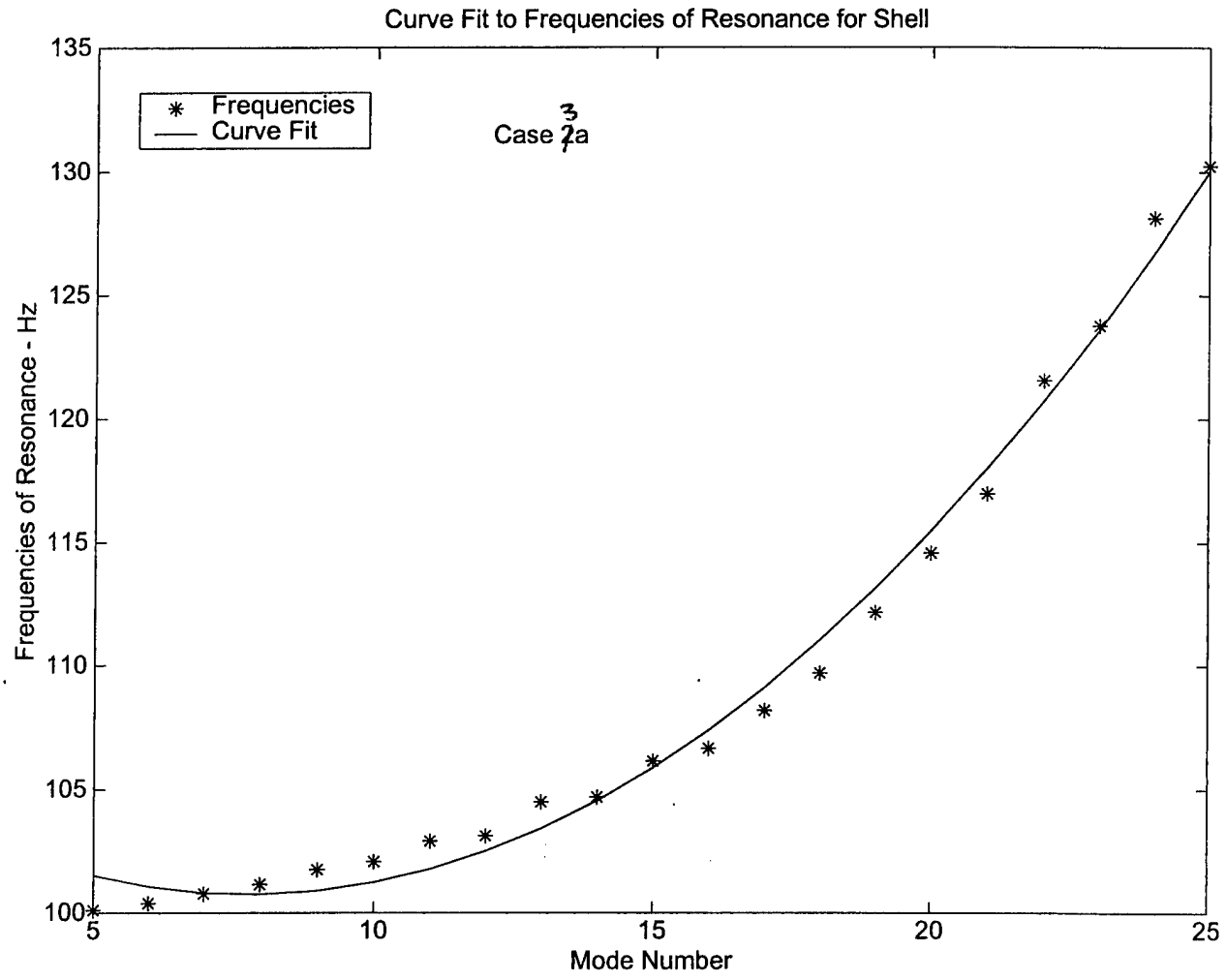

Figure 41. Quadratic Curve Fit to Bending Wave Frequencies of Resonance for Case 3a Prolate Spheroidal Shell

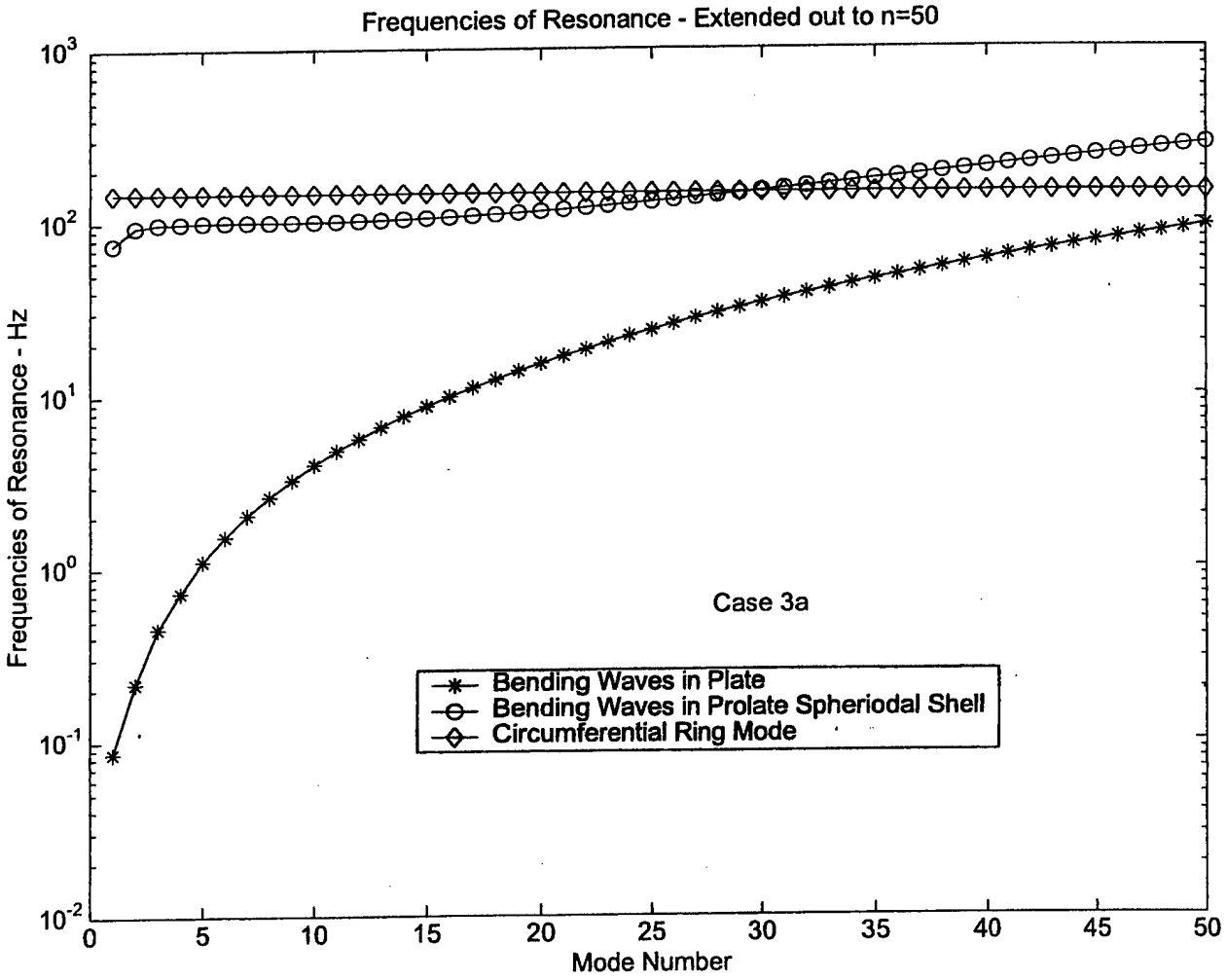

Figure 42. Extrapolation of Frequencies of Resonance for Case 3a Shell and Plate to Mode Number, n=50

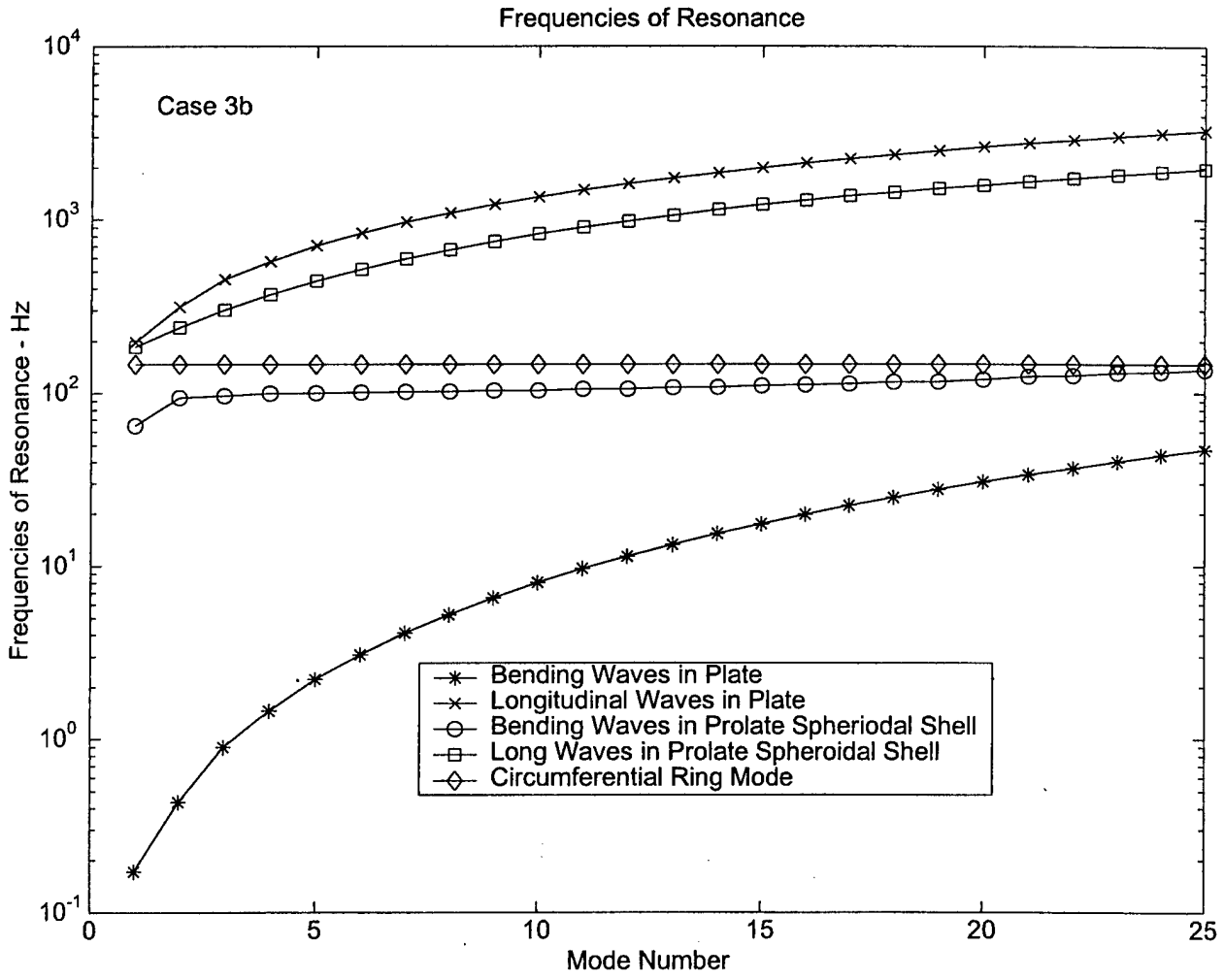

Figure 43. Frequency of Resonance for Case 3b Prolate Spheroidal Shell and And Corresponding Unwrapped Plate.

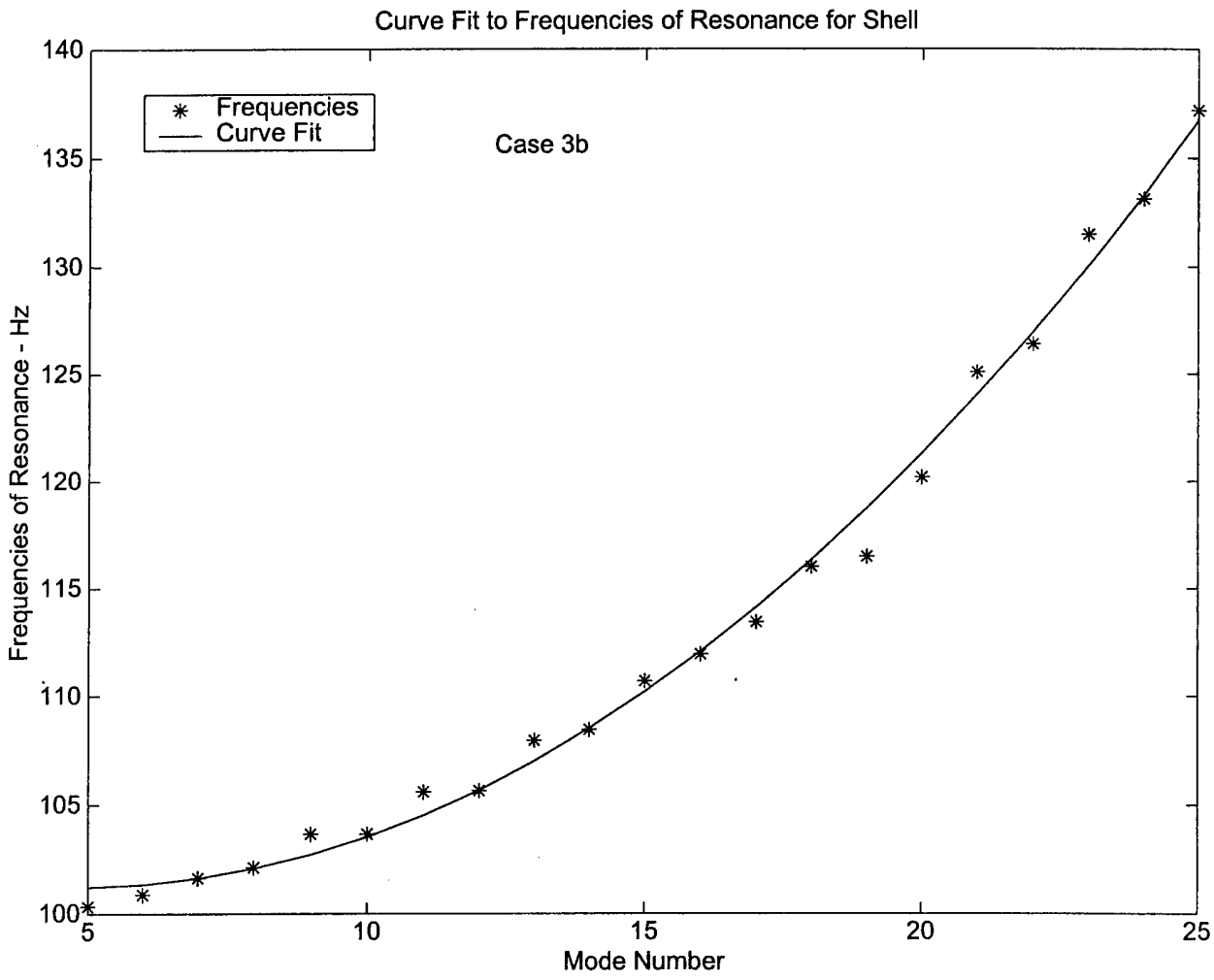

Figure 44. Quadratic Curve Fit to Bending Wave Frequencies of Resonance for Case 3b Prolate Spheroidal Shell

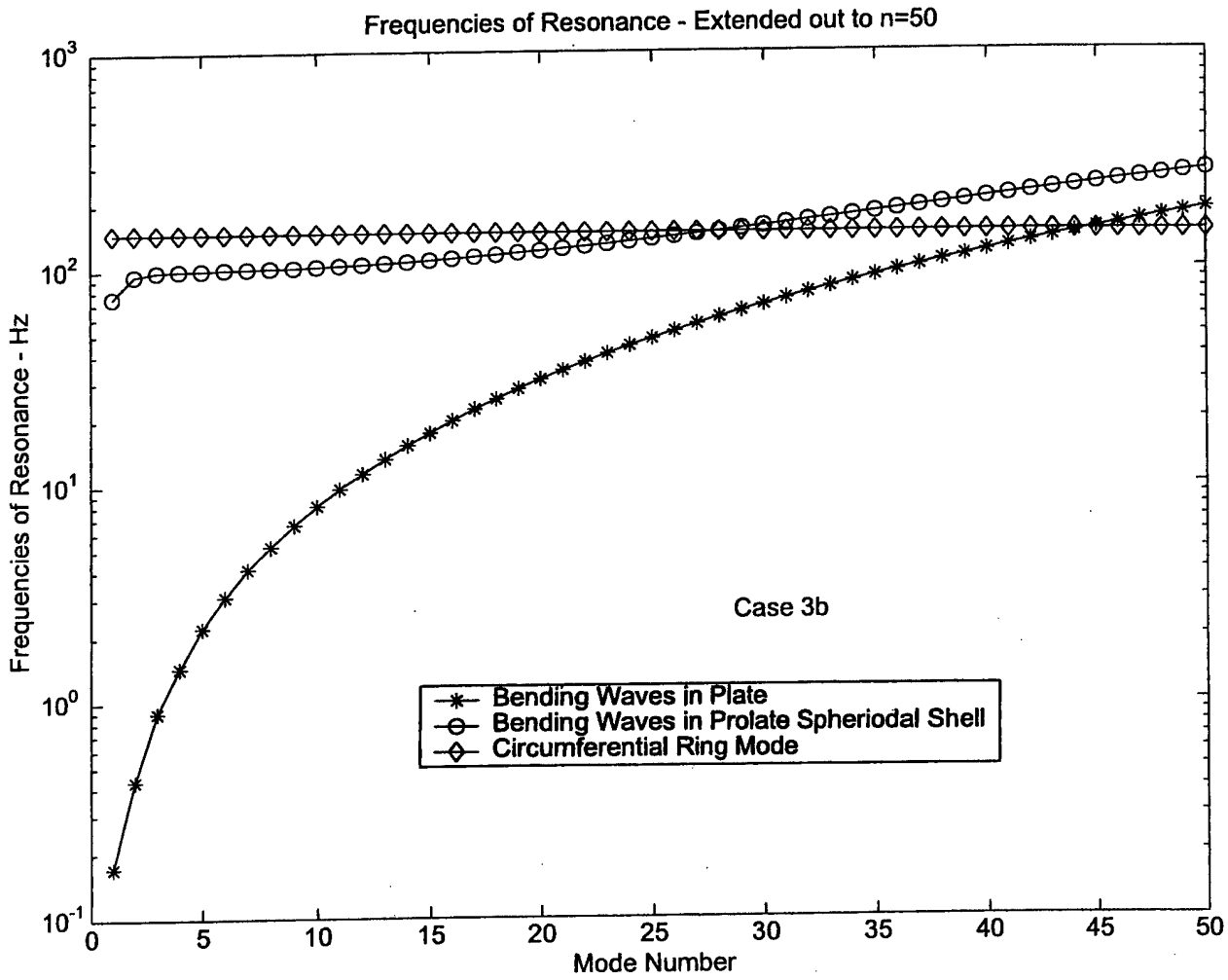

Figure 45. Extrapolation of Frequencies of Resonance for Case 3b Shell and Plate to Mode Number, n=50

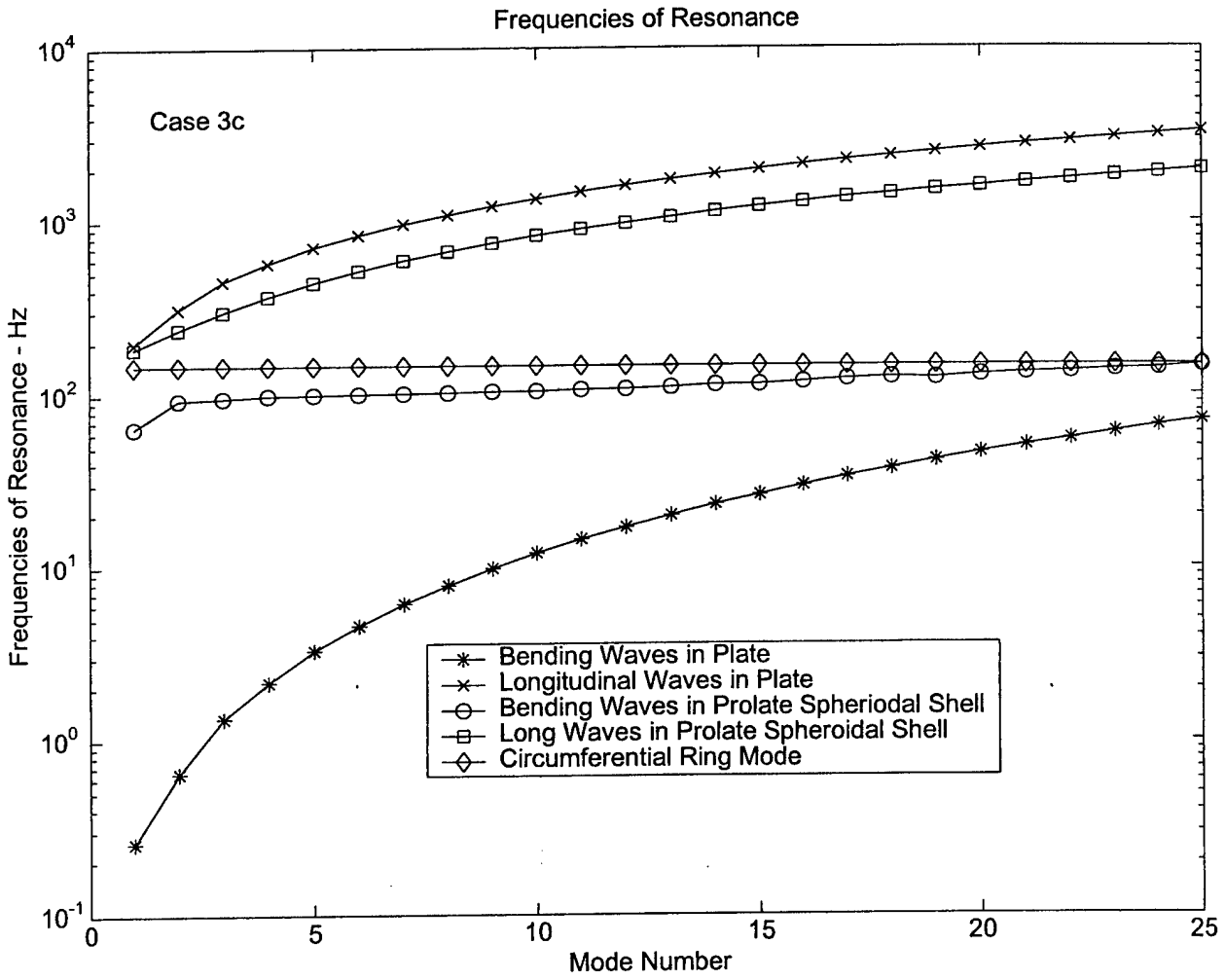

Figure 46. Frequency of Resonance for Case 3c Prolate Spheroidal Shell and And Corresponding Unwrapped Plate.

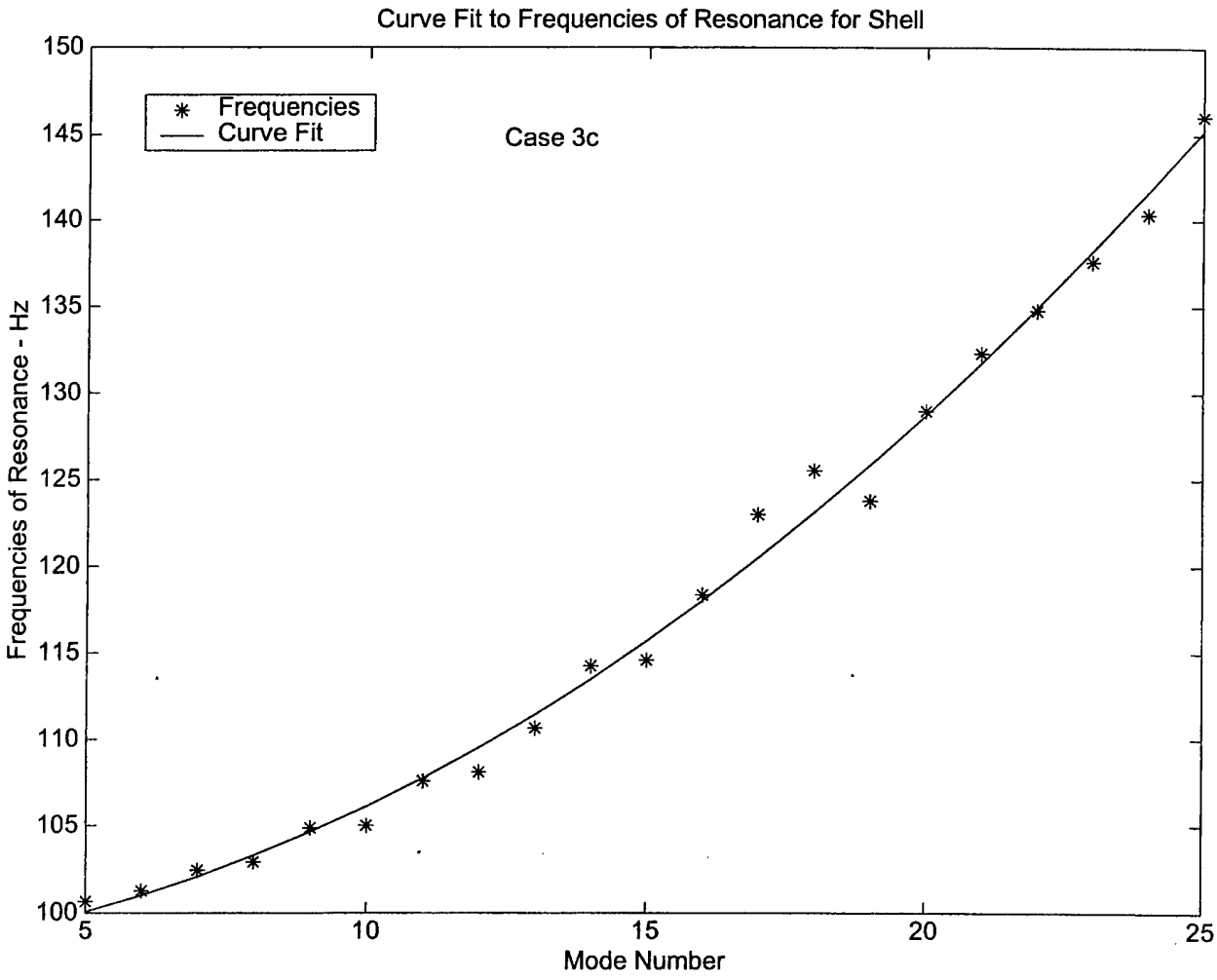

Figure 47. Quadratic Curve Fit to Bending Wave Frequencies of Resonance for Case 3c Prolate Spheroidal Shell

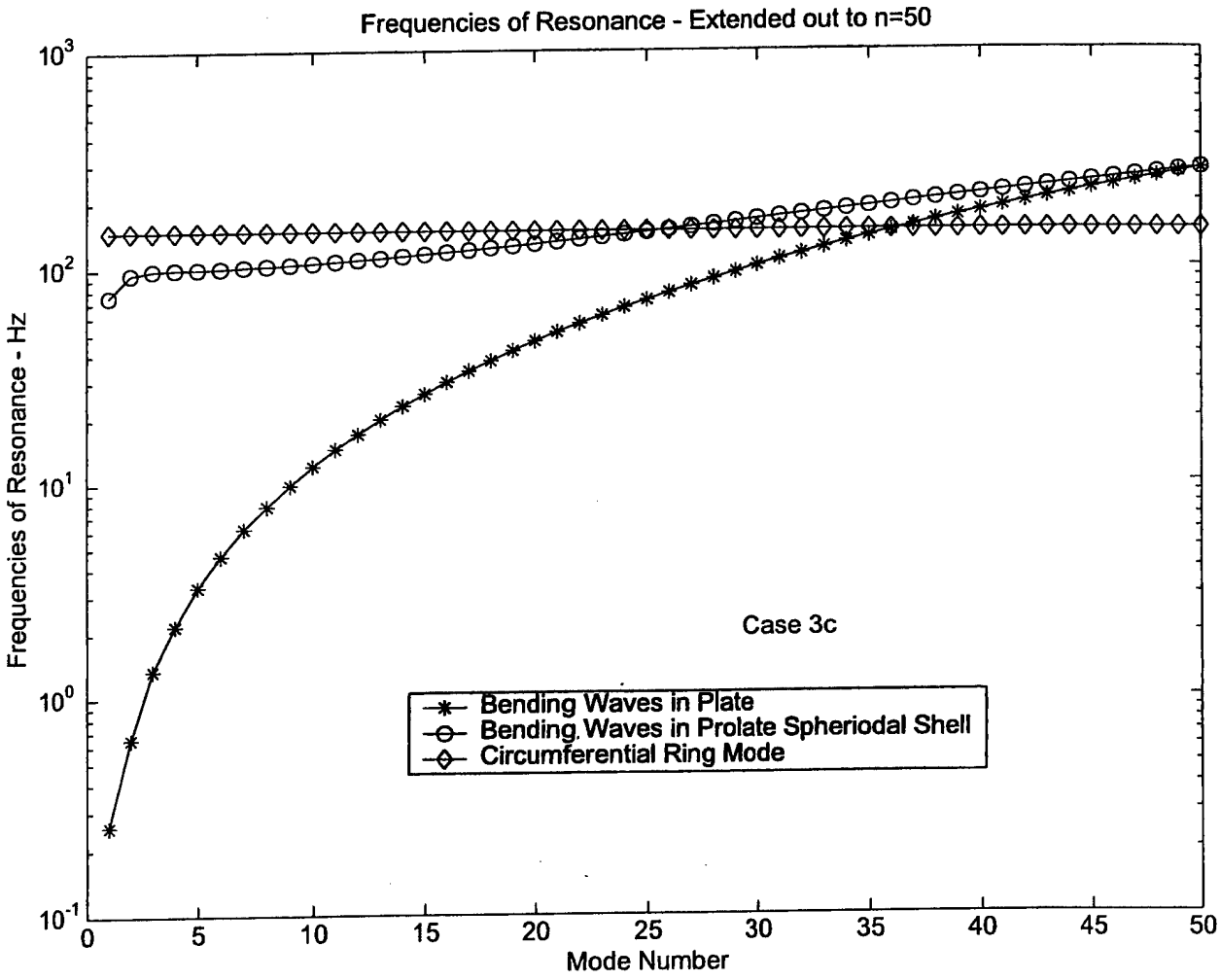

Figure 48. Extrapolation of Frequencies of Resonance for Case 3c Shell and Plate to Mode Number, n=50

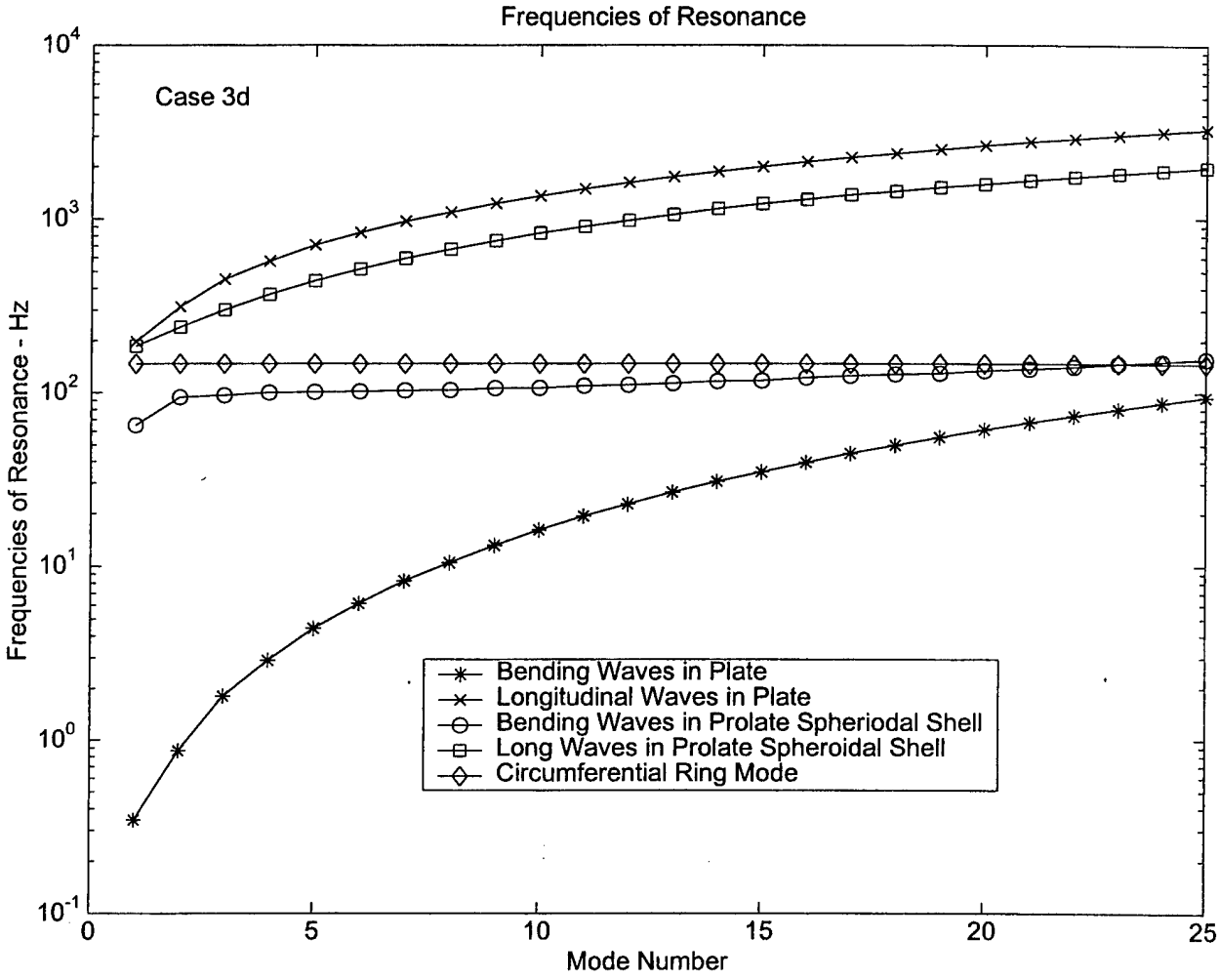

Figure 49. Frequency of Resonance for Case 3d Prolate Spheroidal Shell and And Corresponding Unwrapped Plate.

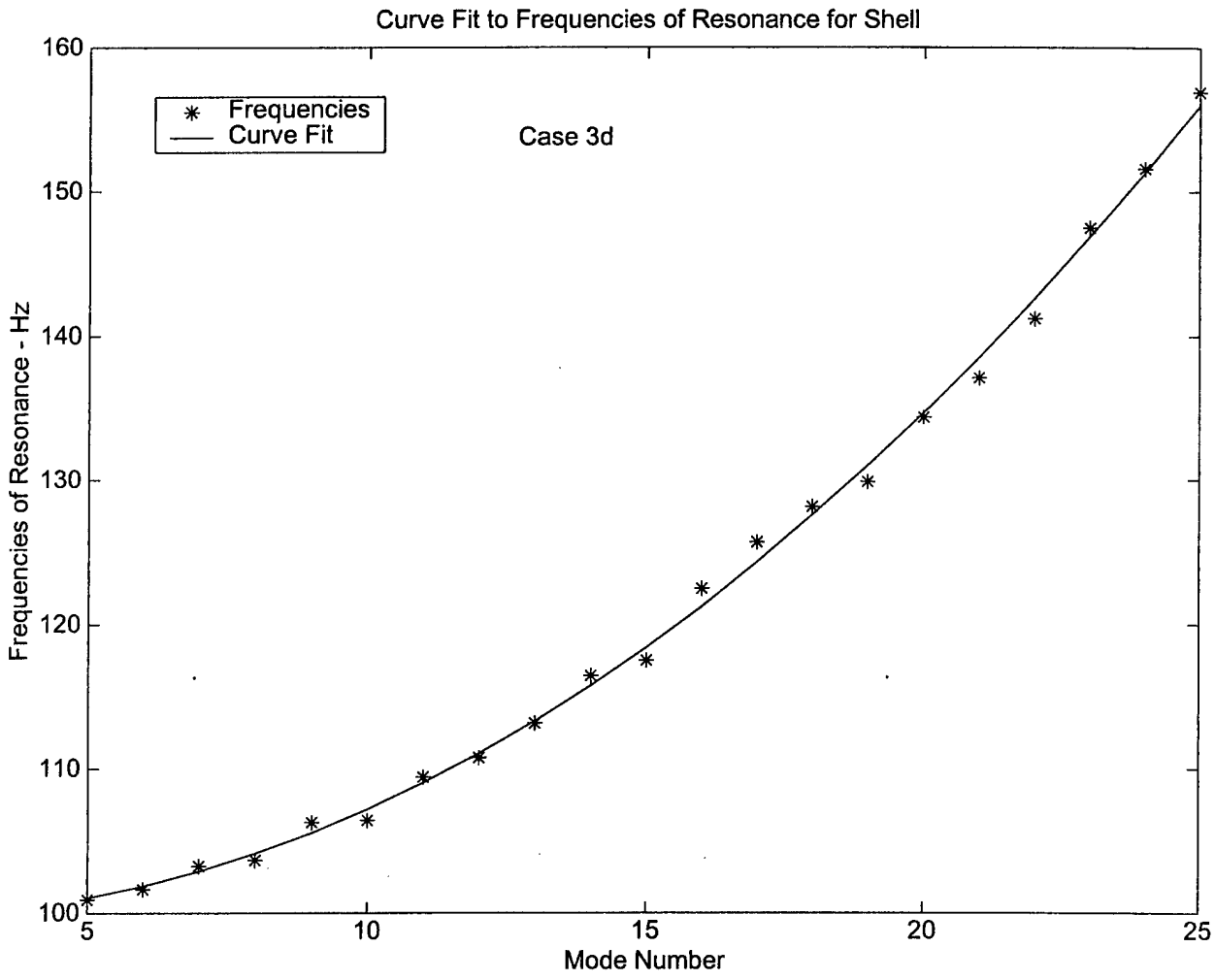

Figure 50. Quadratic Curve Fit to Bending Wave Frequencies of Resonance for Case 3d Prolate Spheroidal Shell

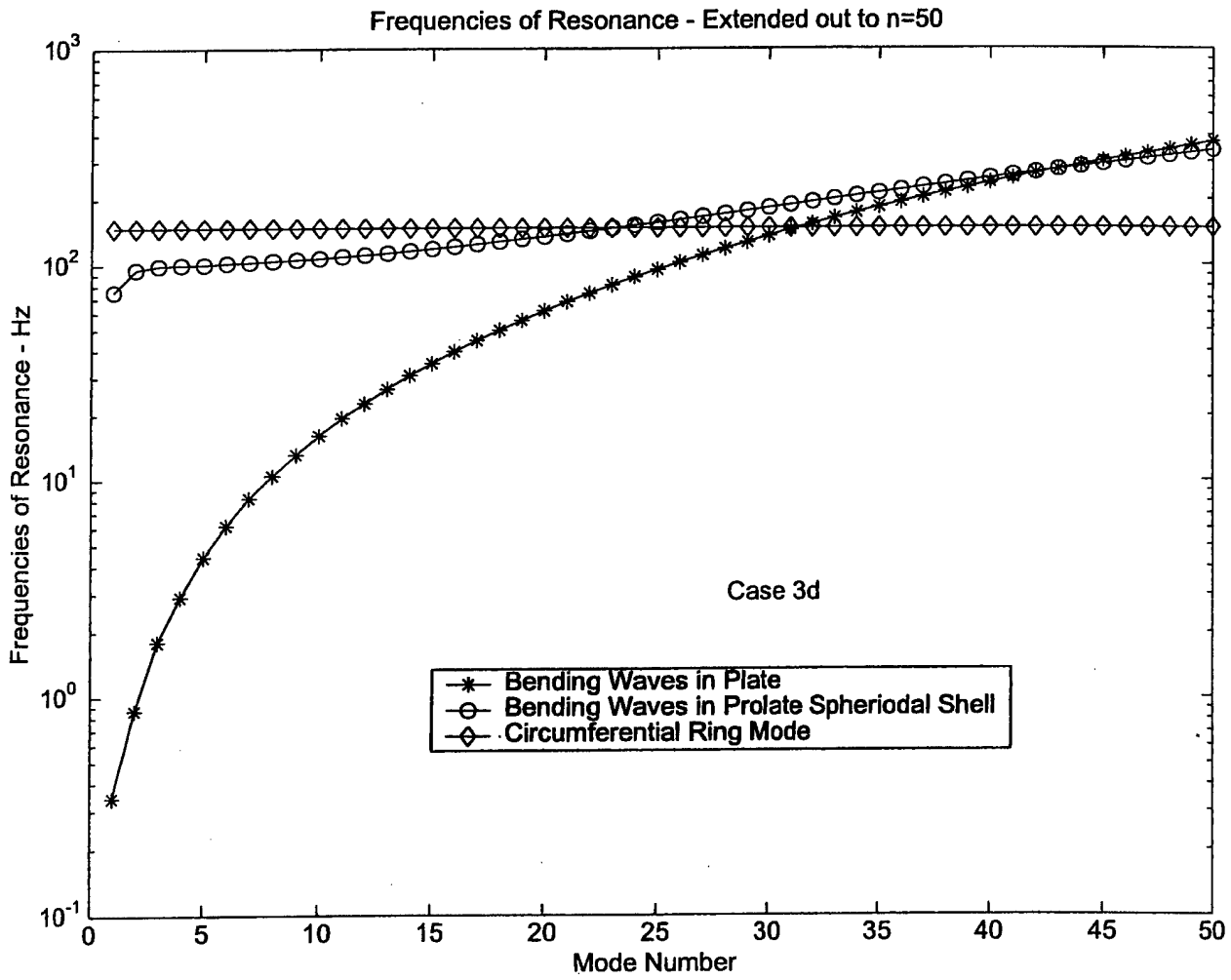

Figure 51. Extrapolation of Frequencies of Resonance for Case 3d Shell and Plate to Mode Number, n=50

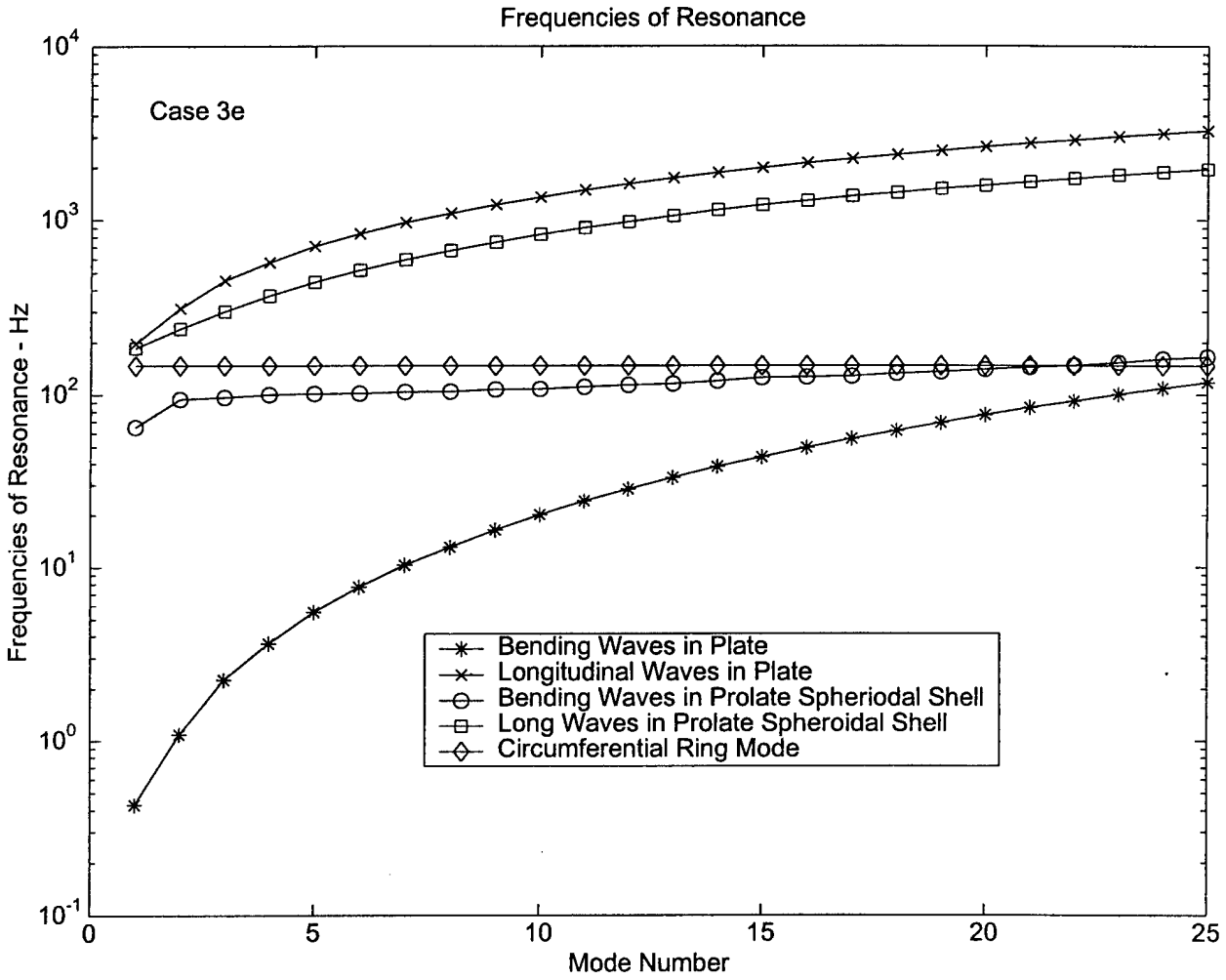

Figure 52. Frequency of Resonance for Case 3e Prolate Spheroidal Shell and And Corresponding Unwrapped Plate.

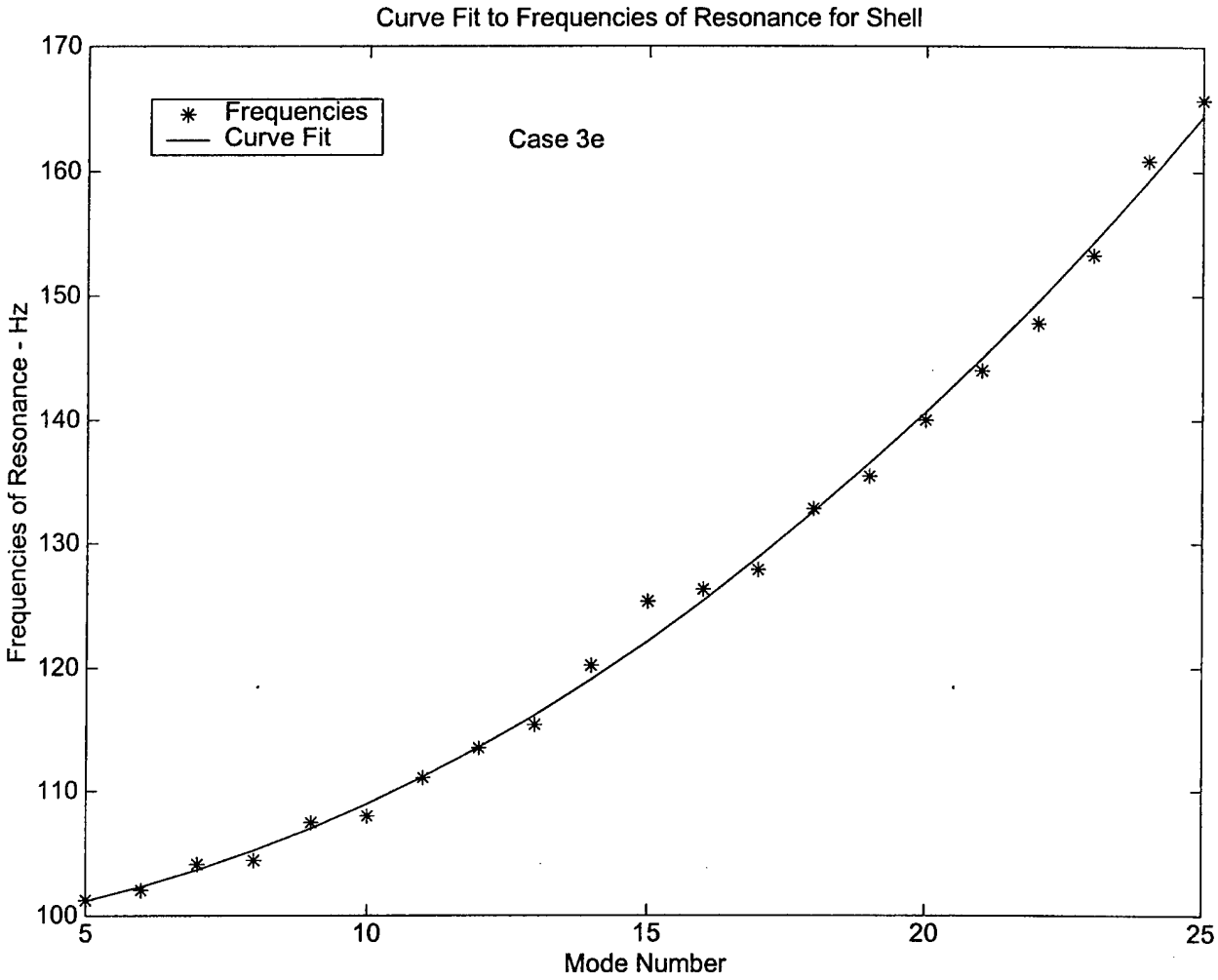

Figure 53. Quadratic Curve Fit to Bending Wave Frequencies of Resonance for Case 3e Prolate Spheroidal Shell

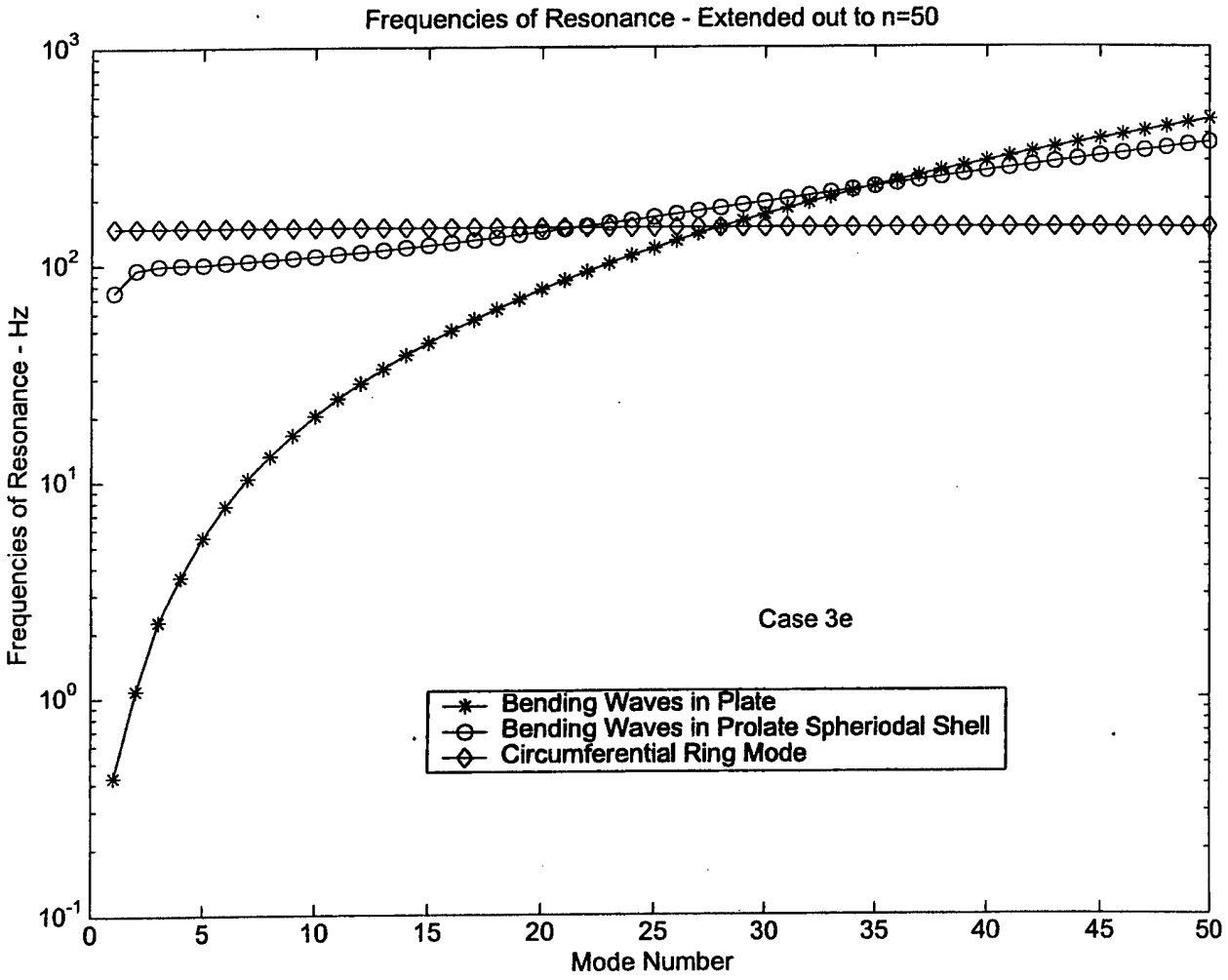

Figure 54. Extrapolation of Frequencies of Resonance for Case 3e Shell and Plate to Mode Number, n=50

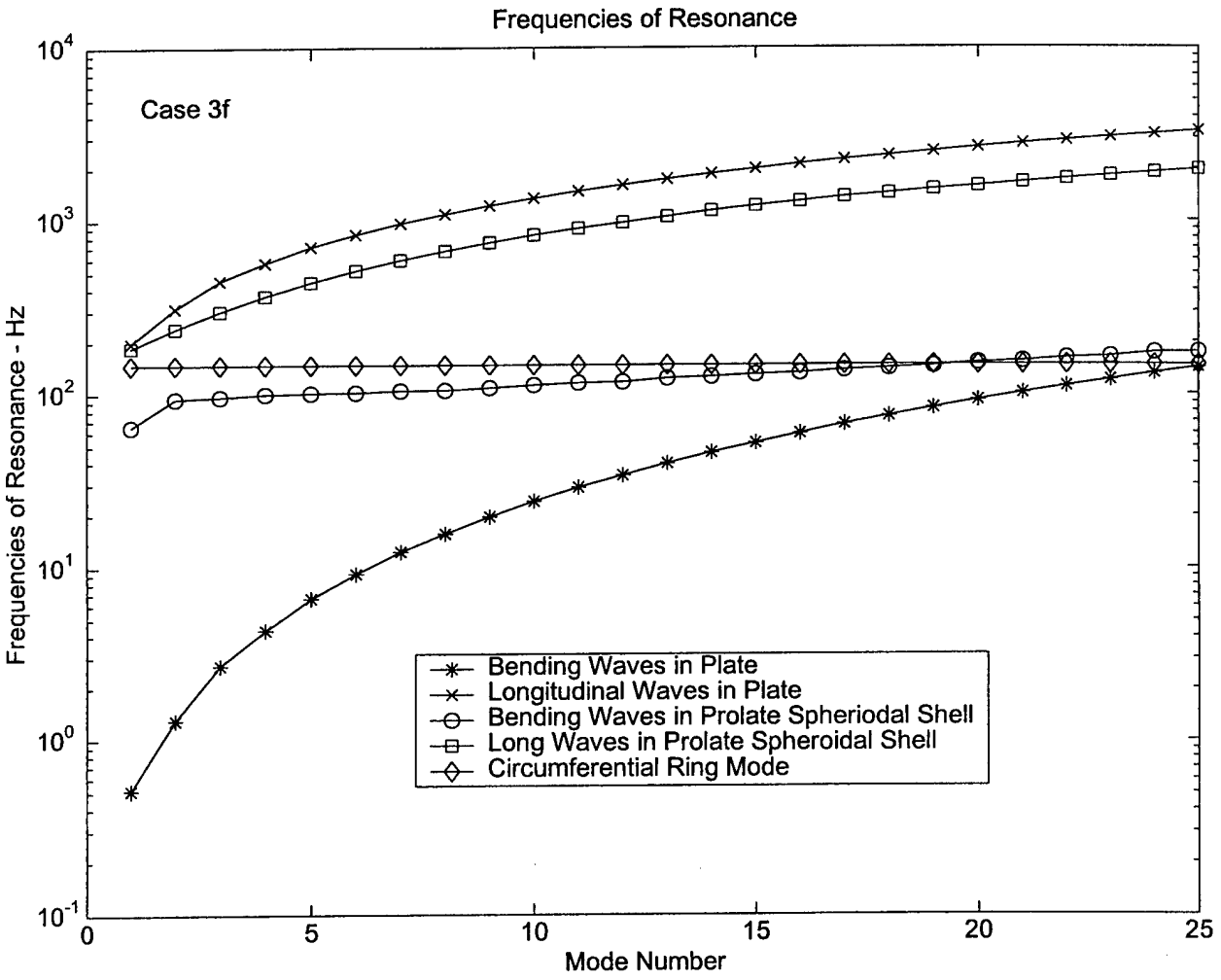

Figure 55. Frequency of Resonance for Case 3f Prolate Spheroidal Shell and And Corresponding Unwrapped Plate.

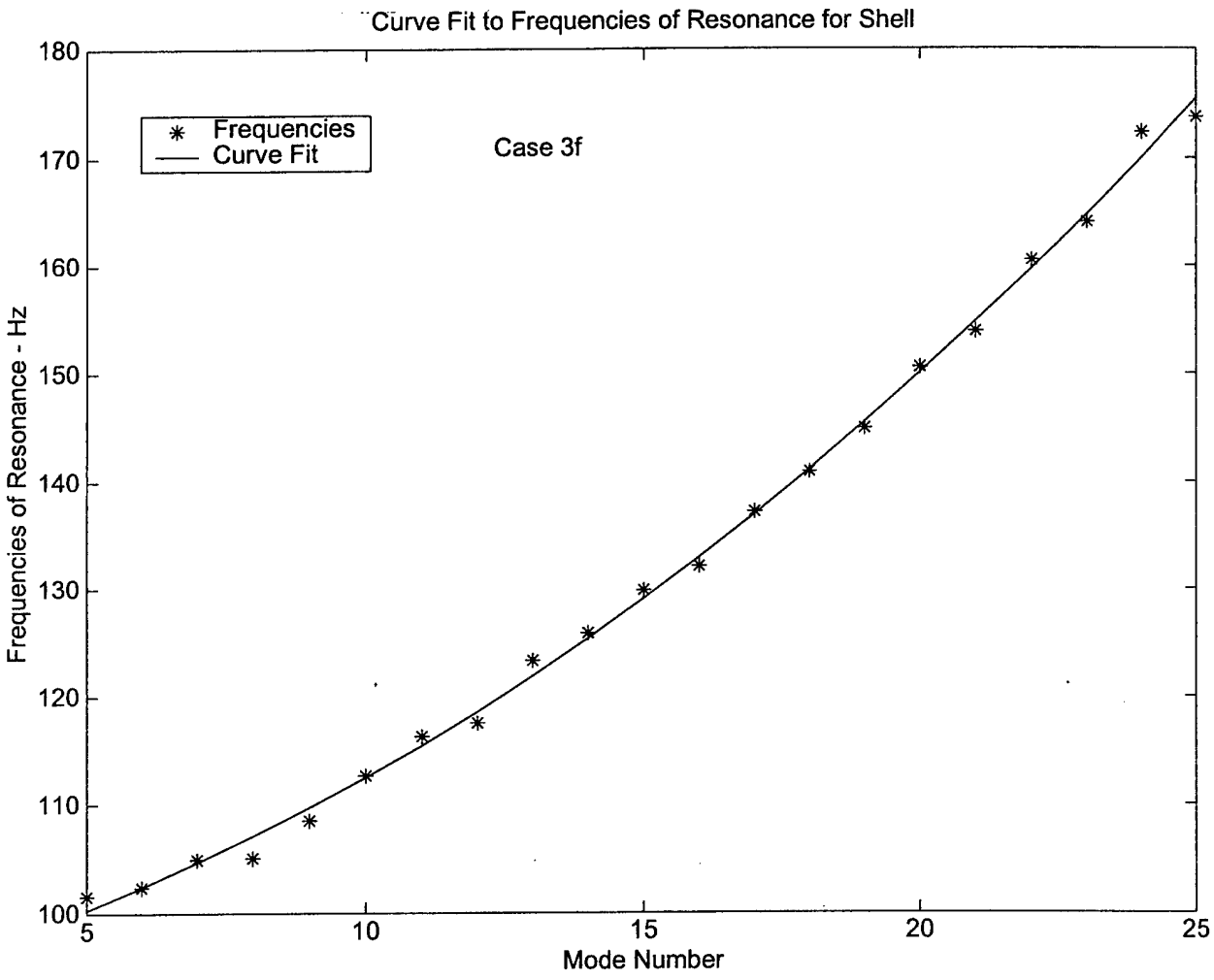

Figure 56. Quadratic Curve Fit to Bending Wave Frequencies of Resonance for Case 3f Prolate Spheroidal Shell

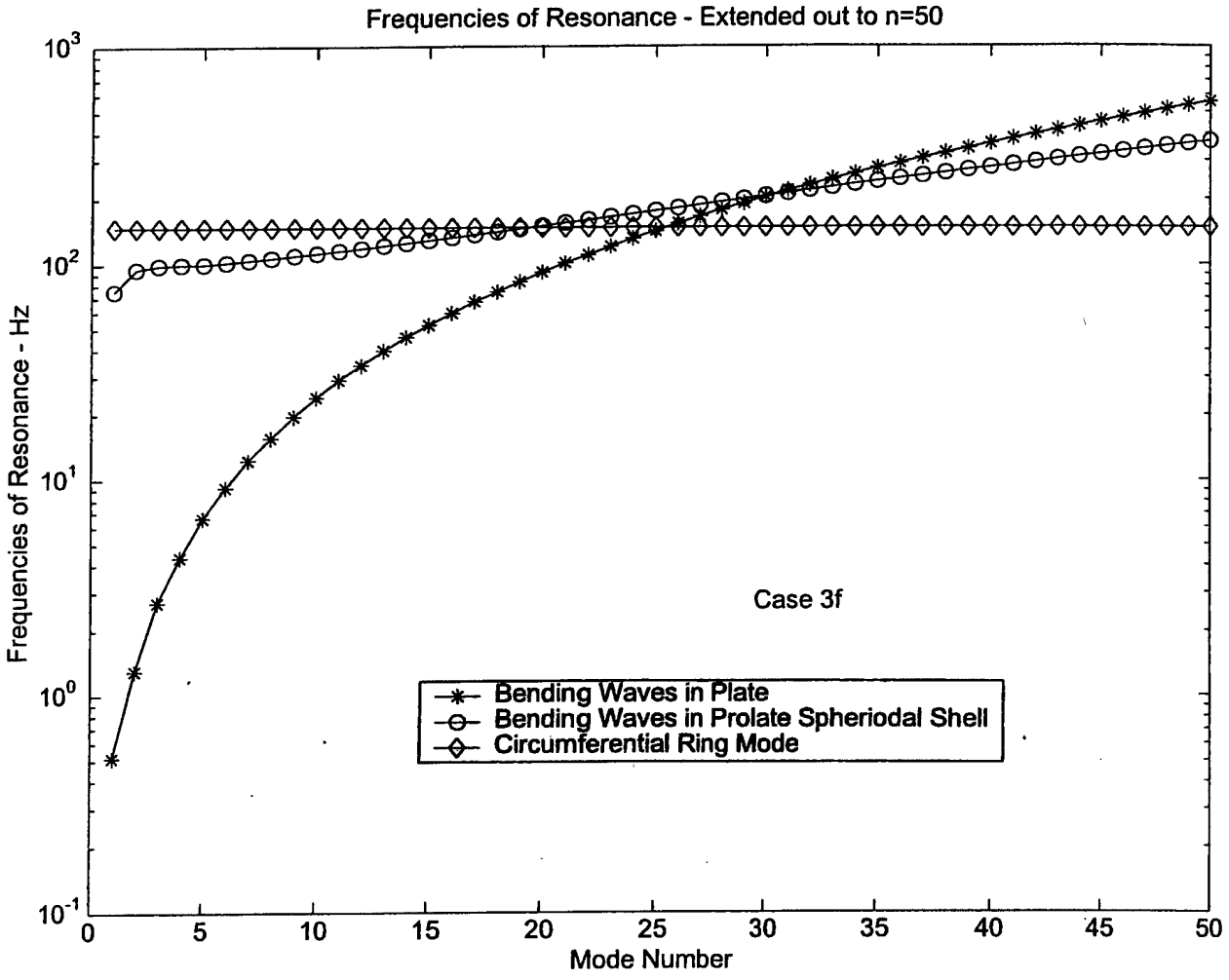

Figure 57. Extrapolation of Frequencies of Resonance for Case 3f Shell and Plate to Mode Number, n=50

5.0 Conclusions

As the mode number increases, the unwrapped plate with a radius equal to the meridian arc length from the apex to the middle of the prolate spheroidal shell provides an increasingly accurate approximation to the frequencies of resonance for the axisymmetric modes of the shell. The ring in-plane circumferential stresses provide a lower bound to the frequencies of resonance for the shell. Thus, the modal density for axisymmetric bending waves in the shell can be approximated with the plate model after the frequencies are shifted up to around the frequency for the ring mode.

For the circular plate, the mode spacing for the higher-order modes can be approximated using asymptotic expressions for the Bessel functions, i.e.

$$J_0(kr) \to \left(\frac{2}{\pi kr}\right)^{1/2} \cos\left(kr - \frac{\pi}{4}\right) \text{ and } J_1(kr) \to \left(\frac{2}{\pi kr}\right)^{1/2} \cos\left(kr - \frac{\pi}{2} - \frac{\pi}{4}\right).$$

Thus, the frequency spacing between modes in a circular plate may be approximated by $\Delta k \approx \frac{\pi}{2a}$ so that the mode count can be approximated as

$$N(\omega) = \frac{k}{\Delta k} = \frac{2kL}{\pi} = \frac{2\omega^{1/2} L}{\pi}\left(\frac{\rho h}{D}\right)^{1/4}$$

where $D = \frac{Eh^3}{12(1-\nu^2)}$ is the bending rigidity. The modal density is then

$$n(\omega) = \frac{\partial N(\omega)}{\partial \omega} = \frac{12^{1/4} L}{\pi}\left[\frac{\rho(1-\nu^2)}{Eh^2}\right]^{1/4}$$

This approximation for the modal density is applicable to the shell only at frequencies above the ring frequency of resonance given by $\omega_r = \frac{c_l}{2\pi R_e}$ where

$$R_e = \frac{a}{4} + \frac{b^2}{4\left(a^2 - b^2\right)^{1/2}} \ln\left[\frac{\left(a^2 - b^2\right)^{1/2} + a}{b}\right]$$

with a and b equal to the major and minor axes for the prolate spheroidal shell. Thus, the proposed approximation for the axisymmetric modes of in-vacuo closed prolate spheroidal shells of constant thickness is

$$n(\omega) = \frac{L^{1/2}}{1.7(\omega c_l h)^{1/2}} \text{ for } \omega > \omega_r$$

and

$$n(\omega) = 0 \text{ for } \omega < \omega_r$$

For $n = 1$ circumferential modes, thein-plane stresses are small so that the derivation of an approximate expression for the modal density should be simpler to obtain than for the $n = 0$ modes. Also, for higher-order circumferential modes, i.e. above the $n = 1$ mode, the effects of curvature in the circumferential direction should be less than for the axisymmetric modes, again making it easier to obtain good approximations for modal densities for bending wave modes in prolate spheroidal shells.

References

1. C.B. Burroughs and E.B. Magrab, "Natural Frequencies of Prolate Spheroidal Shells of Constant Thickness", J. Sound & Vibr., **57(4)**, pp. 571-581 (1978).

2. Arthur Leissa, "Vibration of Plates", Acoust. Soc. Am., Melville NY, 1993, Chapter 2.

3. Arthur Leissa, "Vibration of Shells", Acoust. Soc. Am., Melville NY, 1993, Chapter 2.